Development of π-Extended Porphyrins with Heterole-linked and Heterole-fused Structures

Issei Nishimura

2022

Development of π-Extended Porphyrins with Heterole-linked and Heterole-fused Structures

Issei Nishimura

2022
Laboratory of Photoorganic Chemistry
Department of Molecular Engineering
Graduate School of Engineering
Kyoto University

Preface

The studies of this thesis were carried out under the guidance of Prof. Dr. Hiroshi Imahori at the Department of Molecular Engineering, Graduate School of Engineering, Kyoto University for five years since 2017.

This thesis focuses on the synthesis and structural and electronic properties of π-extended porphyrins. Porphyrin is one of the most famous organic pigments in nature, and has been studied over one century. In particular, π-extended porphyrins have attracted attention to various organic devices as well as their intriguing structural and electronic properties. Incorporation of main group elements in π-extended porphyrins has been investigated due to their unique properties derived from effective interaction between porphyrins and main group elements. Meanwhile π-extended porphyrins with heterole-linked or -fused structures have been still rare owing to lack of their synthetic approaches. The aim of this thesis is to establish synthetic methodologies for π-extended porphyrins with heterole-linked or -fused structures and to understand the effects of heteroles on the structural and electronic properties of π-extended porphyrins.

Contents

General Introduction and Overview of This Thesis
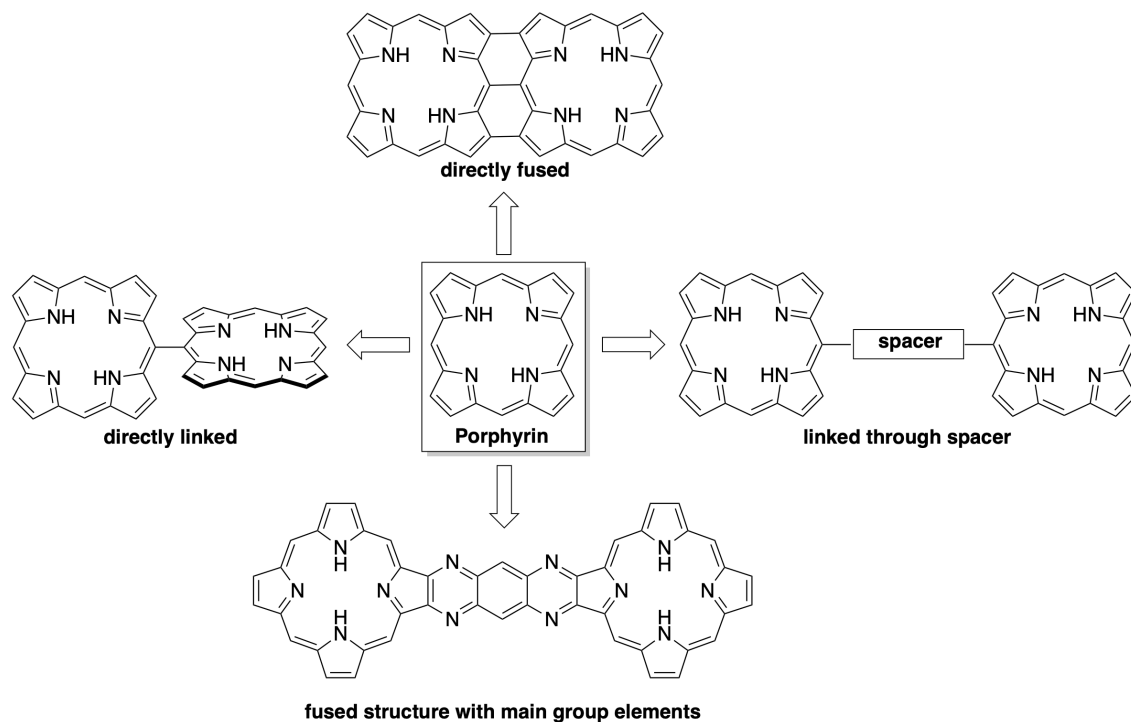
Contents

Porphyrins

General Properties of Porphyrins

Synthesis of *meso*-Tetrasubstituted Porphyrins

Selective Synthesis of *meso*-Free Porphyrins

Functionalization at Porphyrin Peripherally Positions

π-Extended Porphyrins with Main Group Elements

Linked Porphyrin Oligomers

Fused Porphyrins

Overview of This Thesis

Porphyrins

Porphyrin is one of the most important organic pigments because they play vital roles in nature such as chlorophyll *a* for photosynthesis as light harvesting system in plants and hemoglobin *b* for oxygen transporting system in human blood. In addition, *vitamin* B_{12} has similar structure with porphyrin. Therefore, porphyrins and their related compounds are called ''the pigments of life''. Porphyrins have increasingly attracted much attention in light of their potential applications in optoelectronic devices, non-linear optical materials, photocatalysts, biosensors, organic solar cells, and pigments for photodynamic therapy. For these practical applications, various kinds of porphyrins have been synthesized and investigated their unique optical and electrochemical properties.[1]
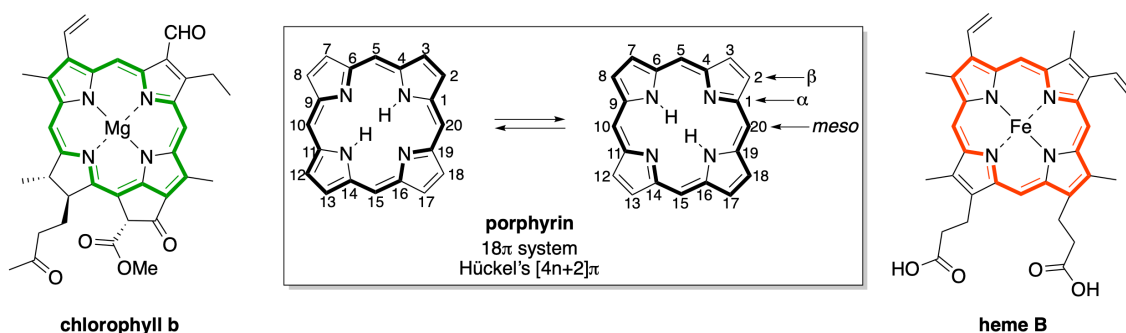
Figure 1. Chemical structures of porphyrin frameworks in nature.

General Properties of Porphyrins

Porphyrin is a macrocyclic compound which is composed of four pyrroles and four bridging-methine carbons. Porphyrin possesses a rigid planar structure and it exhibits strong aromaticity due to the 18π-electron system according with Hückel's [4n+2]π rule. Generally, the conformation of porphyrin shows two *trans*-state tautomers because it is more stable than *cis*-state isomer. In addition, the NH-tautomerism between two *trans*-isomers has been observed by NMR spectroscopy in solution.[2] An absorption spectrum of 5,10,15,20-tetraphenyl-porphyrin (**H₂TPP**) shows one strong band at around 400 nm and four weak bands at around 500–650 nm, which are called as Soret band and Q bands, respectively (Figure 2a). In the 1960s, Gouterman and co-workers explained assignment of Soret and Q bands of porphyrins as Gouterman's four orbital model.[3] Molecular orbitals of porphyrins degenerate HOMO–1/HOMO ($M_L = \pm4$), and LUMO/LUMO+1 ($M_L = \pm5$), where M_L is the magnetic quantum number. According to Gouterman's four orbital model, spin-allowed electronic

transitions with $\Delta M_L = \pm 1$ and ± 9 were assigned allowed and forbidden Soret and Q bands, respectively (Figure 2b).
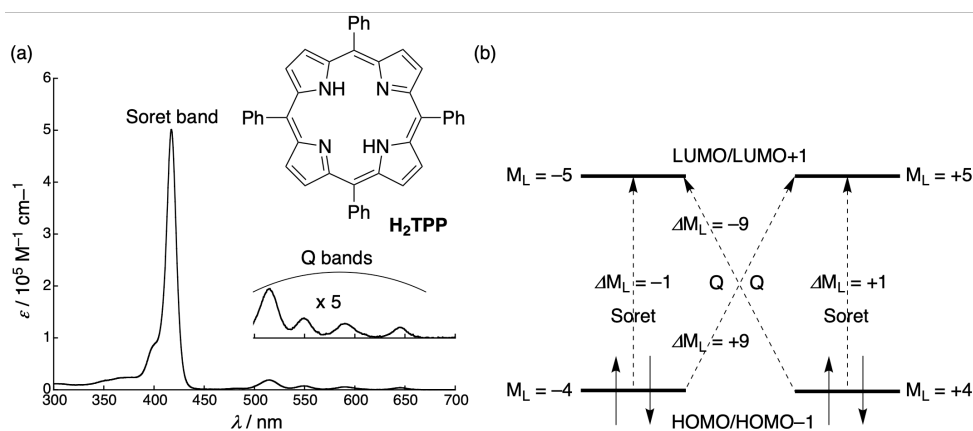
Figure 2. (a) UV-Vis absorption spectrum of **H₂TPP** in CH_2Cl_2 and (b) Gouterman's four orbital model.

The inner cavity surrounded by four nitrogen atoms can accommodate a metal ion to form a wide variety of stable metal complexes called as ''metalloporphyrin'' with alternation of the electronic properties as well as the stereochemical properties. Metalloporphyrins have highly symmetrical D_{4h} (free-base porphyrin: D_{2h}) owing to collapsing their tautomerisms. In contrast to free-base porphyrins, UV/Vis absorption spectra of metalloporphyrins exhibit one Soret band and two weak Q bands because of their highly symmetrical structures. Generally, the fluorescence intensity for metalloporphyrins is significantly weaker than that for free-base porphyrins due to heavy-atom effect of their metal ions. For instance, nickel porphyrins show no fluorescence because of their very short excited states lifetime within a few hundred picosecond order.[4] On the other hand, zinc porphyrins exhibit fluorescence, thus zinc porphyrins have been used as photofunctional molecules in various fields including artificial photosynthesis.

Synthesis of *meso*-Tetrasubstituted Porphyrins

Porphyrins can be classified into β-substituted porphyrins and *meso*-substituted porphyrins (Figure 3). β-Substituted porphyrins are widely found in nature such as chlorophylls or hemes, and their effective synthetic approach has been established by Fisher in the 1930s[5a,5b] and MacDonald in the 1960s.[5c] While *meso*-substituted porphyrins are rarely found in biological or natural pigments, they can be widely applied for functional materials as well as biomimetic models.
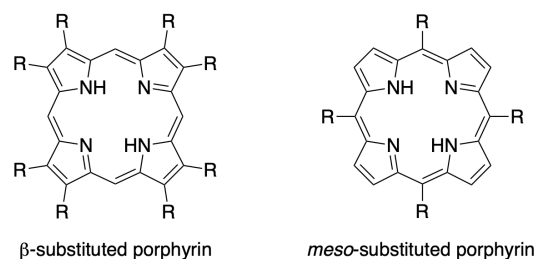
Figure 3. Chemical structures of β-substituted porphyrin and *meso*-substituted porphyrin.

In 1935, the first synthesis of 5,15,15,20-tetramethylporphyrin was successful by Rothemund, who investigated the reaction of pyrrole with gaseous acetaldehyde in methanol (Scheme 1a). The reaction proceeded at room temperature for several weeks, under reflux for 15–25h or at 85–90 ℃ in a sealed tube for 10–12h. Furthermore, reaction yields increased adding pyridine to the reaction mixture.[6] Rothemund was also successful for synthesis of **H₂TPP** in 1941 by the condensation of pyrrole with benzaldehyde in pyridine at 220 ℃ in sealed tubes for 48h.[7] Later, Alder, Longo and co-workers reported the modified Rothemund's condition, in which the reactions of pyrrole with aldehyde in acidic solvents (e.g., acetic acid, chloroacetic acid, or trifluoroacetic acid) in the presence of a metal salt under aerobic condition in refluxing for 30 min afforded *meso*-tetra-substituted porphyrins (Scheme 1b).[8] In the 1980s, Lindsey and co-workers established an effective synthetic methodology for *meso*-tetrasubstituted porphyrins under mild conditions (Scheme 1c).[9] This approach is a two-step one-pot synthesis. In the first step, a solution of pyrrole and aldehyde in chloroform or dichloromethane is treated with trifluoroacetic acid (TFA) or boron trifluoride etherate (BF₃·OEt₂) at room temperature to form porphyrinogens. In the second step, porphyrinogens are oxidized by using a stoichiometric amount of 2,3-dichloro-5,6-dicyano-*p*-benzoquinone (DDQ), *p*-chloranil or aqueous hydrogen peroxide in acetic acid[10] to afford *meso*-substituted porphyrins in moderate yields.
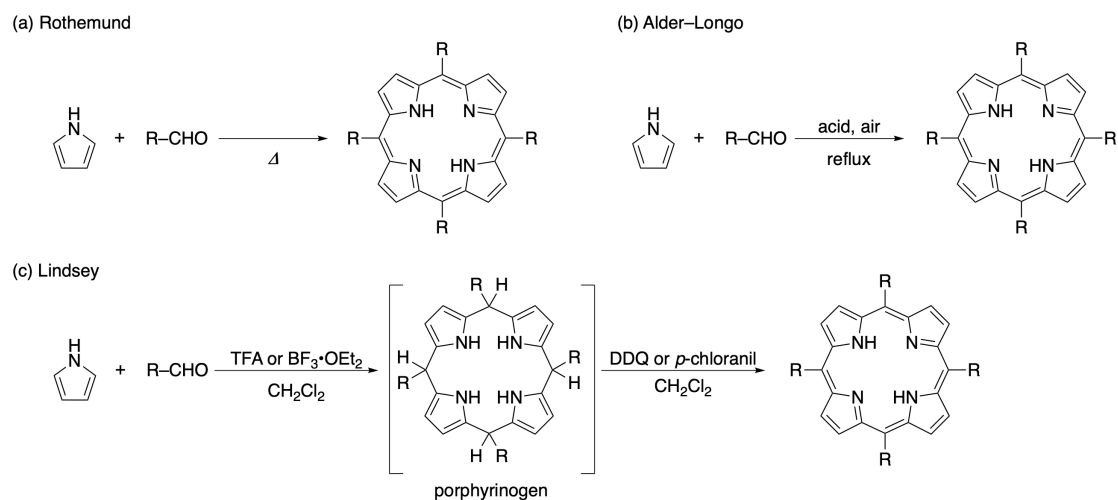
Scheme 1. Typical approaches for synthesis of 5,10,15,20-substituted porphyrins.

Selective Synthesis of *meso*-Free Porphyrins

5,10,15,20-Tetrasubstituted porphyrins (A_4) such as **H₂TPP** have attracted attention to investigate general properties of porphyrins and to construct three-dimensional architectures. However, it is difficult to modulate the structure and properties of tetrasubstituted porphyrins (A_4) because they have no free *meso*-positions for further chemical modifications. Therefore, it is necessary to develop selective synthetic strategies toward partially *meso*-free porphyrins including 5-substituted porphyrin (A_1), 5,15-substituted porphyrin (*trans*A_2), 5,10-substituted porphyrin (*cis*A_2) and 5,10,15-substituted porphyrin (A_3) for realizing porphyrin-based functional materials (Figure 4). Additionally, the number of substitutions (0 to 4) and structural symmetry (*trans*A_2 or *cis*A_2) in porphyrins give perturbation to their electronic properties.[11]
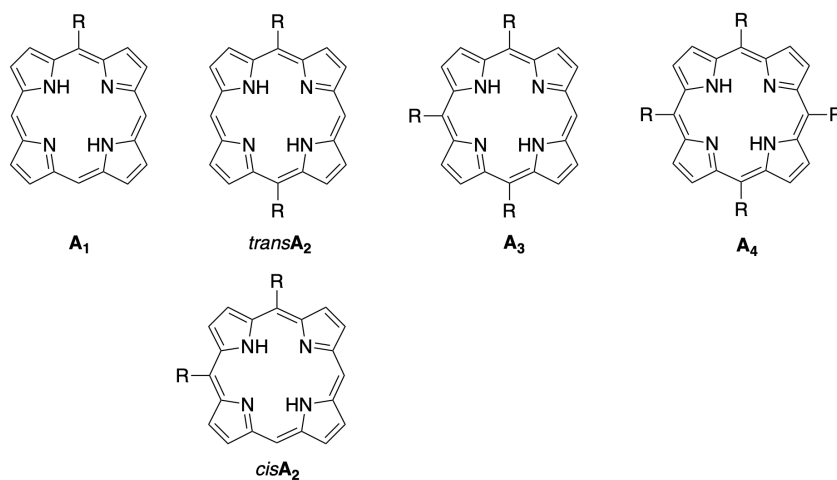
Figure 4. Chemical structures of *meso*-substituted porphyrins.

Senge and co-workers established a synthetic protocol toward A_1-type porphyrins using 2+2+1 condensation of pyrrole-2-carbaldehyde or hydroxymethylpyrrole, aldehyde, and dipyrromethane to afford A_1-type porphyrins in 2–12% yield (Scheme 2a).[12] However, this protocol gives *trans*A_2-type porphyrins as a byproduct due to occurring acid scrambling. Lindsey and co-workers succeeded in the synthesis of 5-arylsubstituted porphyrin zinc complex via 2+2 condensation of *meso*-free dipyrromethane and 1,9-bis(N,N-dimethylaminomethyl)-dipyrromethane in moderate yield (ca. 30%) without scrambling (Scheme 2b).[13]
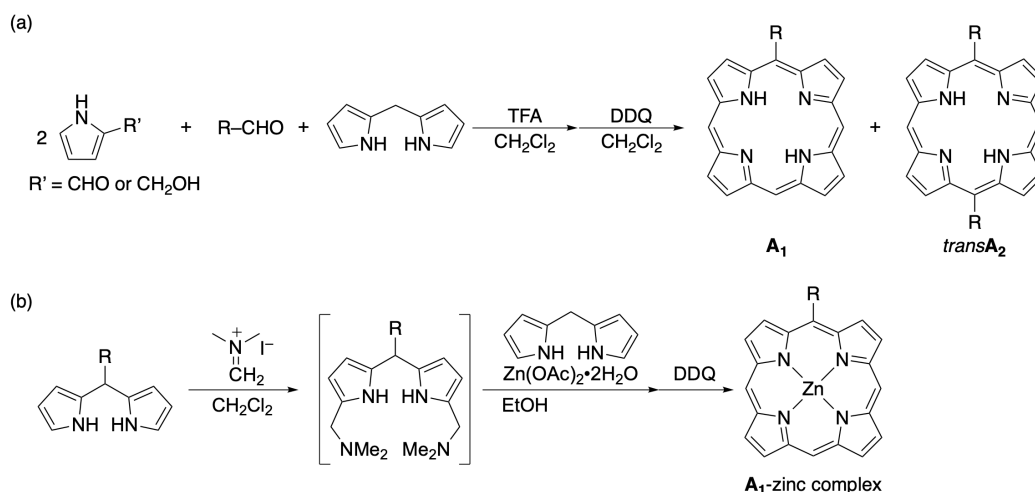
Scheme 2. Synthetic approaches toward 5-substituted porphyrins (A_1).

5,15-Substituted porphyrin (*trans*A_2) was first reported in 1968 by Treibs, Häberle and co-workers, who synthesized 5,15-diphenylporphyrin from benzaldehyde and dipyrromethane in low yield (3%).[14] *trans*A_2-Type porphyrins have drawn significant interest because they are key building blocks for models of light-harvesting antenna systems and non-linear optical materials. Lawrence and co-workers established synthetic approach for symmetrical *trans*A_2-type porphyrins in high yield 73–92%, which is the 2+2 condensation reaction of dipyrromethane with aldehyde in the presence of trifluoroacetic acid (TFA) (Scheme 3).[15] Later, Dolphin and co-workers developed reliable method of synthesis of 5,15-diphenylporphyrin because the reaction under the Lawrence's conditions was difficult to reproduce in their hands. They mentioned that separating excess amount of chloranil from product is very important process to produce pure product (25–40%) because the purification by column chromatography alone using CH_2Cl_2 is insufficient to be similar R_f-values on their TLC analysis.[16] Also, Dolphin and co-workers devised many synthetic methods to afford *trans*A_2-type porphyrins.
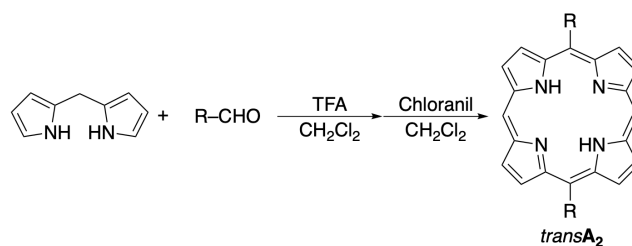
Scheme 3. Synthetic approach for 5,15-arylsubstituted porphyrins (*trans*A_2).

Senge and co-workers developed effective synthetic methodologies for *cis*A_2-type porphyrins, which are 3+1 cyclization reaction using 1:1:2 molar ratio of tripyrrane, pyrrole, and aldehyde (Scheme 4). Both of aryl and aliphatic aldehydes except pivaldehyde can be used in this protocol. Although disubstituted *cis*A_2-type porphyrins were obtained in 11–4% yield, mono-substituted A_1-type porphyrins were also generated as a byproduct.[12b]
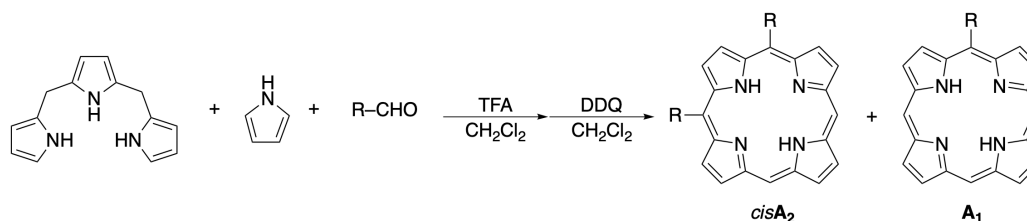
Scheme 4. Synthetic approach for 5,10-arylsubstituted porphyrins (*cis*A_2).

In 1998, Osuka and co-workers synthesized A_3-type porphyrins by cross condensation of *meso*-substituted dipyrromethane, *meso*-free dipyrromethane, with aldehyde in the presence of trifluoroacetic acid.[17] At the same time, Shultz and co-workers also prepared A_3-type porphyrins using boron trifluoride etherate instead of trifluoroacetic acid (Scheme 5).[18]
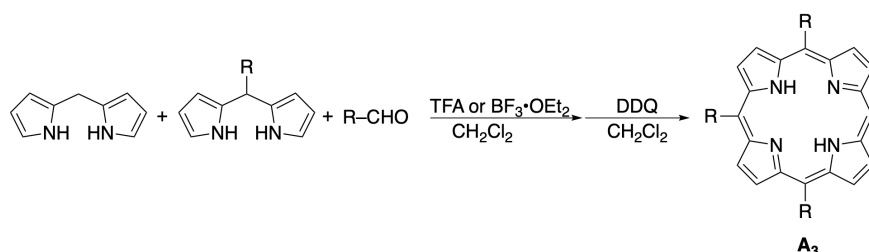
Scheme 5. Synthetic approach for 5,10,15-arylsubstituted porphyrins (A_3).

In contrast to the selective synthesis *via* acid-catalyzed condensation reactions, the reaction of *meso*-free porphyrins with organolithium reagents provided an alternative strategy for functionalization of *meso*-position after the construction of porphyrin macrocycles. Senge and co-workers reported that the treatment of *meso*-free porphyrins with organolithium reagents (RLi) and subsequent oxidation with DDQ gave A_1-type (40–70%) or *cis*A_2-type (50–70%)

porphyrins (Scheme 6).[12b, 19] Funasaki, Neya and co-workers presented that porphine (porphyrins without any substituents) can be prepared from *meso*-tetra-*tert*-butyl substituted porphyrin with sulfuric acid.[20]
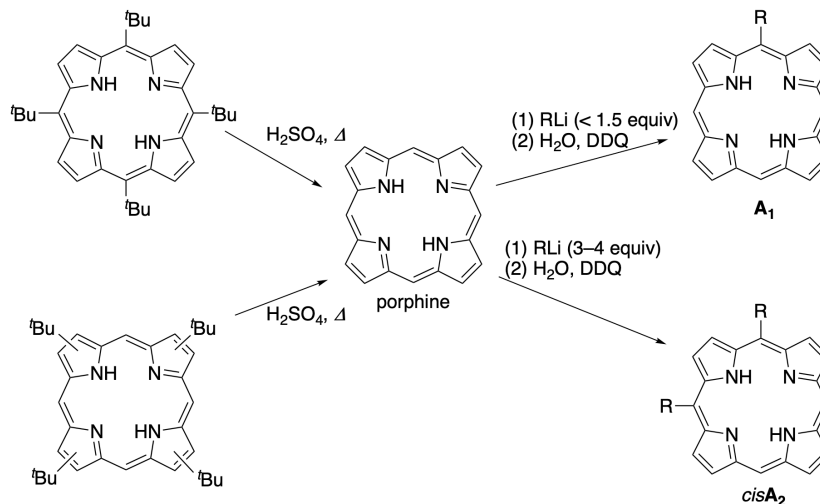
Scheme 6. Synthetic approach for **A₁-** and *cis***A₂**-type porphyrins using organolithium reagents.

Thus, the development of various kinds of *meso*-free porphyrins enables us to synthesize well-designed porphyrins for key building blocks in biomimetic systems and novel functional materials.

Functionalization of Porphyrins at Peripheral Positions

Halogenated porphyrins have attracted attention as key precursors in materials chemistry because they can incorporate main group elements as well as hydrocarbon-based substituents using cross-coupling reactions at their peripheral positions to modulate their properties (Figure 5).[21] For instance, introducing alkyl or aryl groups to porphyrins at their peripheral positions using palladium-catalyzed coupling reactions such as Suzuki, Stille, Negishi, and Kumada coupling reactions. π-Extended porphyrins with vinylene or ethynylene linkages have been synthesized by Heck or Sonogashira coupling reactions. In addition, introduction of carbon–heteroatom (N, S, P, B, and Si) bonds at peripheral positions is also possible by using palladium-catalyzed coupling reactions or organometallic species generated by halogen-metal exchange reactions.
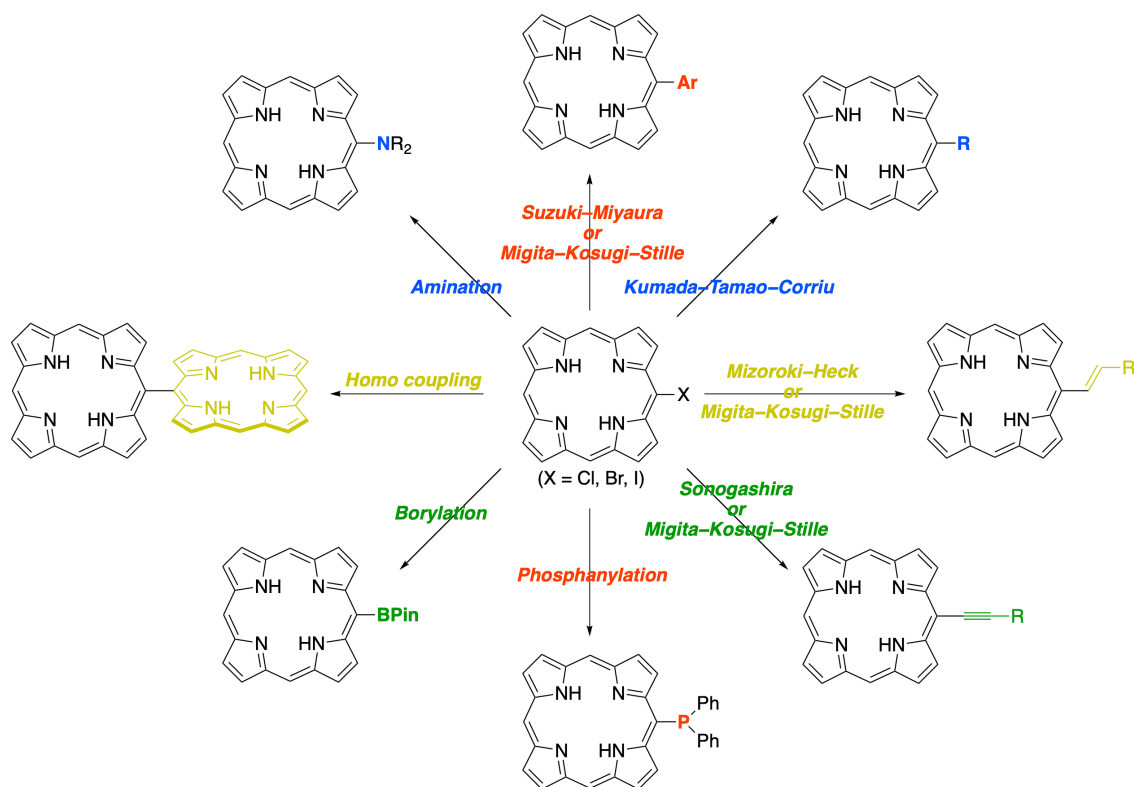
Figure 5. Functionalization of porphyrins at peripheral positions from halogenated porphyrins.

In general, *meso*-halogenated porphyrins can be easily prepared in comparison with β-halogenated porphyrins because the reactivity at *meso*-positions is higher than at β positions. Therien and co-workers reported selective bromination of porphyrin at *meso*-positions by the reaction of 5,15-diphenylporphyrin with N-bromosuccinimide (NBS) in the presence of pyridine, affording *meso*-dibromoporphyrins in high yield (Scheme 7a).[22] The bromination with NBS can be carried out for metalloporphyins, but the reactivity at *meso*-positions depends on the metal ions. Actually, brominations for *meso*-substituted porphyrins sometimes lead to low selectivity depending on substituents or a metal ion. For example, direct bromination of 5,15-dialkynyl substituted free-base or zinc porphyrins was unsatisfactory, with significant amounts of reaction at the β-positions and on the alkynes.[23] This problem can be overcome by using magnesium porphyrins, providing *meso*-brominated porphyrins without brominations at β positions.[24] Moreover, chlorination of porphyrins at the *meso*-position was reported by Chen and co-workers using PhICl$_2$ as a halogen source (Scheme 7b).[25] For zinc porphyrins, yields of *meso*-chloro zinc porphyrins are lower than those of copper and nickel derivatives due to formation of *meso-meso* directly linked porphyrin dimer as a byproduct. Dolphin and co-workers, and Osuka and co-workers synthesized *meso*-iodoporphyrin using

[bis(trifluoroacetoxy)iodo]benzene (PIFA) and iodine[26], and AgPF$_6$ and iodine[27], respectively (Scheme 7c). In addition, these mono- and di- halogenated porphyrins are easily separated by silica gel column chromatography.
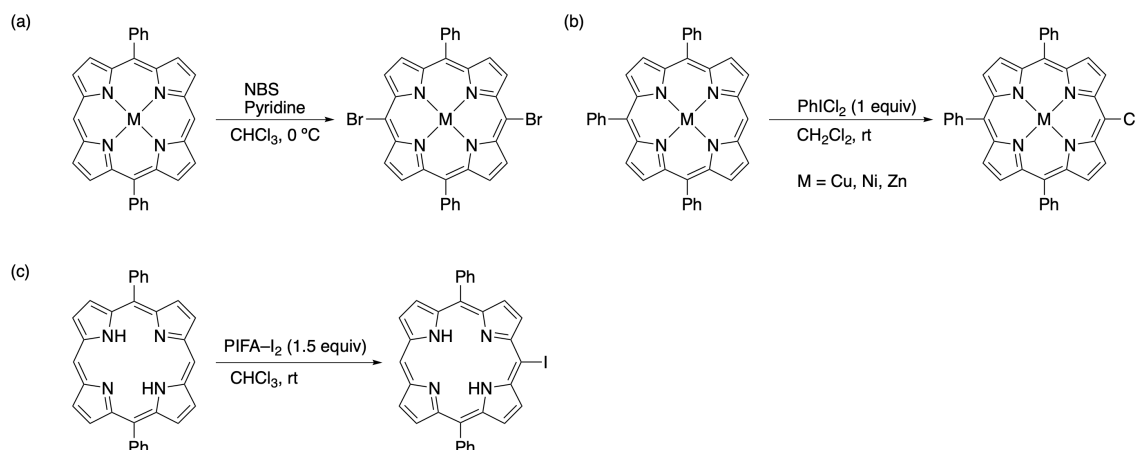
Scheme 7. Examples of synthesis of *meso*-halogenated porphyrins.

While the synthetic approaches of *meso*-halogenated porphyrins have been established so far, the development of synthetic methodologies for β-selective functionalization has been still rare except **A$_4$**-type porphyrins.[28] Although there are a few reports on the β-selective halogenations[29], they cannot be applied to the synthesis of β-halogenated *meso*-free porphyrins. Osuka, Shinokubo and co-workers reported regioselective borylation at β-positions without *meso*-borylations by iridium-catalyzed direct borylation using bis(pinacolato)diboron, 4,4′-di(*tert*-butyl)-2,2′-bipyridyl and [Ir(OMe)(cod)]$_2$ (Scheme 8).[30] The β-borylporphyrins can be converted to various β-functionalized porphyrins using transition metal-catalyzed coupling reactions. Furthermore, Osuka and co-workers presented that β-borylporphyrins can be transformed to β-halogenated porphyrins using N-halosuccinimide (NXS) and copper (I) halide (CuX) in 2:1 mixture of DMF and toluene under air (Scheme 8).[31]
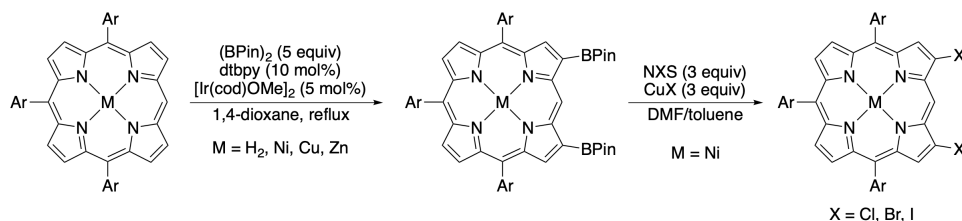
Scheme 8. Synthesis of β-halogenated porphyrins.

π-Extended Porphyrins with Main Group Elements

π-Extended porphyrins exhibit significantly altered their electronic structures by introduction of π-systems at their peripheral positions. Hence, π-extended porphyrins reveal red-shifted absorption and fluorescence spectra, multiple redox and oxidation potentials, and unique structural properties in comparison with those of typical porphyrins. Incorporation of main group elements to π-conjugated molecules is extremely important for development in materials science because of their unique optical and electrochemical properties derived from heteroatoms as well as high stabilities of their compounds. Therefore, porphyrins with main group elements have attracted attention because of their unique optical and electrochemical properties derived effective interaction between porphyrins and main group elements.

Linked Porphyrin Oligomers

Covalently linked porphyrin oligomers[32] have drawn much attention because of their potential applications in molecular electronics,[33] nonlinear optical materials,[34] photovoltaics,[35] and artificial photosynthetic systems (Figure 6).[36] In 1996, Segawa and co-workers synthesized first example of *meso-meso* directly linked oligomers as low yield (dimer: 4%; trimer: 0.5%).[37] Their structures show orthogonal geometries between each porphyrin and their absorption spectra exhibit split Soret band and red-shifted Q bands, implying strong electronic interaction between porphyrins at excited states. Osuka and co-workers investigated effective method for oxidative coupling using $AgPF_6$ to obtain *meso-meso* directly linked porphyrin oligomers as moderated yields (dimer: 25%; trimer: 4%).[38] Later, Chen and co-workers synthesized *meso-meso* directly linked porphyrin dimers by oxidation coupling using PIFA in high yield.[39]

In 1978, Arnold, Johnson and co-workers synthesized 1,3-butadiyne-linked porphyrin dimer by oxidative coupling using $Cu(OAc)_2$ from *meso*-ethynylporphyrin as a first example of ethyne-linked porphyrin oligomers.[40] In the 1990s, Arnold and co-workers investigated their optical and electrochemical properties and demonstrated the strong electronic communication between porphyrins.[41] Anderson and co-workers synthesized 1,3-butadiyne-linked porphyrin oligomers (N = 2–6) by the Glaser–Hay coupling using CuCl·TMEDA under aerobic conditions, and isolated them by silica gel column chromatography and evaluated their optical properties.[42] Therien and co-workers synthesized a series of *meso*-to-*meso* and β-to-β ethyne-linked porphyrin oligomers by the metal-mediated cross-coupling methodologies. The

ethyne-linked porphyrin oligomers exhibit significantly red-shifted and broadened absorption spectra in comparison to the corresponding porphyrin monomers.[43] In addition, *meso*-to-*meso* ethyne-linked derivatives reveal considerably split Soret bands and red-shifted absorption spectra compared with β-to-β-linked derivatives, which suggests that introducing ethyne linkers at *meso*-positions realizes stronger electronic communications between porphyrins through ethyne moieties than those at β-positions.
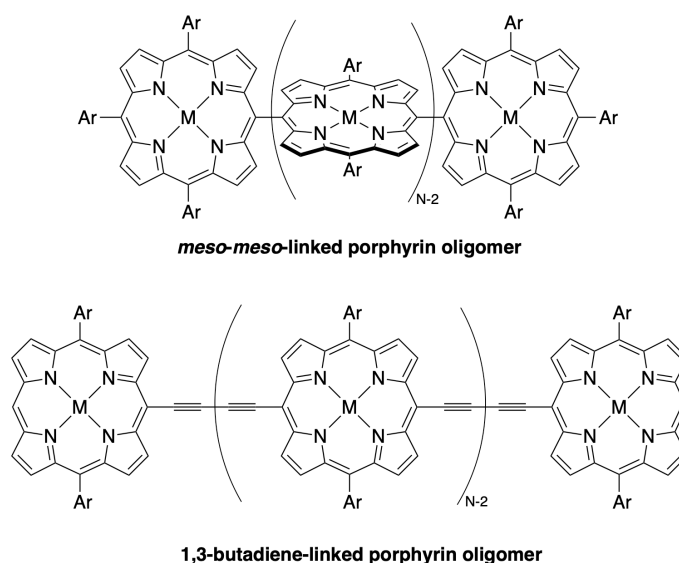
Figure 6. Representative examples of linked porphyrin oligomers.

   Porphyrin oligomers with main group elements have been reported so far (Figure 7). Anderson and co-workers synthesized imino-linked porphyrin dimer **1** in 2002.[44] Later, Arnold and co-workers prepared azo-linked porphyrin dimer **2**, which exhibits strong electronic coupling between porphyrins through azo linker than those of ethane- and ethyne-linked porphyrin dimers.[45] Amino-linked porphyrin dimer **3** was synthesized by Arnold and co-workers in 2006.[46] Later, Ruppert and co-workers reported *meso*-to-β and β-to-β amino-linked porphyrin dimers as well as *meso*-to-*meso* dimer **3**, which reveal broadened and split Soret band.[47] The aminium radical cation of **3** was prepared by chemical oxidation and the carbocation was delocalized over the two porphyrins, showing absorption peaks at 1120 nm. Senge and co-workers synthesized sulfur-linked porphyrin dimers **4** from *meso* 2-ethylhexyl-3-mercaptopropionate substituted porphyrins.[48] Osuka and co-workers prepared β-to-β disilane-linked porphyrin dimers **5**, **6** by silylation at β-positions.[49]
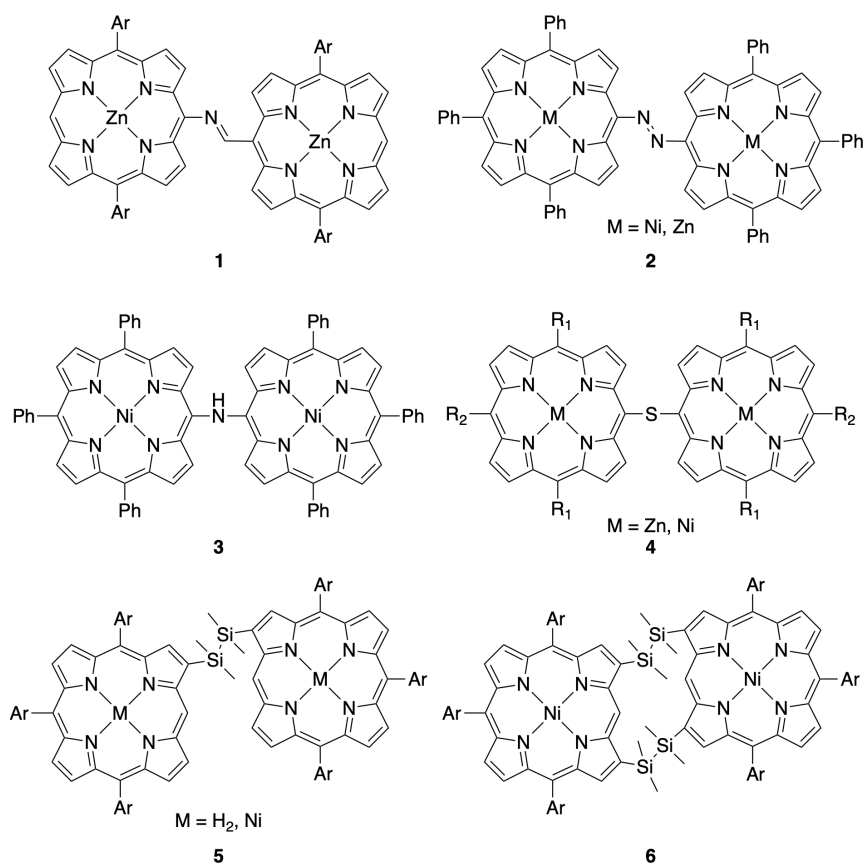
Figure 7. Examples of linked porphyrin dimers with main group elements.

In addition, heterocycle-linked porphyrin oligomers have been synthesized (Figure 8). Arnold and co-workers synthesized *meso*-to-*meso* furan-linked porphyrin dimer **7** by the reaction of 1,3-butadiyne-linked porphyrin dimer with sulfuric acid.[50] *Meso*-to-*meso* furan-linked porphyrin dimer **7** shows broadened Soret and Q bands, which are similar to those of *p*-phenylene-linked porphyrin dimers. Osuka and co-workers prepared β-to-β doubly thiophene-linked porphyrin dimers **8**, which exhibit large two-photon absorption cross sections because of their coplanar structure between porphyrins.[51] Osuka and co-workers reported *meso*-to-*meso* pyrrole-linked porphyrin dimer **9**, which reveals split Soret bands, indicating effective electronic interaction two porphyrins.[52] Osuka and co-workers synthesized β-to-β doubly 2,6-pyridylene-linked porphyrin dimer Pd(II)-complex **10**, in which the Pd(II) ion coordinates with two *meso*-carbon and pyridyl nitrogen atoms. Pd(II)-complex **10** possesses bent structures and exhibits large a two-photon absorption cross section value at 800 nm.[53]
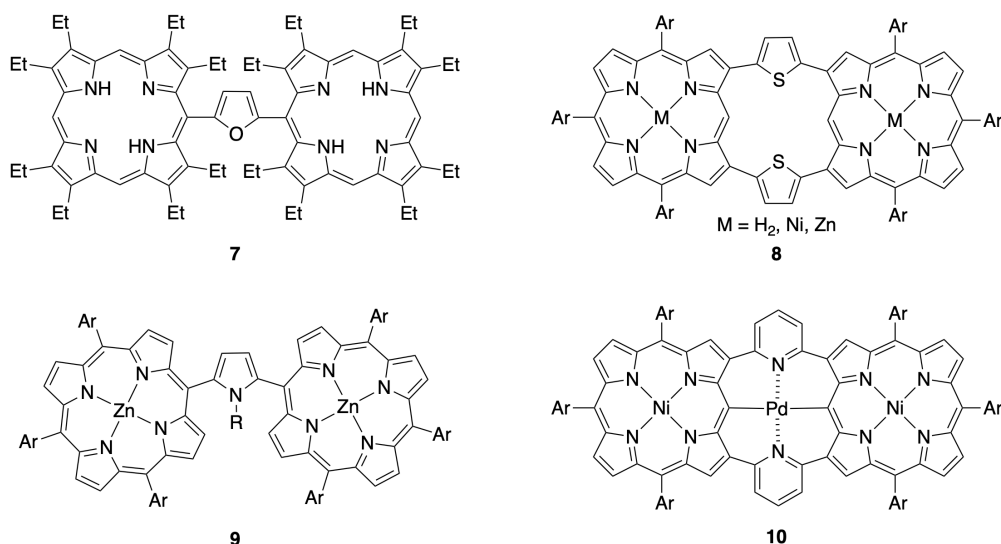
Figure 8. Examples of linked porphyrins with heterocycles.

Fused Porphyrins

Incorporation of aromatic-fused structures into porphyrins gives large perturbation to structural properties and physicochemical properties of porphyrins. Representative examples of fused porphyrin oligomers are *meso-meso*, β-β triply linked porphyrin arrays[54] such as porphyrin tapes prepared by Osuka and co-workers and pyrazinoquinoxaline-fused porphyrin oligomers[55] reported by Crossley and co-workers (Figure 9). Their fused oligomers exhibit extremely red-shifted absorption spectra and small HOMO–LUMO gaps increasing the number of porphyrin units, indicating effective π-conjugation through the whole molecule due to their highly planar structures.

porphyrin tape

pyrazinoquinoxaline-fused porphyrin oligomer
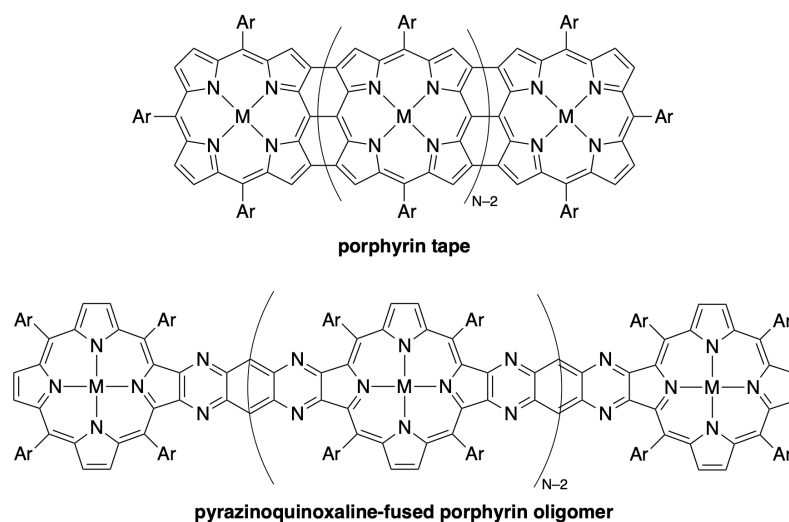
Figure 9. Examples of fused porphyrin oligomers.

In recent years, heterole-fused porphyrins including main group elements have attracted attention due to their unique optical and electrochemical properties owing to effective π-conjugation between porphyrin and heterole moieties. For example, porphyrins with thiophene-fused structures have been synthesized so far (Figure 10). The first examples of benzothiophene-fused porphyrin **11** was synthesized by Ogawa and co-workers in 1996.[56] Crossley and co-workers reported thiophene-fused porphyrin through pyrazine units **12** in 1997.[57] Matsuo and co-workers synthesized thiophene-fused porphyrin with a five-membered ring **13**, in which the overall aromaticity can be modulated by the direction of fused thiophene ring.[58] In 2015, Li and co-workers prepared porphyrin with thiophene-fused structure **14** by the aromatization of tetrahydrothiophene-fused porphyrin.[59] Osuka and co-workers prepared thiophene-fused porphyrins with a phosphorus atom **15** in 2017.[60] In 2019, Imahori and

co-workers synthesized methylene-bridged thiophene-fused porphyrin **16** as a high performance
sensitizers in dye-sensitized solar cells.[61]
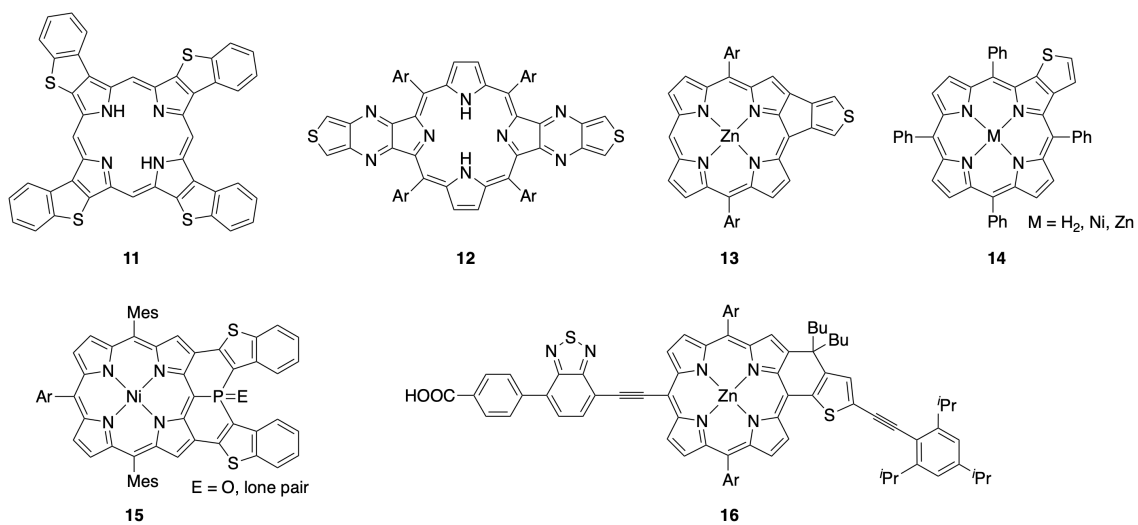
Figure 10. Examples of porphyrins with thiophene-fused structures.

Recently, indole-fused porphyrins have been reported as nitrogen-incorporated fused porphyrins. Cavaleiro and co-workers prepared indole-fused porphyrin **18** by the reaction of β-aminoporphyrin **17** with 1,4-benzoquinone in the presence of catalytic amount of H_2SO_4 (Scheme 9a).[62] Gryko and co-workers synthesized indole-fused porphyrin **20** by intramolecular oxidative coupling (Scheme 9b).[63a] On the other hands, *trans***A**$_2$-type of indole-fused porphyrin **22** cannot be obtained from doubly indole-linked porphyrin **21** due to the decomposition under a reaction condition (Scheme 9c).[63b] However, the electronic properties of these indole-fused porphyrins have not been fully investigated so far.
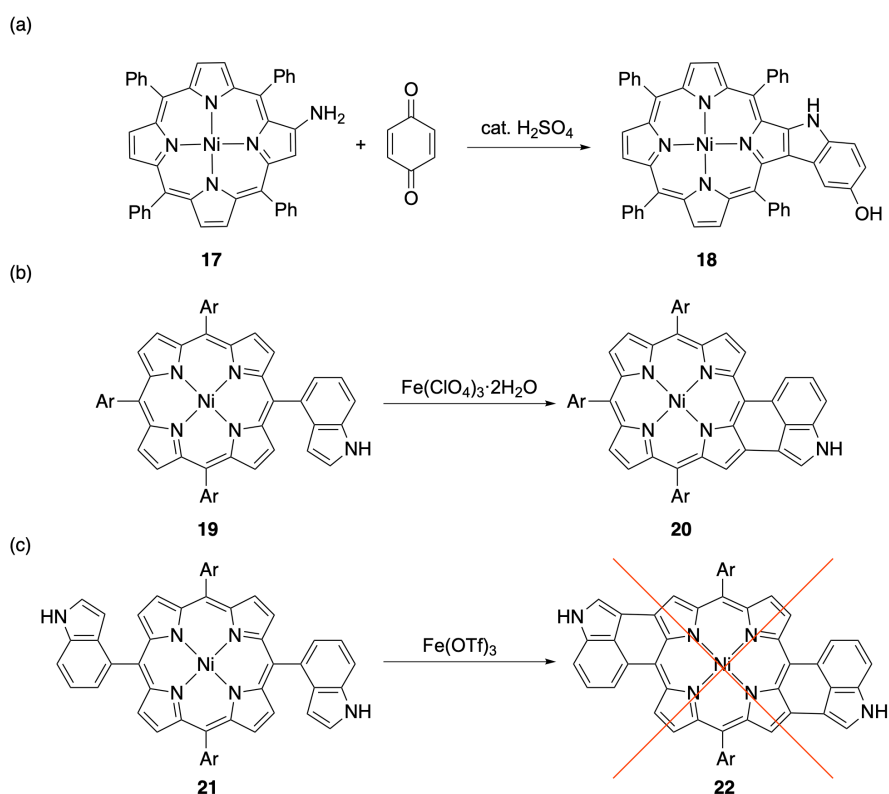
Scheme 9. Synthesis of indole-fused porphyrins.

In contrast to a variety of thiophene-fused porphyrins, phosphole- and silole-fused porphyrins are still rare due to their synthetic difficulties. Imahori and co-workers prepared phosphole-fused porphyrin dimer **25** by acid-catalyzed condensation of bis(pyrrolo)phosphole **23** and tripyrrane dicarbinol **24** in low yield (0.7%) (Scheme 10a).[64] Phosphole-fused porphyrin dimer **25** exhibits effective π-conjugation between two porphyrins through central phosphole unit, indicating broadened and red-shifted absorption and low reduction potential, which reflects the electron-accepting character of phosphole. Silole-fused porphyrin **27** was prepared by Osuka and co-workers using intramolecular sila-Friedel–Crafts reaction of **26** (Scheme 10b).[65] Silole-fused porphyrins indicate slightly negative-shifted first redox potential in comparison with the reference porphyrins.
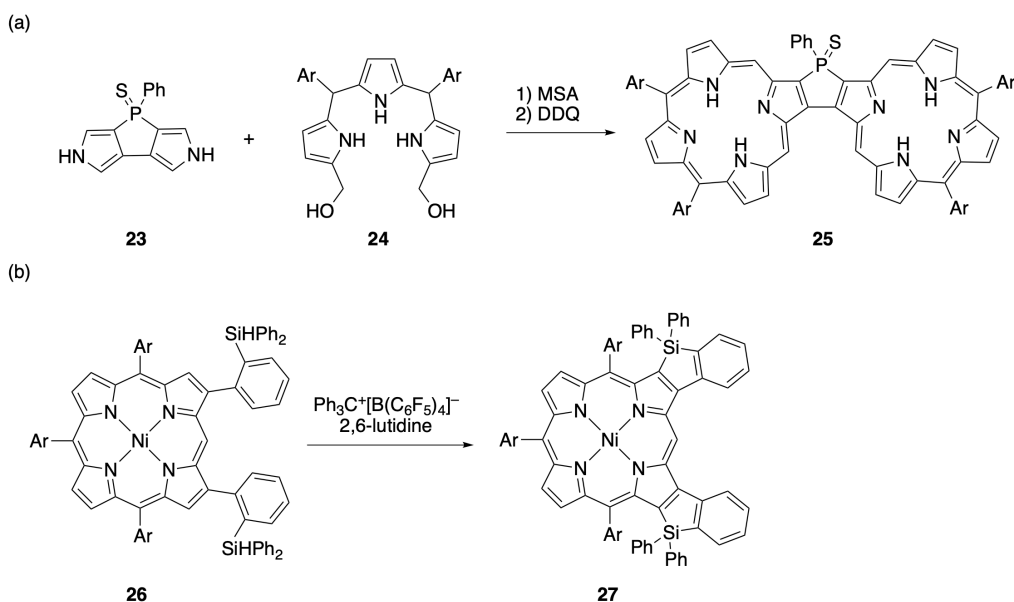
Scheme 10. Synthesis of (a) phosphole-fused porphyrin dimer **25** and (b) benzosilole-fused porphyrin **27**.

Overview of This Thesis

π-Extended porphyrins with heterole structure have been still limited in spite of their unique optical and electrochemical properties because of their synthetic difficulties. In this context, the author established the synthetic approach to construct heterole-linked or -fused structures in porphyrins and evaluated their structural, optical and electrochemical properties.

In Chapter 1, *meso*-to-*meso* or β-to-β phosphole-bridged porphyrin dimers were reported as the first example of phosphole-linked porphyrin oligomers. Their optical and electrochemical properties were discussed in comparison with thiophene- and phenylene-linked porphyrin dimers.

In Chapter 2, the synthesis of a series of phosphole-fused porphyrins by [2+2+1] intramolecular cyclization reaction via titanium intermediates were described. Their optical and electrochemical properties were found to be modulated by the oxidation states of the phosphorus centers.

In Chapter 3, the synthesis and properties of pyrrole-fused porphyrins were reported. Effects of heteroatoms on the whole aromaticity and electronic properties were investigated in comparison with phosphole-fused porphyrins in Chapter 2.

In Chapter 4, thiophene-fused helical porphyrin dimers were presented as the rare examples of helical porphyrins. Their unique structural and electronic properties were discussed.

Chapter 1. Synthesis and Properties of Phosphole-bridged Porphyrin Dimers
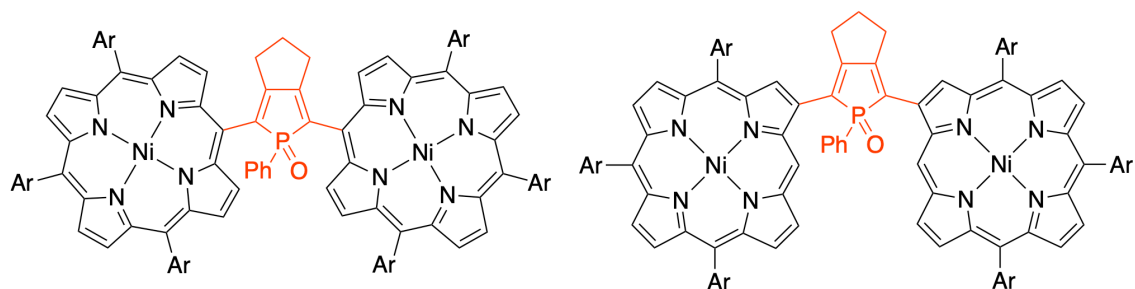
Contents

1-1. Introduction

As described in general introduction, covalently linked porphyrin oligomers[32] have attracted attention because of their potential various applications in novel functional materials as well as biometric systems.[33–36] The electronic perturbations in the oligomers depend on the linker. For instance, 1,3-butadiyne-bridged porphyrin oligomers exhibit unique optical and electrochemical properties that result from their effective π-conjugation.[41b,66,67] On the other hand, aromatic linkers in the oligomers show different effects. Although *p*-phenylene linkers are widely used to construct various porphyrin oligomers, the π-conjugation is often disturbed by their large torsion angles.[68] In contrast, π-conjugation through thienylene linkers is more effective because of their small torsion angles.[69] Meanwhile, π-conjugated phospholes have also attracted interest due to their characteristic properties such as high electron-accepting ability.[70] In particular, phospholes with π-conjugated moieties at 2,5-positions have been studied because of their synthetic accessibilities and effective interactions between the phosphole and π-conjugated moieties. However, phosphole-containing porphyrins are still rare. In this context, we aimed to evaluate the effect of phospholes on the optical and electrochemical properties of phosphole-bridged porphyrin dimers. Considering that 2,5-diarylphospholes possess smaller HOMO–LUMO gaps than those of the corresponding 2,5-diarylthiophenes due to effective π-conjugation through the phosphole linker,[71] we expected an effective π-conjugation through the phosphole linker in phosphole-bridged porphyrin dimers. Herein, we report the synthesis of phosphole-bridged porphyrin dimers *meso*-**28** and β-**28** (Figure 1-1). As far as we know, these are the first examples of covalently linked porphyrin dimers with a phosphole linker. We also assessed the optical and electrochemical properties of thienylene- and *p*-phenylene-bridged porphyrin dimers *meso*-**29**, β-**29** and *meso*-**30**, β-**30** as references (Figure 1-1).
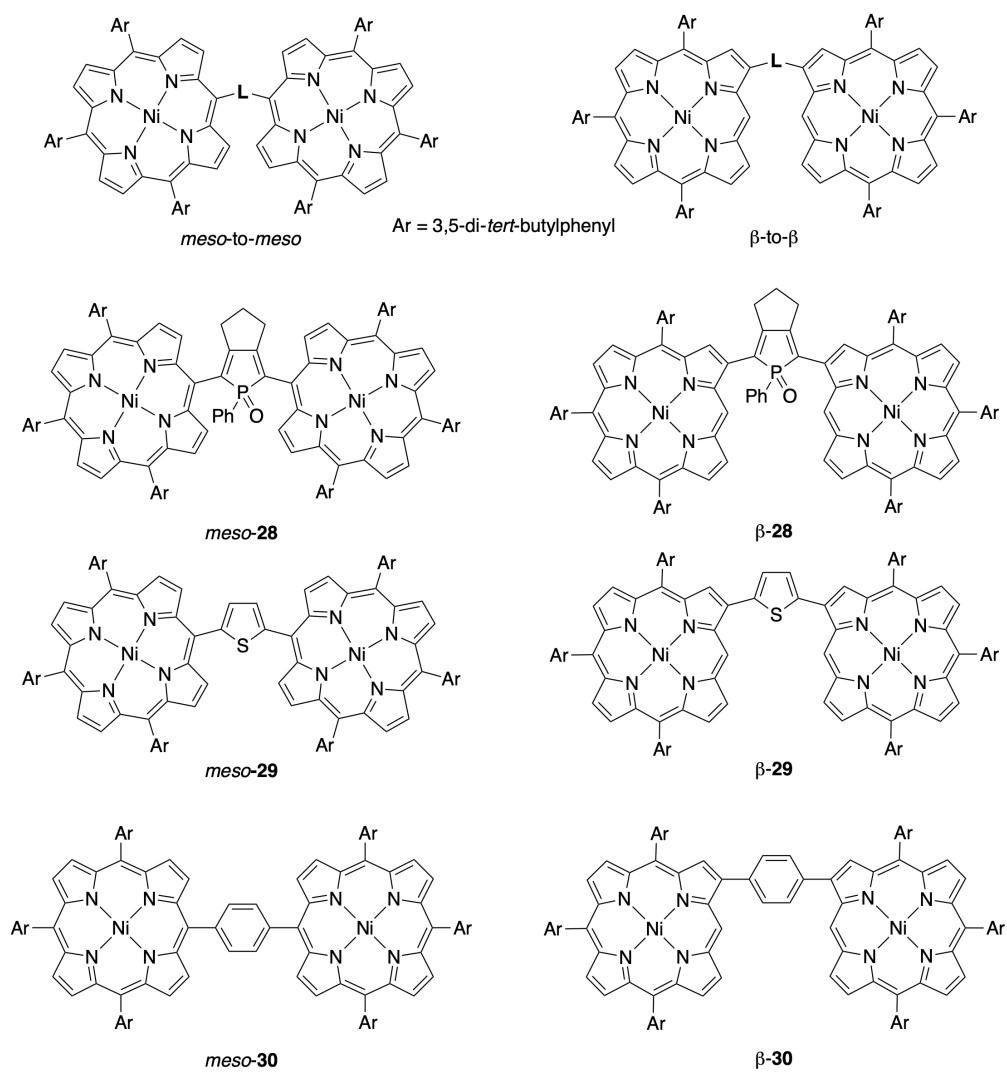
Figure 1-1. Molecular structures of covalently linked porphyrin dimers.

1-2. Synthesis

Synthetic schemes of phosphole-bridged porphyrin dimers are shown in Scheme 1-1. The Stille coupling of nickel bromoporphyrins **31** and **33**[31] with bis(tributylstannyl)-phosphole **32**[72] in the presence of Pd(PPh$_3$)$_4$ (30 mol%), CuI (60 mol%), and CsF (4 equiv) afforded the porphyrin dimers *meso*-**28** and, β-**28** in 41% and 10% yield, respectively (Scheme 1-1a,b). It is noteworthy that reactions of the corresponding free-base or zinc porphyrins with **32** gave complicated mixtures and no desired product was obtained. We also synthesized the reference thienylene- and *p*-phenylene-bridged porphyrin dimers ***meso*-29**, **30** and ***β*-29**, **30** (Scheme 1-1c,d).

(a)

31

Ar = 3,5-di-*tert*-butylphenyl

32

Pd(PPh₃)₄
CuI, CsF
DMF

meso-**28**

(b)

33

Ar = 3,5-di-*tert*-butylphenyl

32

Pd(PPh₃)₄
CuI, CsF
DMF

β-**28**

(c)

34

Ar = 3,5-di-*tert*-butylphenyl

Pd(PPh₃)₄
CsCO₃
toluene

L =

meso-**29**

meso-**30**

(d)

35

Ar = 3,5-di-*tert*-butylphenyl

Pd(PPh₃)₄
CsCO₃
toluene

L =

β-**29**

β-**30**
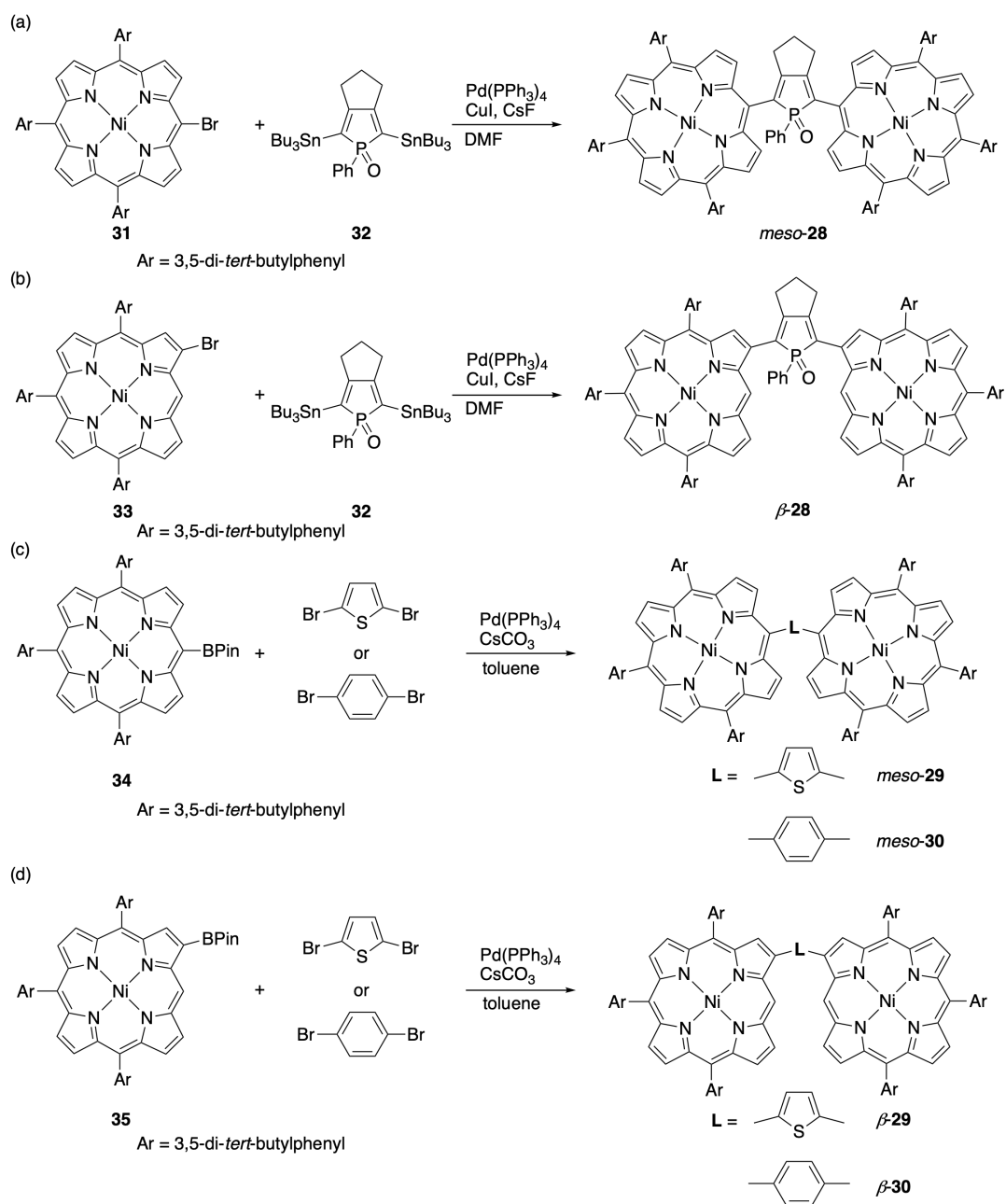
Scheme 1-1. Synthesis of phosphole- and reference thienylene and *p*-phenylene- bridged porphyrin dimers.

1-3. UV/Vis Absorption Spectra

The UV/vis absorption spectra of porphyrin dimers *meso*-**28**–**30**, β-**28**–**30** and a porphyrin monomer [5,10,15-tris(3,5-di-*tert*-butylphenyl)porphyrinato]nickel(II) (**NiP**) were measured in CH$_2$Cl$_2$ (Figure 1-2 and Table 1-1). The *meso*-bridged porphyrin dimers *meso*-**28**–**30** exhibit red-shifted Soret- and Q-bands by 10–20 nm relative to **NiP**. The Soret- and Q-bands of *meso*-**29** are red-shifted in comparison with those of *meso*-**30**. On the other hand, the Soret-band of *meso*-**28** is blue-shifted. Although *meso*-bridged porphyrin dimers often have trivial spectral changes because of their large torsion angles, the broadened Soret-band and red-shifted Q-bands of *meso*-**28** suggest effective electronic interaction between the porphyrins through the phosphole linker. Compared to *meso*-**28**–**30**, β-bridged porphyrin dimers β-**28**–**30** reveal more broadened Soret-bands and red-shifted Q-bands, while the red-shifts of the Soret-bands are smaller. The red-shifted lowest energy Q-bands of β-**28**–**30** indicate effective π-conjugation between the porphyrins owing to smaller dihedral angles, which is attributed the less hindered β-positions. Similar to *meso*-**28**, the broadened Soret-band and red-shifted Q-bands of β-**28** also indicate the effective interaction between the porphyrins and phosphole linker as well as the porphyrins.

Table 1-1. Optical properties of porphyrin dimers and **NiP** in CH$_2$Cl$_2$.

	λ_{abs} / nm (ε [10^4 M^{-1} cm^{-1}])
NiP	409 (24), 521 (1.2), 551 (0.55)
meso-**28**	420 (22), 534 (3.2), 581 (1.0)
meso-**29**	427 (35), 534 (4.1)
meso-**30**	423 (42), 529 (4.2)
β-**28**	414 (13), 530 (2.5), 589 (2.0)
β-**29**	418 (25), 531 (3.9), 576 (3.0)
β-**30**	417 (33), 527 (3.9), 562 (1.8)
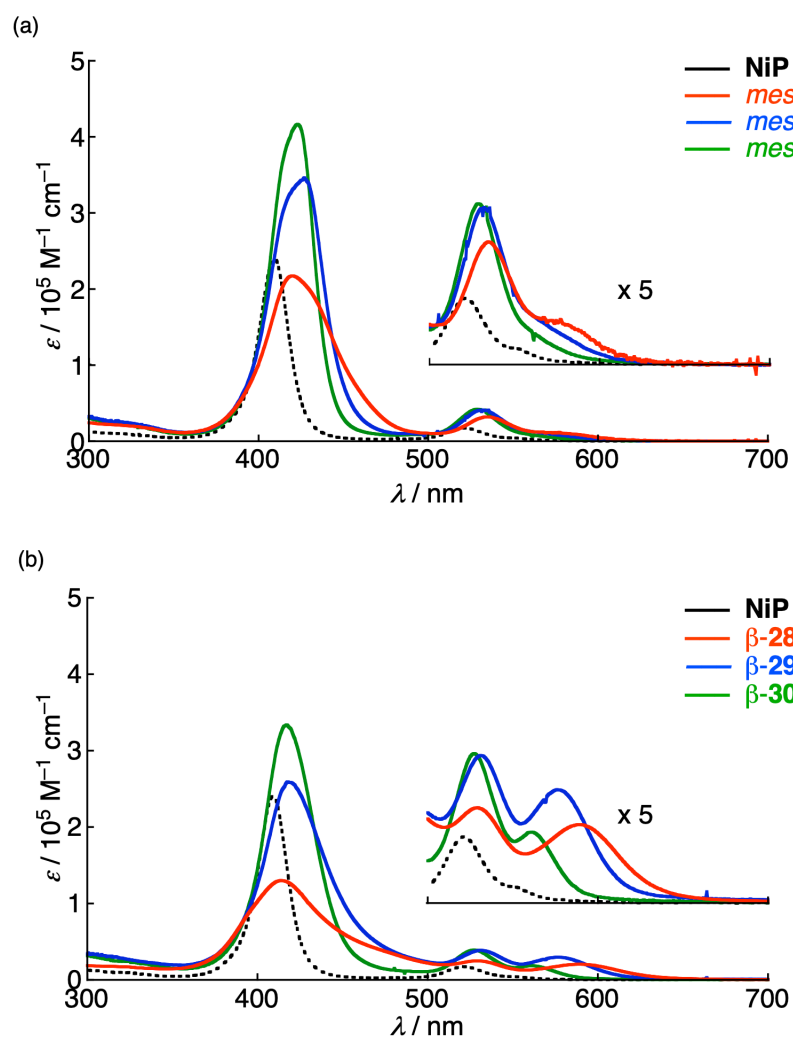
Figure 1-2. UV/Vis absorption spectra of (a) *meso*-bridged dimers (*meso*-**28–30**) and (b) β-bridged dimers (β-**28–30**) and porphyrin monomer **NiP** in CH₂Cl₂.

Chapter 1

1-4. Electrochemical Properties

To evaluate the electrochemical properties of the porphyrin dimers, we conducted cyclic voltammetry (CV) and differential pulse voltammetry (DPV) measurements in CH_2Cl_2 versus ferrocene/ferrocenium ion (Fc/Fc$^+$) with tetrabutylammonium hexafluorophosphate (n-Bu$_4$NPF$_6$) as an electrolyte (Figure 1-3 and 1-4). All the porphyrin dimers show reversible oxidation peaks with largely comparable oxidation potentials (ca. 0.5 V), and no meaningful second oxidation peak appears at potentials up to 1.3 V. Meanwhile, *meso*-**28**–**30** and β-**28**–**30** reveal irreversible and reversible reduction peaks, respectively. The oxidation and reduction potentials of β-**28**–**30** are slightly shifted to a positive direction than those of the corresponding *meso*-**28**–**30**. It should be noted that the reduction potentials of *meso*-**28** (–1.65 V) and β-**28** (–1.64 V) are shifted to a positive direction relative to those of *meso*-**29**, **30** (−1.79 and −1.80 V), and β-**29**, **30** (−1.72 and −1.76 V). The more positive reduction potentials of *meso*-**28** and β-**28** reflect electron-accepting nature of the phosphole linker. The electrochemical HOMO–LUMO gaps of the porphyrin dimers are largely consistent with their optical HOMO–LUMO gaps. Namely, the smaller electrochemical HOMO–LUMO gaps of *meso*-**28** (2.13 eV) and β-**28** (2.14 eV) than those of *meso*-**29**, **30** (2.25 and 2.32 eV) and β-**29**, **30** (2.19 and 2.29 eV) agree with the red-shifted absorption owing to effective interaction in *meso*-**28** and β-**28**.
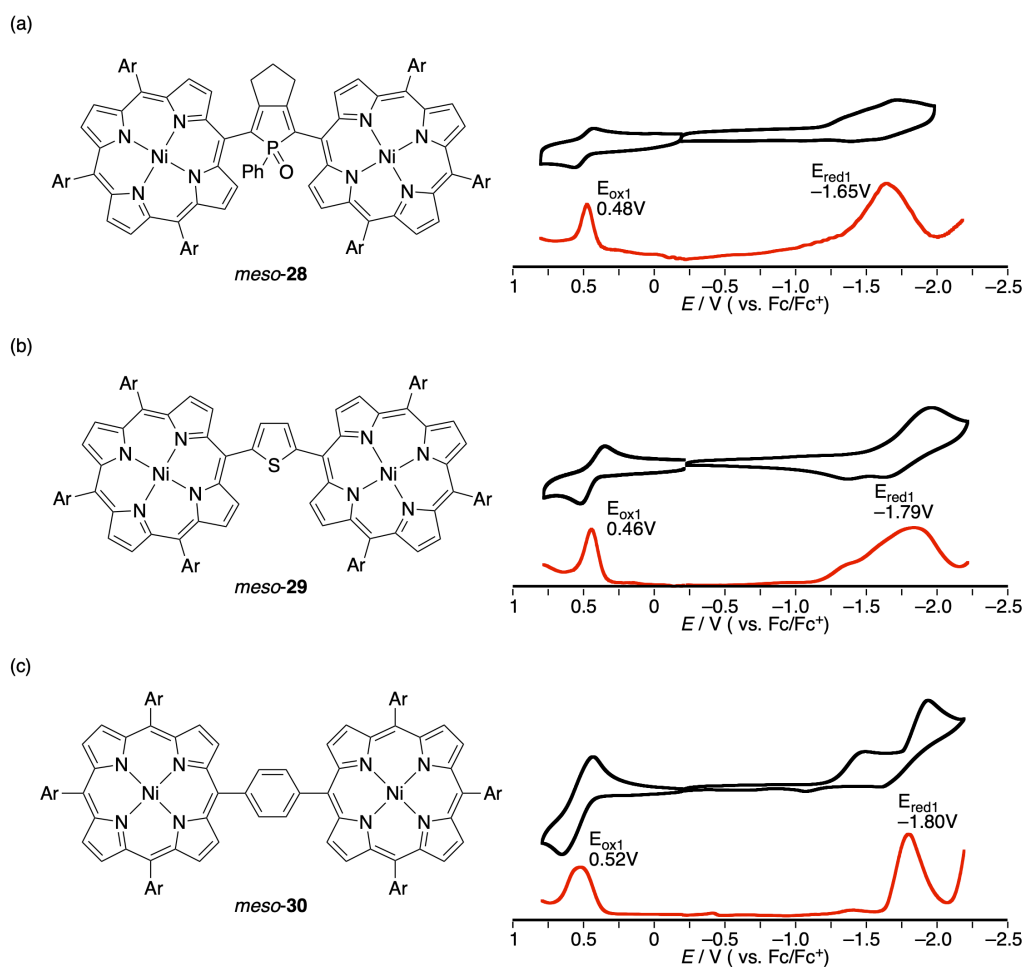
Figure 1-3. Cyclic voltammograms (black) and differential pulse voltammetry (DPV) curves (red) of porphyrins (a) *meso*-**28**, (b) *meso*-**29**, and (c) *meso*-**30**. Redox potentials were determined by DPV. Solvent: CH_2Cl_2; scan rate: 0.1 V s^{-1}; working electrode: glassy carbon; reference electrode: Ag/Ag$^+$ (0.01 M AgNO$_3$); electrolyte: 0.1 M n-Bu$_4$NPF$_6$.
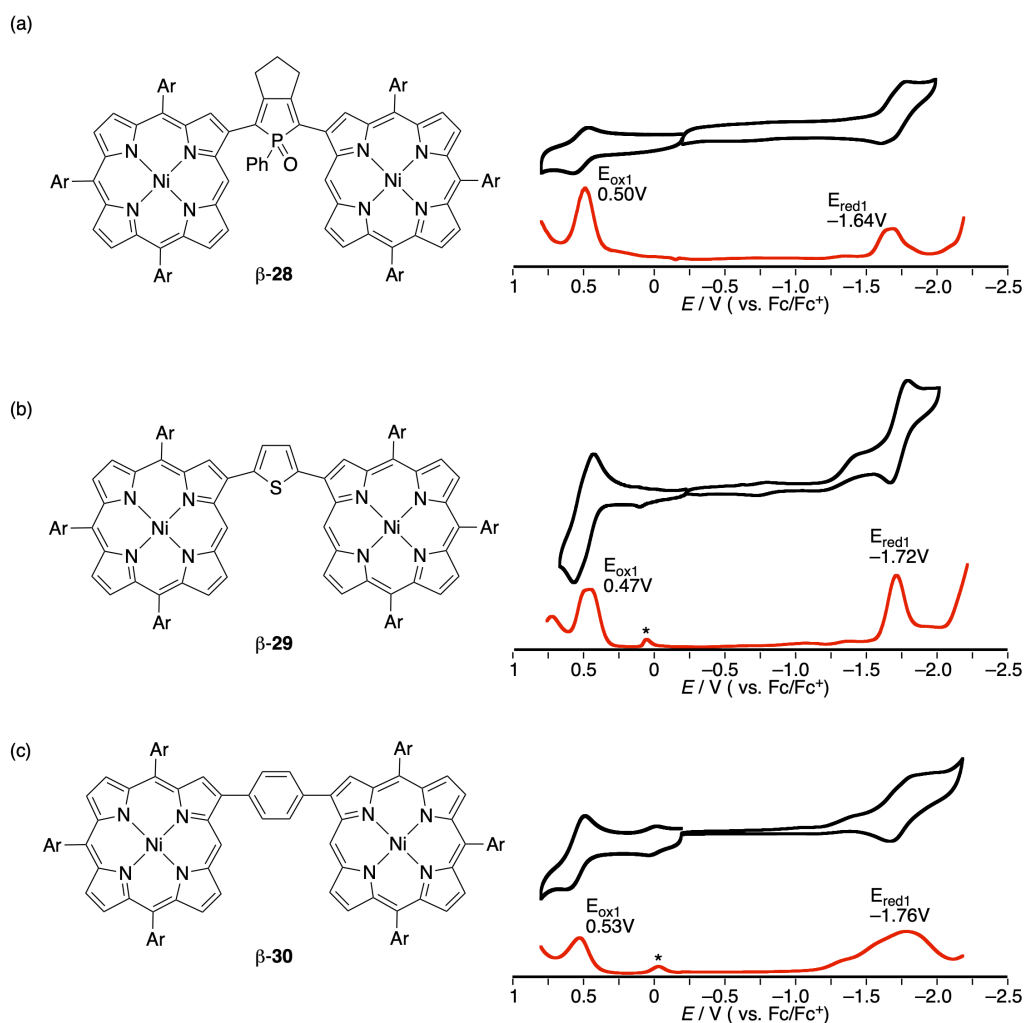
**Figure 1-4.** Cyclic voltammograms (black) and differential pulse voltammetry (DPV) curves (red) of porphyrins (a) β-**28**, (b) β-**29**, and (c) β-**30**. Redox potentials were determined by DPV. Solvent: CH_2Cl_2; scan rate: 0.1 V s^{-1}; working electrode: glassy carbon; reference electrode: Ag/Ag$^+$ (0.01 M AgNO$_3$); electrolyte: 0.1 M n-Bu$_4$NPF$_6$. Peaks marked with * arise from impurity.

1-5. Theoretical Calculations

To gain further insights into the structures and electronic properties of the porphyrin dimers, we performed density functional theory (DFT) calculations on model compounds in which the *meso*-aryl groups were replaced with hydrogen atoms.[73] We obtained the optimized structures at B3LYP/6-31G(d,p) level with C_s symmetry. The torsion angles of *meso*-**28m** and β-**28m** are smaller than those of *meso*-**29m–30m** and β-**29m–30m**, respectively (Figure 1-5). These small torsion angles of *meso*-**28m** and β-**28m** result from the effective through-bridged interaction between the porphyrins, which is consistent with their broad absorption.
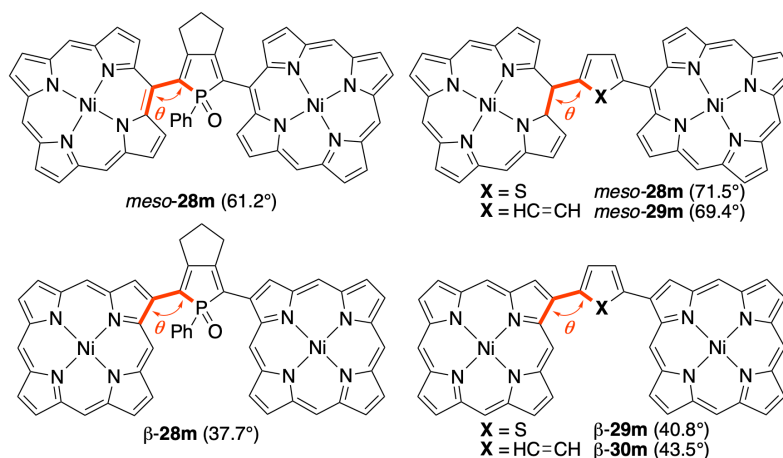
Figure 1-5. Torsion angles on model compounds of porphyrin dimers.

The frontier orbitals of porphyrin dimers and the corresponding porphyrin monomer **NiPm** are illustrated in Figures 1-6 and 1-7. Since the orbital distributions of HOMOs and LUMOs of *meso*-**29m** and *meso*-**30m** are mainly localized on the porphyrin rings, their shifts in the energy levels relative to **NiPm** are small. On the other hand, the LUMO of *meso*-**28m** has the large orbital distribution on the phosphole linker. The similar energy levels of HOMOs of *meso*-**28-30m** are in good agreement with their largely similar oxidation potentials. In contrast, the energy level of LUMO of *meso*-**28m** is significantly stabilized, which is consistent with the more positive reduction potential of *meso*-**28**. Consequently, the calculated HOMO–LUMO gap of **28m** (2.73 eV) is smaller than those of *meso*-**28m** (2.97 eV) and *meso*-**30m** (2.96 eV). The frontier orbitals of β-**28m-30m** also exhibit similar feature to those of *meso*-**28–30m**. Thanks to the smaller torsion angles of β-**28–30m** than *meso*-**28m–30m** (Figure 1-5), the HOMO–LUMO gaps of β-**28m–30m** are smaller than those of *meso*-**28m–30m**. It is noticeable that *meso*-**28m–30m** and β-**28m–30m** possess non-degenerated LUMO/LUMO+1 because of the remarkable stabilization of LUMO by effective σ*-π* interactions of the phosphole linker. The

non-degenerated LUMO/LUMO+1 probably induces the small blue shifts of their Soret-bands. These calculation results support the effective interaction between the porphyrins through the phosphole linker.
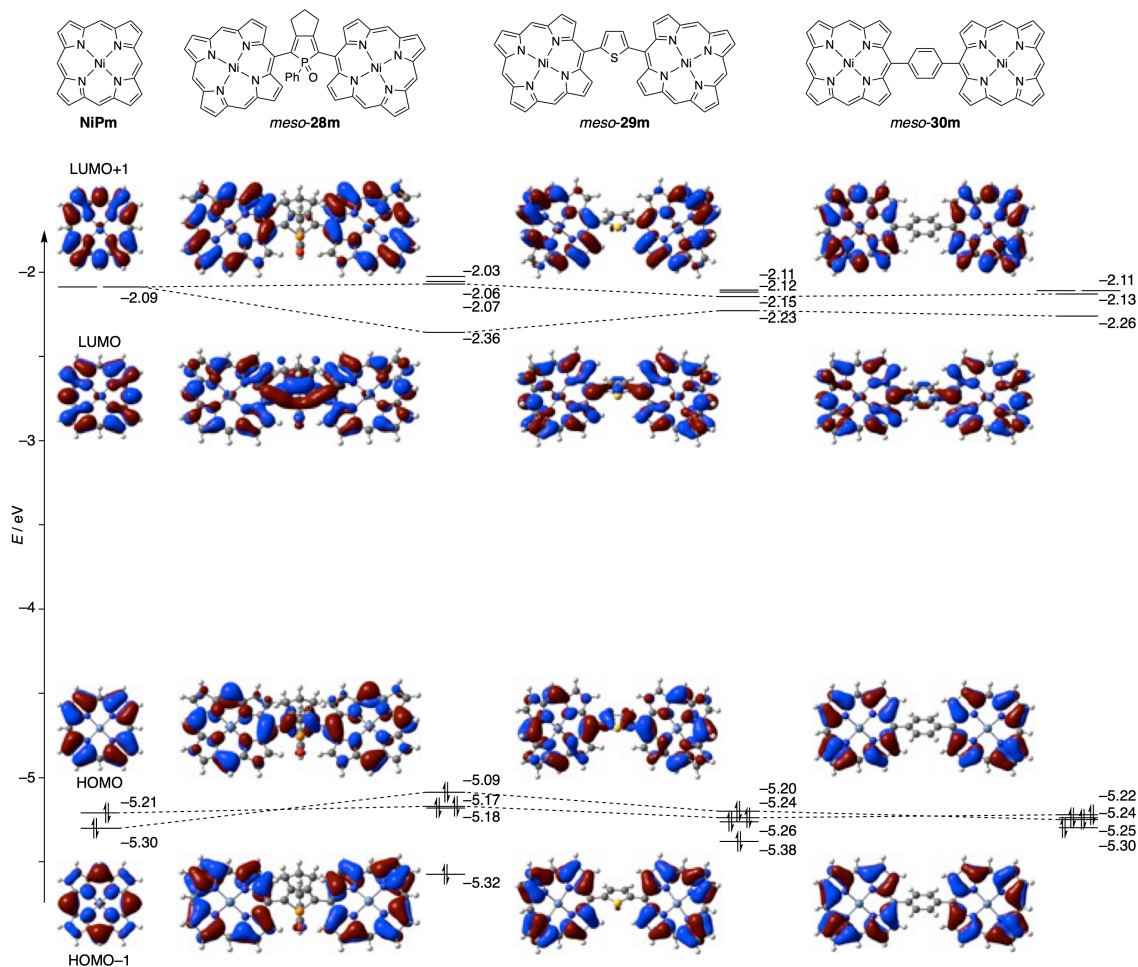
Figure 1-6. Selected Kohn-Sham orbitals of model porphyrins **NiPm** and meso-**28m**–**30m**.
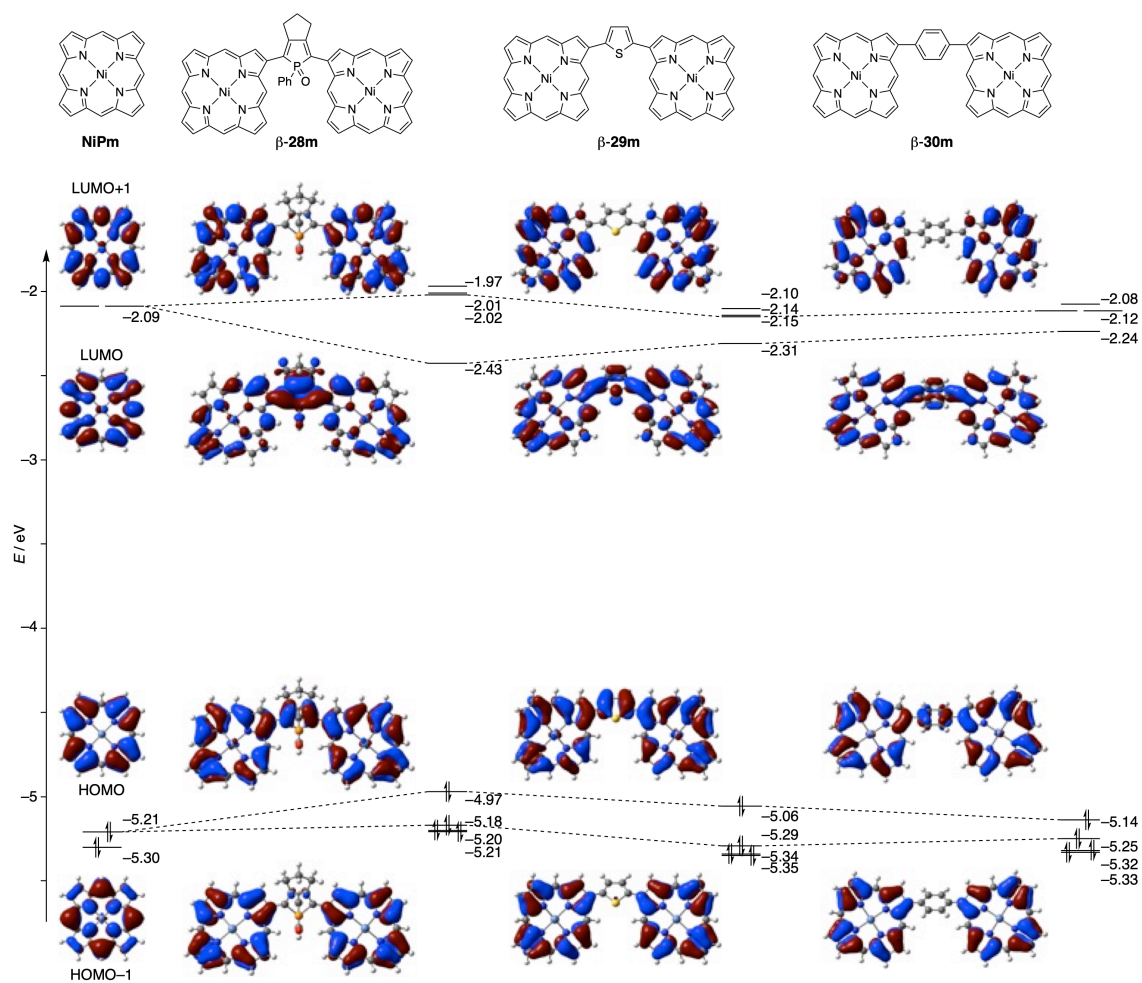
Figure 1-7. Selected Kohn-Sham orbitals of model porphyrins **NiPm** and β-**28m**–**30m**.

1-6. Summary

In summary, we synthesized phosphole-bridged porphyrin dimers and evaluated their optical and electrochemical properties. The porphyrin dimers exhibited broadened and red-shifted absorption relative to the thienylene- and *p*-phenylene-bridged reference dimers, suggesting effective π-conjugation between the porphyrins through the phosphole linker. The more positive reduction potentials of phosphole-bridged porphyrin dimers compared to the reference dimers are attributed to the electron-accepting ability of the phosphole linker, which is supported by DFT calculations.

Chapter 2. Phosphole-fused Dehydropurpurins via Titanium-mediated [2+2+1] Cyclization Strategy

E = O, S, lone pair
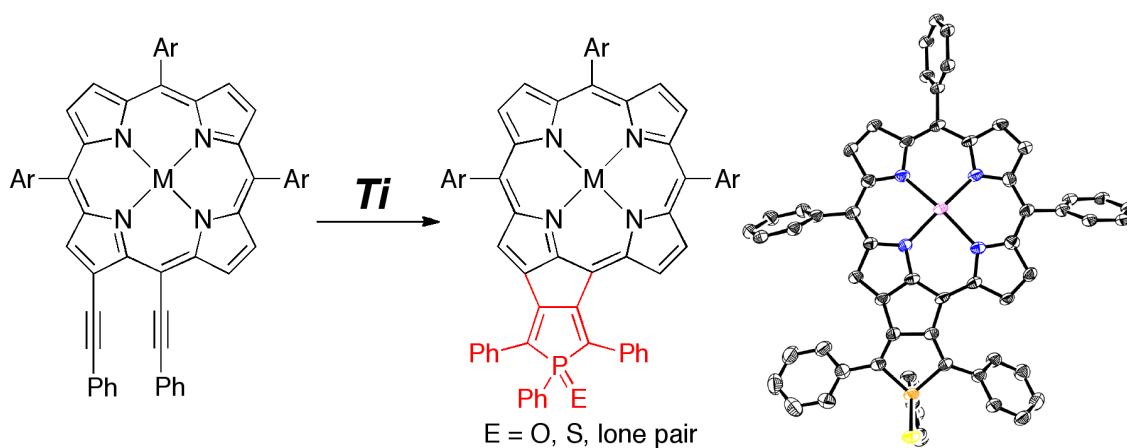
Contents

2-1. Introduction

Porphyrins with peripherally fused structures have emerged as promising organic functional materials for near infrared (NIR) absorption and/or fluorescence, solar energy conversion, and nonlinear optical response.[34c,63,74] In particular, porphyrins with a fused five-membered ring, *i.e.*, 7,8-dehydropurpurins[73] and related aromatic-fused porphyrins,[58,76] are unique porphyrinoids because of their altered absorption and weakened aromaticity. Although various benzene-fused dehydropurpurins have been synthesized,[76] a thiophene-fused dehydropurpurin has appeared as the sole example of heterole-fused dehydropurpurins due to their synthetic difficulty in fusing a heterole to a large π-system of a porphyrin.[58] Thus, a new synthetic approach to heterole-fused dehydropurpurins is needed to expand a world of fused porphyrinoids.

The reactions of 1,6-diynes using low-valent zirconium[77] or titanium[78] species, generated *in situ*, followed by treatment with suitable electrophiles afford various heteroles with a five-membered ring. If the 1,6-diyne-like structure was introduced into a porphyrin to give 3,5-bis(alkynyl)porphyrin, the analogous cyclization would offer the corresponding heterole-fused 7,8-dehydropurpurin (Scheme 2-1). However, to the best of our knowledge, no such cyclizations of porphyrins using low-valent zirconium or titanium species have been achieved despite the remarkable progress of organometallic approaches for porphyrinoids.[21,79] In fact, we recently presented phosphole-bridged porphyrin dimers, but our trials *via* this cyclization strategy of alkynylporphyrins fell through.[80] As such, this synthetic breakthrough has been waited for the developments of organometallic synthetic methodologies as well as heterole-fused dehydropurpurins.
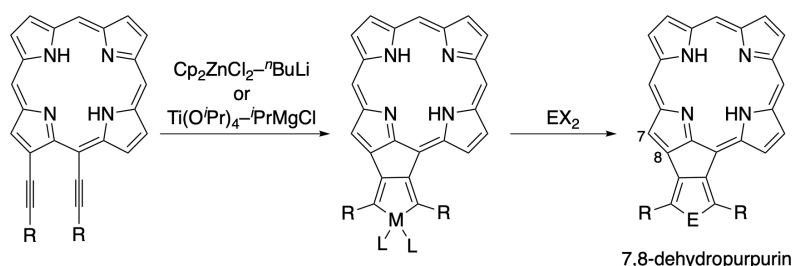
Scheme 2-1. [2+2+1] Cyclization strategy on 3,5-bis(alkynyl)porphyrin.

Phospholes are actively studied heteroles owing to their intriguing optical and electrochemical properties as well as potential for diverse applications.[70a-b,70d-f,81] For example, phospholes have high electron-accepting properties arising from the effective hyperconjugation between the σ*-orbital of the P−C bonds and the π*-orbital of the butadiene moiety.

Furthermore, their structural and electronic properties can be tuned by chemical modifications, such as oxidation, metal-coordination, and alkylation, of the phosphorus center. Nevertheless, there are no examples of porphyrins with phospholes at their peripheral positions except our works.[64,80] Specifically, we previously reported the phosphole-fused porphyrin dimer as the first example of porphyrin-phosphole hybrids where the two porphyrins are directly fused at the β-positions through the phosphole unit (Figure 2-1a).[64] It exhibited unique optical and electrochemical properties owing to intrinsic features of the phosphole.
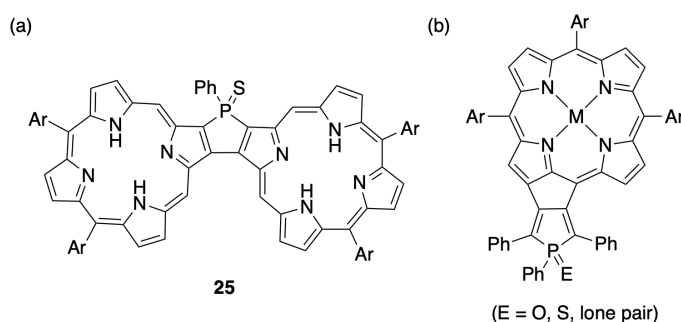
Figure 2-1. Examples of phosphole-fused porphyrins.

   As describe in Chapter 1, porphyrin dimers linked at *meso-* or β-positions through a phosphole bridge were synthesized in moderate yield by recently developed organometallic approaches.[80] On the other hand, the phosphole-fused porphyrin dimer **25** was prepared in the quite low yield (0.7%) from the condensation of bis(pyrrolo)phosphole and tripyrrane.[64] The phosphole P=S derivative was the sole example due to this synthetic limitation which is an obstacle to elucidate the effects of phosphorus atoms on the intrinsic electronic properties of phosphole-fused porphyrins. The common synthetic approach for aromatic-fused phospholes is a halogen-lithium exchange followed by a treatment with chlorophosphines (RPCl$_2$).[70a-b,70d-f,81] But examples of a halogen-lithium exchange for porphyrins are still limited,[82] thus an alternative synthetic approach for phosphole-fused porphyrins are required. Meanwhile, aromatic-fused porphyrins with an embedded phosphorus atom have been recently described as attractive π-extended porphyrins for functional materials.[60,83] Totally, fusion of a phosphole moiety to the peripheral positions of a porphyrin core is a promising strategy for creating an exotic π-system. Herein, we succeeded in synthesizing a systematic series of phosphole-fused dehydropurpurins as new families of heterole-fused dehydropurpurins as well as π-extended phosphorus-embedded porphyrins (Figure 2-1b). The effects of oxidation states of the phosphorus atom on their electronic properties have been elucidated for the first time. Thus, we demonstrated that the titanium-mediated [2+2+1] cyclization strategy is an effective synthetic approach for phosphole-fused porphyrins.

2-2. Synthesis

To establish the titanium-mediated cyclization reaction on porphyrins, we attempted the reaction of 3,5-bis(phenylethynyl)porphyrin **34M** using (η^2-propene)Ti(O^{i}Pr)$_2$, generated *in situ* from Ti(O^{i}Pr)$_4$ and ^{i}PrMgCl, followed by treatment with PhPCl$_2$ and H$_2$O$_2$ (Table 2-1). The reaction of **34Ni** under the typical condition, with 1 equivalent of Ti(O^{i}Pr)$_4$ and 2 equivalent of ^{i}PrMgCl, resulted in complete recovery of **34Ni** (entry 1). The reaction with excess amounts of Ti(O^{i}Pr)$_4$ and ^{i}PrMgCl afforded the complicated mixture with complete conversion of **34Ni**, and no phosphole-fused dehydropurpurin was detected (entry 2). Fortunately, when the reaction with the same excess amounts of Ti(O^{i}Pr)$_4$ and ^{i}PrMgCl was performed under the diluted condition ([**34M**] = 1 mM), we succeeded in isolation of the phosphole-fused dehydropurpurin **35Ni** in low yield (entry 3). These results suggest that the reactivity of 3,5-bis(alkynyl)porphyrin with low-valent titanium species is low, while the titanacycle intermediate may easily react with other porphyrins under high concentration to give the complicated mixture. Finally, we found that the reaction with the large excess amounts of Ti(O^{i}Pr)$_4$ and ^{i}PrMgCl provided **35Ni** in 62% yield (entry 4). In addition, the treatment with S$_8$ in place of H$_2$O$_2$ furnished **36Ni** in 79% yield (entry 5).

Table2-1. Synthesis of phosphole-fused 7,8-dehydropurpurins.[a]
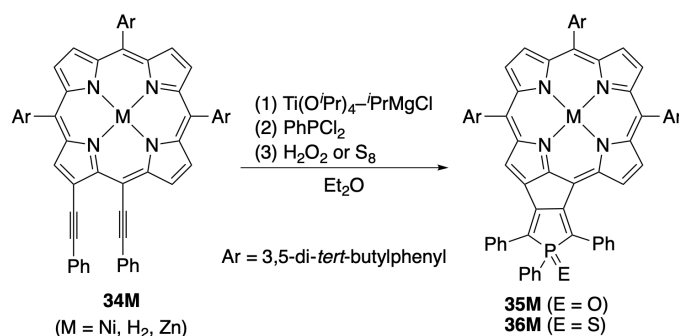
entry	**34M**	Ti(O^{i}Pr)$_4$ / eq.	iPrMgCl / eq.	PhPCl$_2$ / eq.	[**34M**] / mM	Product (yield)
1	**34Ni**	1	2	1	30	**35Ni** (0%)
2	**34Ni**	3	6	3	30	**35Ni** (0%)
3	**34Ni**	3	6	3	1	**35Ni** (23%)
4	**34Ni**	10	40	50	1	**35Ni** (62%)
5	**34Ni**	10	40	50	1	**36Ni** (79%)
6	**34Zn**	10	40	50	1	**35Zn** (0%)
7	**34H$_2$**	10	40	50	1	**35H$_2$** (0%)

[a] After the reaction, the crude phosphorus(III) product was oxidized by the treatment with H$_2$O$_2$.

[b] S$_8$ was used instead of H$_2$O$_2$.

We also attempted the same reactions for the corresponding zinc porphyrin **34Zn** or free-base porphyrin **34H₂**, but could not obtain the corresponding phosphole-fused dehydropurpurins (entries 6,7). Luckily, demetalation of **35Ni** and **35Ni** with sulfuric acid in trifluoroacetic acid gave free-base dehydropurpurins **35H₂** and **36H₂**, respectively (Scheme 2-2). Then, the treatment of **35H₂** and **36H₂** with Zn(OAc)₂·2H₂O provided zinc dehydropurpurins **35Zn** and **36Zn**. Dehydropurpurins **35M** could be also converted to the corresponding **36M** by the reaction with Lawesson's reagent. Notably, the reaction of **36M** with P(NMe₂)₃ yielded phosphorus(III) derivatives **37M**. However, phosphorus(III) derivatives **37M**, are gradually oxidized to **35M** under air, probably owing to the electron-rich nature of the porphyrin core.

All phosphole-fused dehydropurpurins **35M**–**37M** were characterized by high-resolution mass spectrometry and ^{1}H, ^{13}C, and ^{31}P NMR spectroscopies.
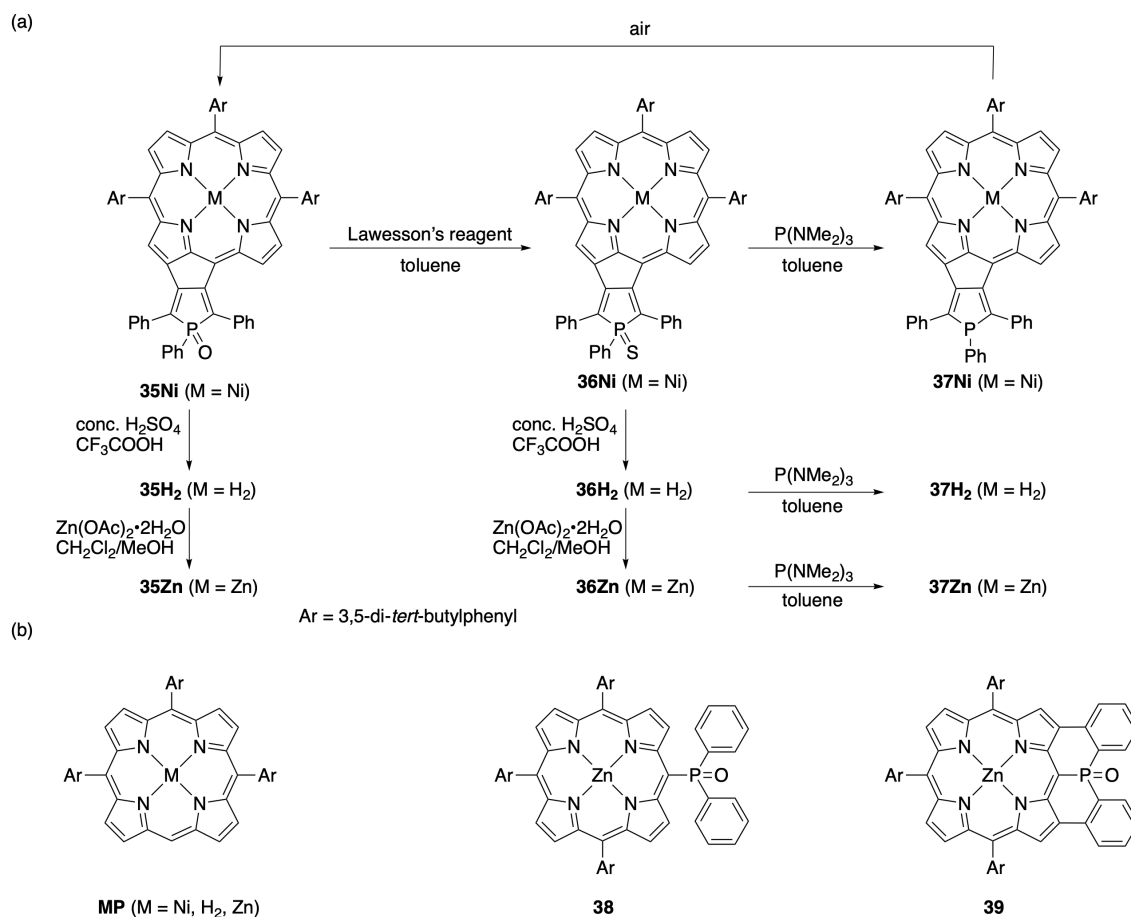
Scheme 2-2. (a) Transformations of dehydropurpurins and (b) structures of reference porphyrins.

2-2. ^{1}H NMR Spectra

The ^{1}H NMR spectrum of **35Zn** displays broad signals in CDCl$_3$ (Figure 2-2a), while the sharp signals similar to those of **36Zn** (Figure 2-3) appear by the addition of C$_5$D$_5$N (Figure 2-2b). The broad signals of **35Zn** in CDCl$_3$ suggest the formation of a dimeric structure originated from the coordination of the oxygen atom of **35Zn** to the zinc atom of **35Zn**, as seen in the complementary dimer formation of phosphorus-containing porphyrins **38**[84]and **39**[82a] (Scheme 2-2b). The dimer formation of **35Zn** is also suggested by the X-ray crystal structure of **35Zn**.
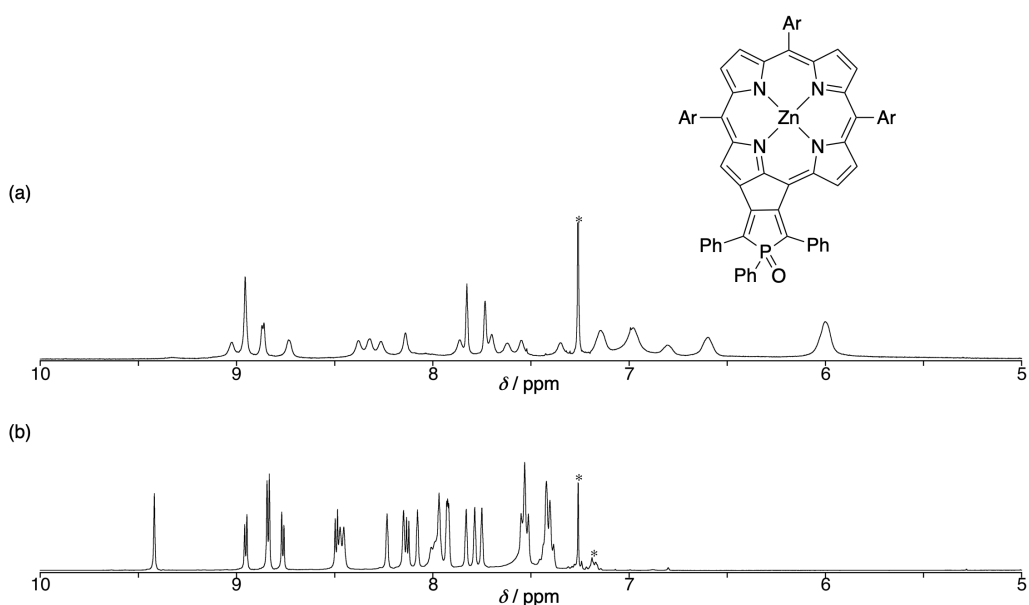
Figure 2-2. ^{1}H NMR spectra of **35Zn** in (a) CDCl$_3$ and (b) CDCl$_3$ in presence of C$_5$D$_5$N at 25 ºC. Peaks marked with ∗ are due to residual solvents and impurities.
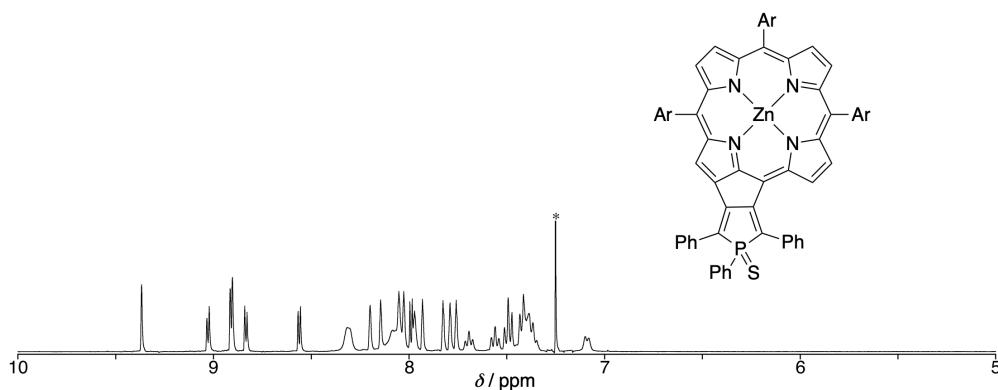
Figure 2-3. ^{1}H NMR spectra of **36Zn** in CDCl$_3$ at 25 ºC. Peaks marked with ∗ are due to residual solvents and impurities.

The ^{1}H NMR spectrum of **37H$_2$** exhibits upfield-shifted signals of the β-protons at 7-position (δ = 8.89 ppm) relative to those of **35H$_2$** and **36H$_2$** (9.41 and 9.34 ppm). Furthermore, the signals of the inner NH protons of **37H$_2$** (–0.62 and –1.69 ppm) show downfield shifts in comparison with those of **35H$_2$** (–1.19 and –2.08 ppm) and **36H$_2$** (–1.12 and –2.05 ppm) (Figure 2-4). These trends are observed nickel and zinc porphyrins in their ^{1}H NMR spectra.
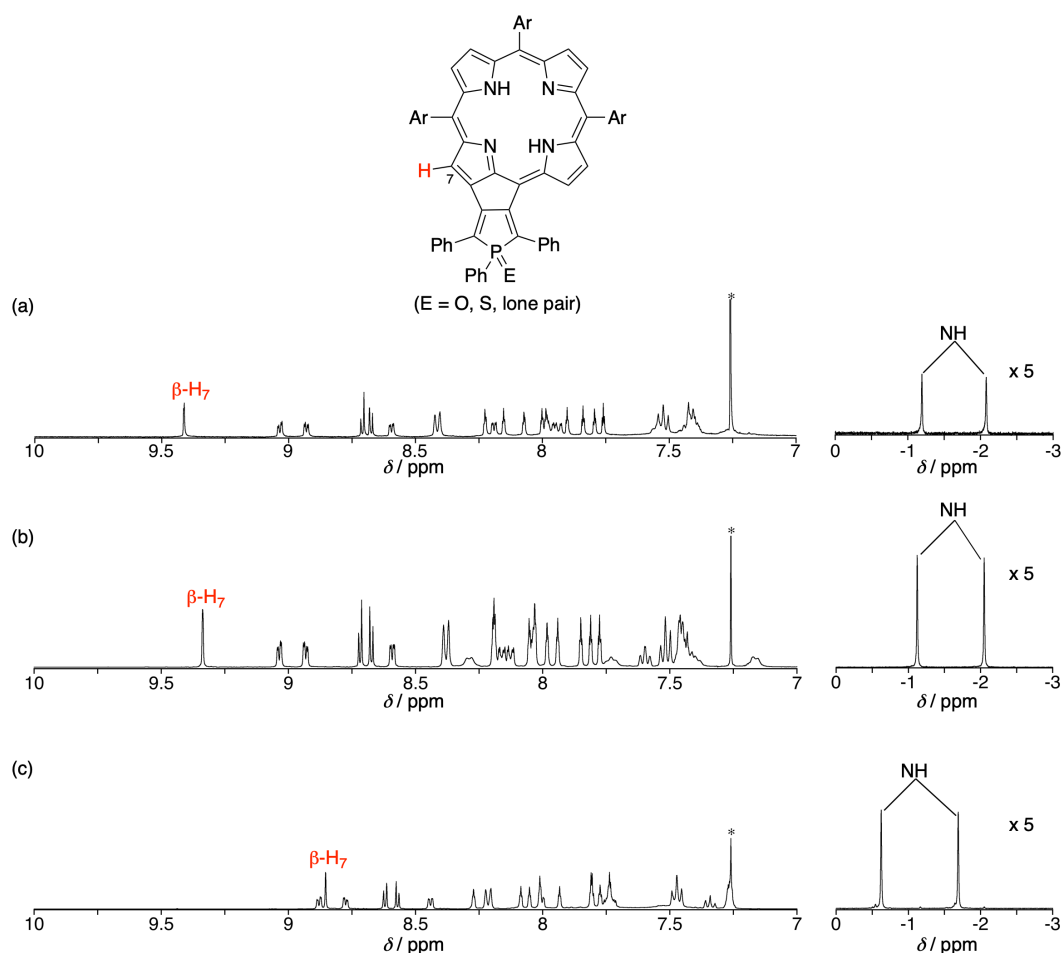
Figure 2-4. ^{1}H NMR spectra of (a) **35H$_2$**, (b) **36H$_2$**, and (c) **37H$_2$** in CDCl$_3$ at 25 ºC. Peaks marked with ∗ are due to residual solvents.

These results imply the weakened aromatic characters of **37M**, which can be rationalized by the contribution of 24π-antiaromatic character derived from a 24π-electron pathway including the lone-pair of the phosphorus(III) atom (Figure 2-5a). This type of 24π-electron pathway is also proposed for the thiophene-fused dehydropurpurin.[58] In contrast, the contribution of 24π-antiaromatic character to **35M** and **36M** should be negligible because the oxidized phosphorus(V) centers (P=O and P=S) without a lone-pair disrupt the 24π-electron pathways (Figure 2-5b). Therefore, the contribution of 18π-aromatic character is dominant in **35M** and **36M**. It is noteworthy that the electronic properties of the porphyrinoids can be greatly altered by their aromaticity and π-circuits.[85] Namely, the whole electronic properties of the phosphole-fused dehydropurpurins can be switched by the oxidation state of the phosphorus center.
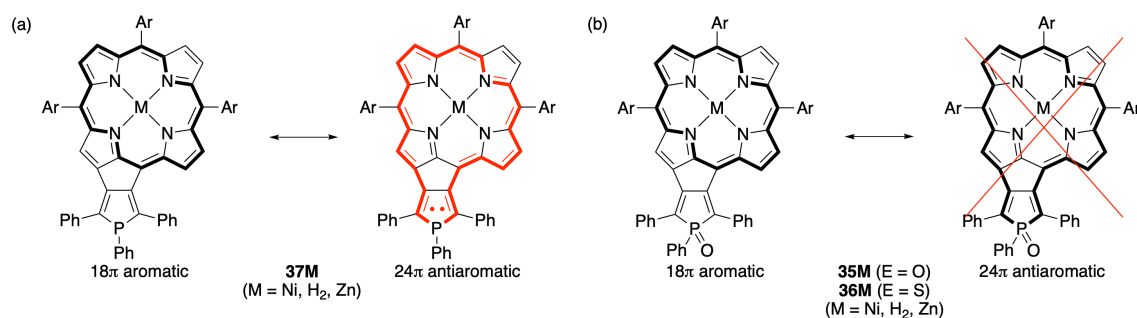
Figure 2-5. 18π- and 24π- electron pathways for (a) **37M** and (b) **35M** and **36M**.

2-3. X-Ray Crystal Structure

Fortunately, we obtained single crystals suitable for X-ray diffraction analysis by vapor diffusion of acetonitrile into a CH_2Cl_2 solution of **36Zn** (Figures 2-6). The crystal structure of **36Zn** reveals an antiparallel face-to-face dimer, which is similar to those of dimeric structures of phosphorus-containing porphyrins **38**[84] and **39**.[83a] However, because of the weaker coordination ability of the sulfur atom than the oxygen atom to the zinc atom, the ^{1}H NMR spectrum of **36Zn** in $CDCl_3$ (Figure 2-3) indicates no dimeric structure of **36Zn**. This is opposite to **35Zn**: the crystal structure of **35Zn** could not be obtained, whereas the broad ^{1}H NMR signals in $CDCl_3$ supported the dimer formation of **35Zn** (Figure 2-2a). The C8–C8' and C10–C10' bond lengths of **36Zn** are 1.446(6) and 1.489(6) Å, which are almost identical to those of other dehydropurpurins (1.45–1.49 Å).[75a-c] On the other hand, the C8'–C10' bond length (1.519(6) Å) is remarkably larger than those of other dehydropurpurins (ca. 1.38 Å), [75a-c] reflecting the butadiene-like character of the phosphole ring.
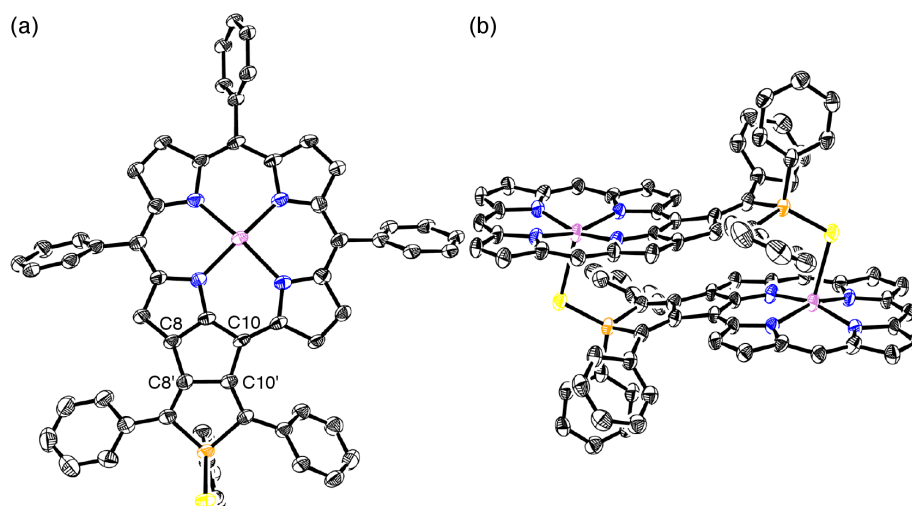
Figure 2-6. X-Ray crystal structure of **36Zn**: top view and (b) dimeric structute. Thermal ellipsoids represent 50% probability. *tert*-Butyl groups and all hydrpgen atoms are omitted for clarity.

2-4. UV/Vis Absorption and Fluorescence Spectra

The UV/vis absorption and fluorescence spectra of **35M–37M** and the reference porphyrins **MP** were measured in CH_2Cl_2 (Figures 2-7, Table 2-2). The phosphole-fused dehydropurpurins display markedly red-shifted absorption and fluorescence spectra compared to **MP**. In contrast to split Soret-bands of non-fused dehydropurpurins,[75] the phosphole-fused dehydropurpurins reveal one broadened characteristic Soret-band (ca. 470–480 nm), which is attributed to the butadiene-like character of the phosphole ring. Moreover, the wavelengths of the lowest energy Q-bands for **35Zn–37Zn** (663–675 nm) are shorter than those of the benzo-fused zinc dehydropurpurins (ca. 750–770 nm).[76c,d,e] The nickel **35Ni–37Ni** and free-base porphyrins **35H₂–37H₂** also display the blue-shifted Q-bands.[76d] These blue-shifts suggest the weaker π-conjugation through the phosphole-fused structure than the benzo-fused structure, which stems from the weak interaction of the phosphorus lone pair in the phosphole π-system. [70a-b,70d-f,81] Since the absorption spectra of **35M** and **36M** with the same central metal are almost identical, the phosphorus(V) centers (P=O and P=S) have comparable impact on the absorption spectra. On the other hand, **37M** shows diminished absorption and slightly red-shifted Q-bands. These spectral features result from the weak 24π antiaromatic character, which is consistent with the results obtained by the comparison of the ^{1}H NMR spectra of **35M–37M**. The fluorescence quantum yields (Φ_F) of P=S derivatives **36H₂** and **36Zn** (0.01–0.03) are smaller than those of P=O **35H₂** and **35Zn** (0.13–0.14), which agrees with the trend in acenaphtho[1,2-*c*]phospholes.[86] In contrast, the smaller Φ_F values of phosphorus(III) derivatives **37H₂** and **37Zn** (0.07) than those of **35H₂** and **35Zn** contradict the larger Φ_F values of phosphorus(III) derivatives than those of P=O derivatives for acenaphtho[1,2-*c*]phospholes.[71c] The smaller Φ_F values of **37H₂** and **37Zn** may be caused by the 24π antiaromatic character generated by the fusion of the phosphole(III) moiety to the large π system of the porphyrin.
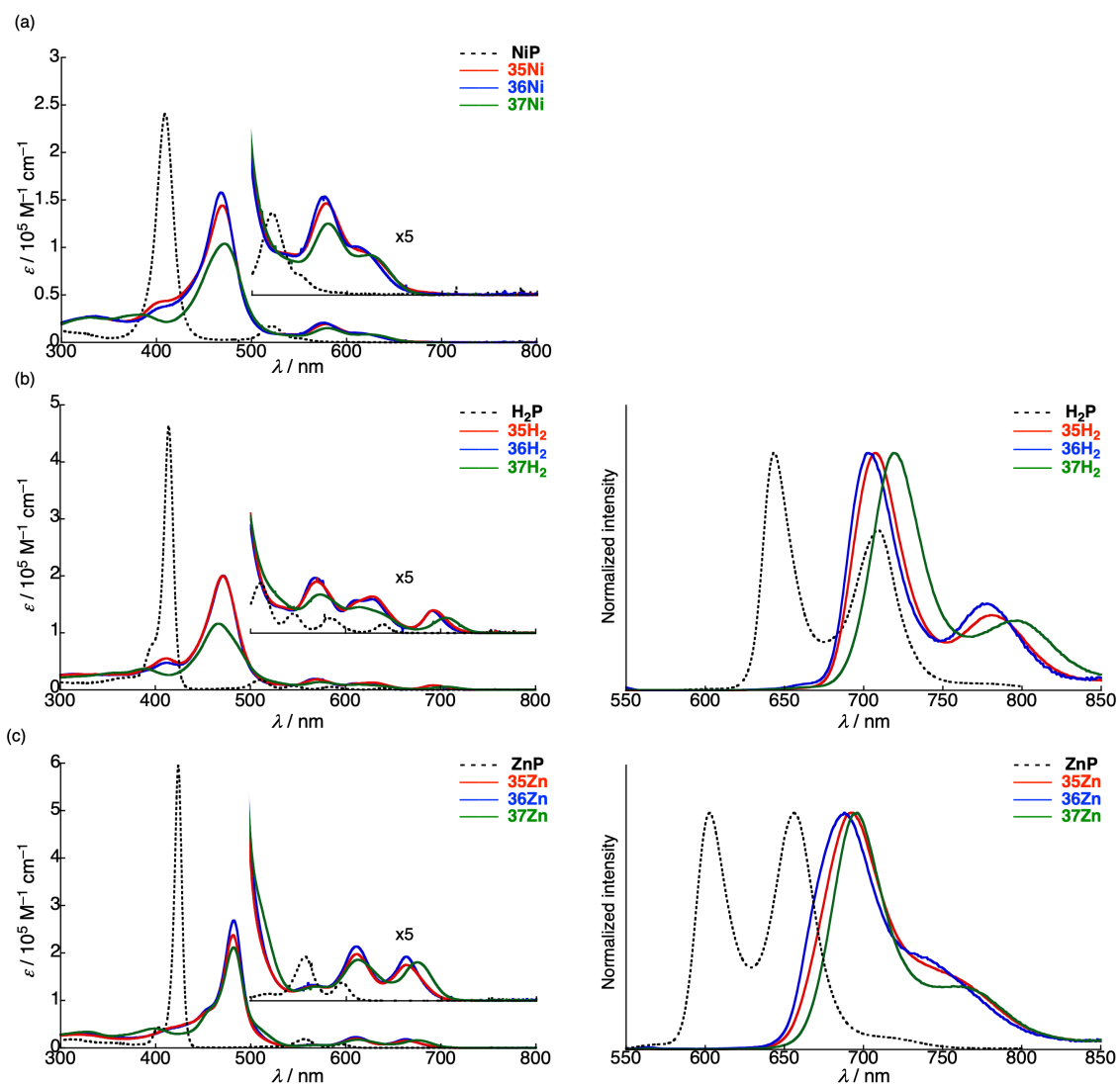
Figure 2-7. UV/Vis absorption (left), and fluorescence spectra (right) of (a) **35M** (red), **36M** (blue), **37M** (green), and **MP** (black) in CH$_2$Cl$_2$. For fluorescence measurements, the samples were excited at wavelengths for Soret band maxima.

Table 2-2. Optical properties of **35M–37M** and **MP** in CH_2Cl_2.

	λ_{abs} / nm (ε [10^4 $M^{-1}cm^{-1}$])	λ_{em}[b] /nm (Φ_F[c])
35Ni	332 (2.7), 409 (4.4), 469 (14), 578 (1.9), 620 (0.89)	_[d]
36Ni	334 (2.8), 408 (3.8), 468 (16), 576 (2.1), 613 (1.0)	_[d]
37Ni	330 (2.6), 384 (2.9), 472 (10), 580 (1.5), 623 (0.85)	_[d]
NiP	409 (24), 521 (1.7), 551 (0.42)	_[d]
35H₂	412 (5.5), 471 (20), 570 (1.9), 628 (1.3), 692 (0.80)	707, 780 (0.13)
36H₂	411 (4.8), 471 (20), 568 (1.9), 612 (1.2), 628 (1.2), 692 (0.78)	703, 778 (0.01)
37H₂	387 (3.7), 466 (12), 573 (1.4), 613 (0.91), 705 (0.54)	719, 797 (0.07)
H₂P	395 (7.6), 414 (46), 511 (1.8), 546 (0.69), 584 (0.50), 639 (0.32)	643, 709 (0.09)
35Zn[a]	321 (2.8), 481 (24), 611 (2.0), 663 (1.5)	692 (0.14)
36Zn[a]	319 (3.2), 482 (27), 610 (2.3), 663 (1.9)	688 (0.03)
37Zn[a]	331 (3.4), 398 (4.1), 482 (21), 612 (1.7), 675 (1.6)	694 (0.07)
ZnP[a]	403 (4.2), 423 (59), 557 (1.9), 596 (0.71)	603, 656 (0.05)

[a] In pyridine/CH_2Cl_2 (v/v=1:99).

[b] The samples were excited at wavelengths for Soret band maxima.

[c] Φ_F values were determined using 5,10,15,20-tetraphenylporphyrin as a standard (Φ_F =0.11).[87]

[d] Fluorescence were not observed.

Considering the interactions between the zinc and oxygen or sulfur atoms for **35Zn** and **36Zn**, we measured the absorption spectra under various concentrations (Figure 2-8). As observed in the ^{1}H NMR spectra, the P=O derivative **35Zn** exhibits distinct absorption spectral changes (Figure 2-8a). In contrast, the P=S derivative **36Zn** reveals no peak shift with increasing the concentration (Figure 2-8b). These results are consistent with our interpretation on the dimer formation of **35Zn** and no dimer formation of **36Zn** in nonpolar solvents. From the dimerization isotherms, the dimerization constant (K_D) for **35Zn** was determined to be 1.9×10^5 M^{-1} (Figure 2-9). This value is one order of magnitude smaller than those of *meso*-phosphorylporphyrins **38** (5.9×10^6 M^{-1})[84] and **39** (1.2×10^6 M^{-1}).[83a] The smaller K_D is attributable to steric hindrance of the phenyl groups at the α-positions of the phosphole moiety.
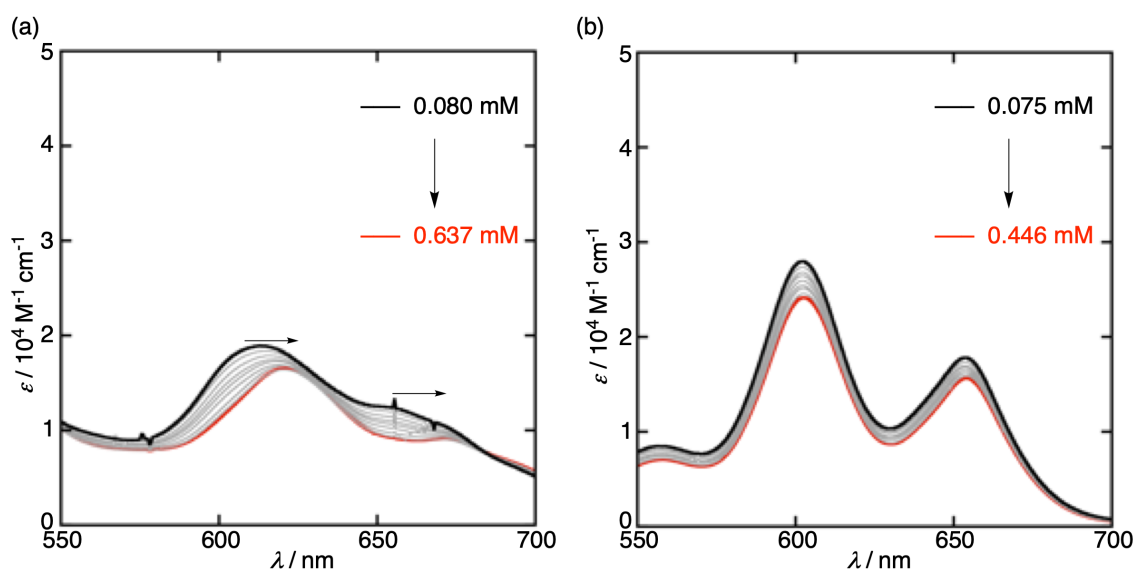
Figure 2-8. Concentration dependent absorption spectra of (a) **35Zn** and (b) **36Zn** in CH_2Cl_2. These measurements were performed using a 1 mm cuvette instead of a 1 cm cuvette due to their highconcentration.

(a)

(b)
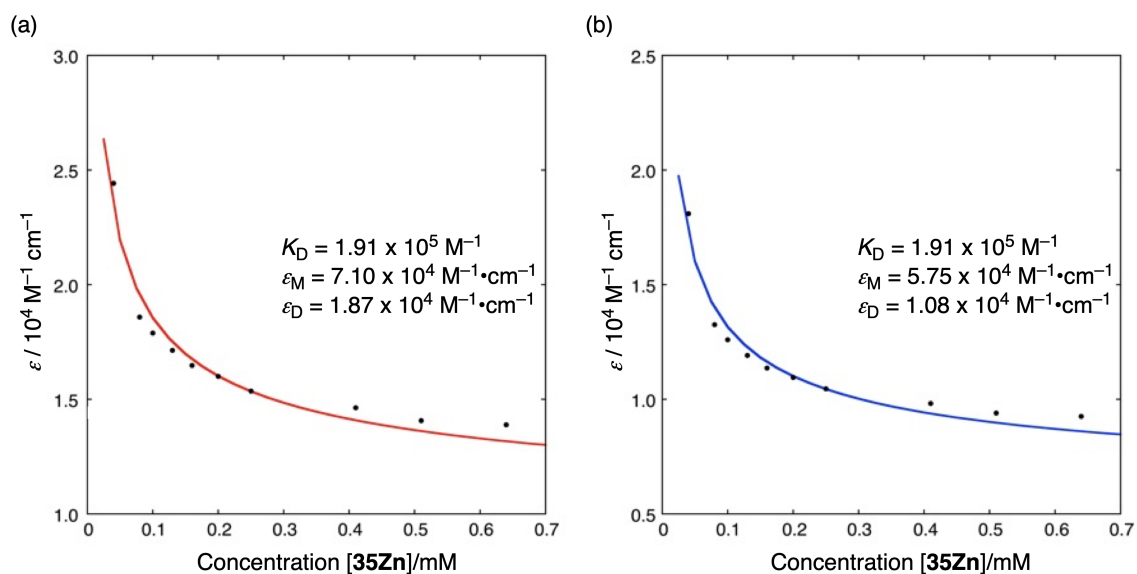
Figure 2-9. Plots of the spectral change of **35Zn** versus the concentration of **35Zn** (0.080–0.637 mM) in CH_2Cl_2 at (a) 608 nm (red) and (b) 655 nm (blue). The fitting curves obtained by the following equation are overlaid.

$$\varepsilon = \frac{\left(2\varepsilon_M - \varepsilon_D\right)\left(\sqrt{1+8K_D[\mathbf{35Zn}]} - 1\right)}{8K_D[\mathbf{35Zn}]} + 4K_D\varepsilon_D$$

2-5. Electrochemical Properties

The electrochemical properties of **35M**–**37M** and **MP** (versus ferrocene/ferrocenium ion (Fc/Fc$^+$)) were studied by cyclic voltammetry (CV) and differential pulse voltammetry (DPV) (Figures 2-10–12 and Table 2-3). Phosphole-fused dehydropurpurins **35M** and **36M** reveal two reversible oxidation peaks. For **35Zn**, the oxidation peaks are split in the absence of pyridine, which matches with the dimer formation. On the other hand, **35M** and **36M** display three reversible or quasi-reversible reduction peaks. The oxidation and reduction potentials of **35M** and **36M** are almost identical. The first reduction potentials (E_{red1}) of **35M** and **36M** are shifted to the positive direction by ca. 0.3 V compared to **MP** by the strong electron-withdrawing character of the phosphorus(V) centers (P=O and P=S). It is noteworthy that the E_{red1} values of **35M** and **36M** are comparable to those of aromatic-fused phospholes,[71c,88] suggesting their potential utility as electron-accepting materials. The phosphorus(III) derivatives **37M** exhibit irreversible first oxidation peaks at 0.17–0.39 V, which are assigned to one electron oxidation of the phosphorus(III) atom. Meanwhile, the reduction potentials of **37M** are shifted to the negative direction relative to those of the corresponding **35M** and **36M** due to the weakened electron-accepting character of the phosphorus(III) center. The electrochemical HOMO–LUMO gaps of **37M** (1.81–1.96 eV) are smaller than those of the corresponding **35M** and **36M** (1.84–2.04 eV), which is associated with the contribution of 24π antiaromatic character in **37M**.
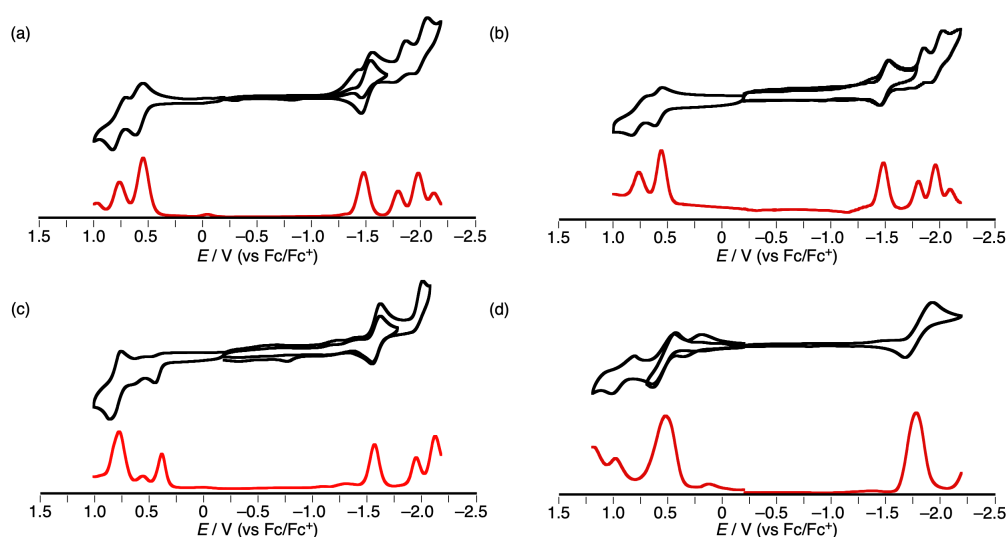
Figure 2-10. Cyclic voltammograms (black) and differential pulse voltammetry (DPV) curves (red) of nickel dehydropurpurins (a) **35Ni**, (b) **36Ni**, (c) **37Ni**, and (d) **NiP**.
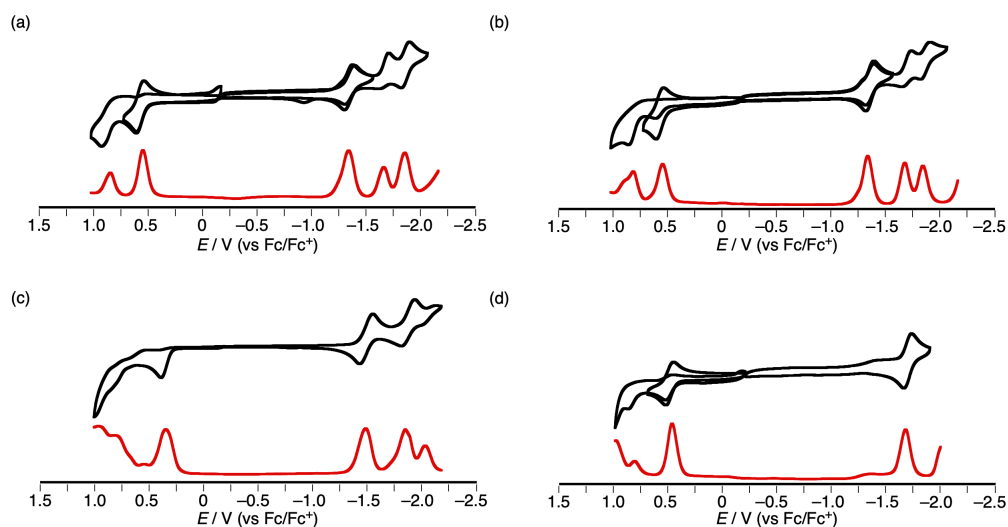
Figure 2-11. Cyclic voltammograms (black) and differential pulse voltammetry (DPV) curves (red) of nickel dehydropurpurins (a) **35H₂**, (b) **36H₂**, (c) **37H₂**, and (d) **H₂P**.
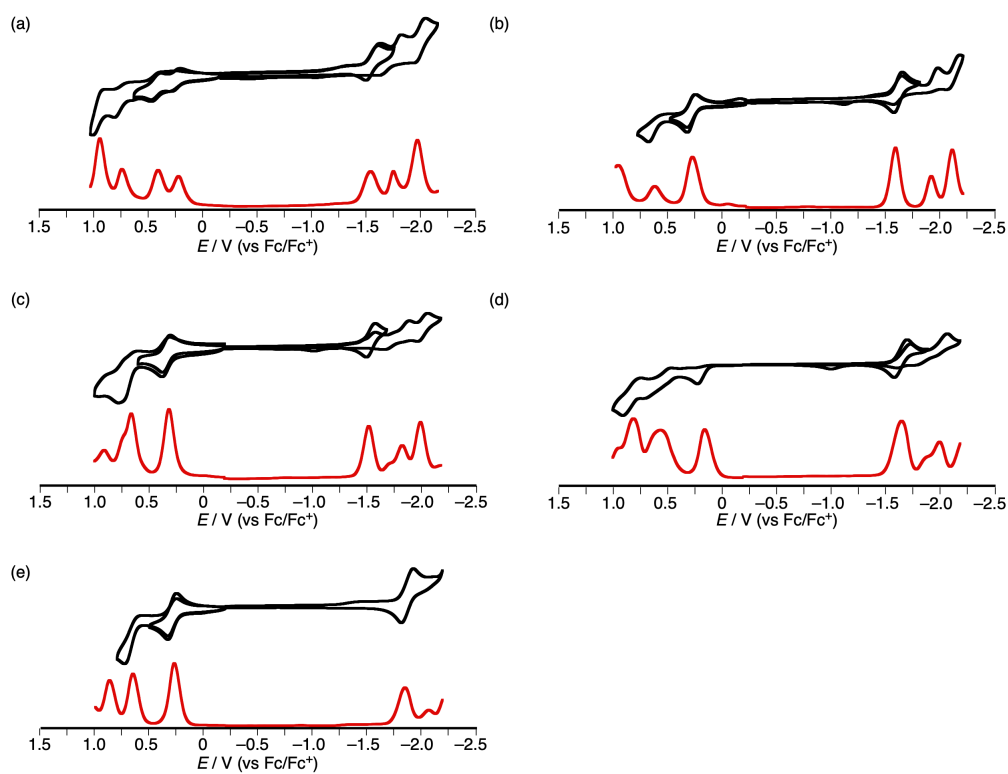
Figure 2-12. Cyclic voltammograms (black) and differential pulse voltammetry (DPV) curves (red) of nickel dehydropurpurins (a) **35Zn**, (b) **35Zn** in the presence of pyridine, (c) **36Zn**, (d) **37Zn**, and (e) **ZnP**.

Table 2-3. Electrochemical oxidation and reduction potentials of phosphole-fused dehydroperpurins and reference porphyrins versus Fc/Fc$^+$.

	E_{ox4}	E_{ox3}	E_{ox2}	E_{ox1}	E_{red1}	E_{red2}	E_{red3}	E_g^{CV}
35Ni	–	–	0.76	0.55	–1.49	–1.80	–1.99	2.04
36Ni	–	–	0.78	0.57	–1.47	–1.80	–1.96	2.04
37Ni	–	–	0.78	0.39	–1.57	–1.95	–2.13	1.96
NiP	–	–	0.99	0.53	–1.78	–	–	2.31
35H$_2$	–	–	0.85	0.55	–1.34	–1.67	–1.86	1.89
36H$_2$	–	–	0.82	0.55	–1.34	–1.68	–1.85	1.89
37H$_2$	–	–	–	0.35	–1.49	–1.85	–2.04	1.84
H$_2$P	–	–	0.82	0.47	–1.68	–	–	2.15
35Zn	0.95	0.74	0.41	0.22	–1.55	–1.76	–1.98	1.77
35Zn[a]	–	–	0.63	0.28	–1.59	–1.92	–2.11	1.87
36Zn	–	–	0.67	0.32	–1.52	–1.83	–2.00	1.84
37Zn	–	0.82	0.57	0.17	–1.64	–2.00	–	1.81
ZnP	–	–	0.66	0.28	–1.85	–	–	2.13

[a] In the presence of pyridine.

Redox potentials were determined by DPV. Solvent: CH$_2$Cl$_2$; scan rate: 0.05 V s^{-1}; working electrode: glassy carbon; reference electrode: Ag/Ag$^+$ (0.01 M AgNO$_3$); electrolyte: 0.1 M *n*-Bu$_4$NPF$_6$.

2-6. Theoretical Calculations

To obtain further insight into the structural and electronic properties of **35M–37M**, we performed density functional theory (DFT) calculations at the B3LYP/6-31G(d,p) level of theory. The optimized structures of **35M–37M** adopted their highly planar conformations (Figures 2-13–15). Because the C–C bond lengths on the phosphole-fused structure are almost identical for all the porphyrins, the oxidation state of the phosphorus atom has little impact on the ground-state geometries. The orbital distributions of HOMO are delocalized over the porphyrin and phosphole moieties, while those of LUMO are significantly localized on the porphyrin core (Figures 2-16–18). We also simulated ^{1}H chemical shifts and nucleus-independent chemical shifts (NICS)[89] values for the optimized structures (Figures 2-19). The simulated ^{1}H chemical shifts at the 7-position of **37M** (8.56–8.98 ppm) show upfield shifts relative to those of the corresponding **35M** and **36M** (8.92–9.40 ppm), which are in parallel with the ^{1}H NMR spectra. Additionally, the NICS value at the center of the porphyrin macrocycle for **37H₂** (–12.50 ppm) is more positive than those for **35H₂** (–12.83 ppm) and **36H₂** (–12.97 ppm). Besides, the NICS values at the five-membered ring between the porphyrin and phosphole rings for **37M** (7.44–8.02 ppm) are more positive than those for **35M** and **36M** (2.97–3.81 ppm). These theoretical calculations also support the contribution of 24π antiaromatic character in **37M**.
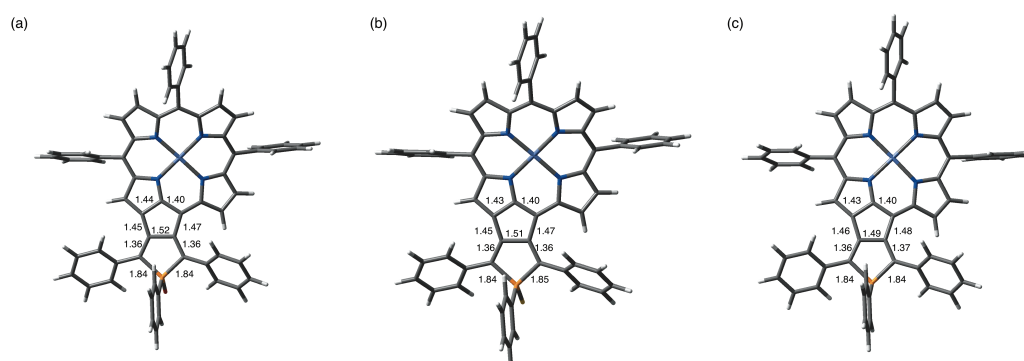
Figure 2-13. Optimized structures of (a) **35Ni**, (b) **36Ni**, and (c) **37Ni**. Selected bond lengths are indicated in Å. *tert*-Butyl groups are omitted for clarity.
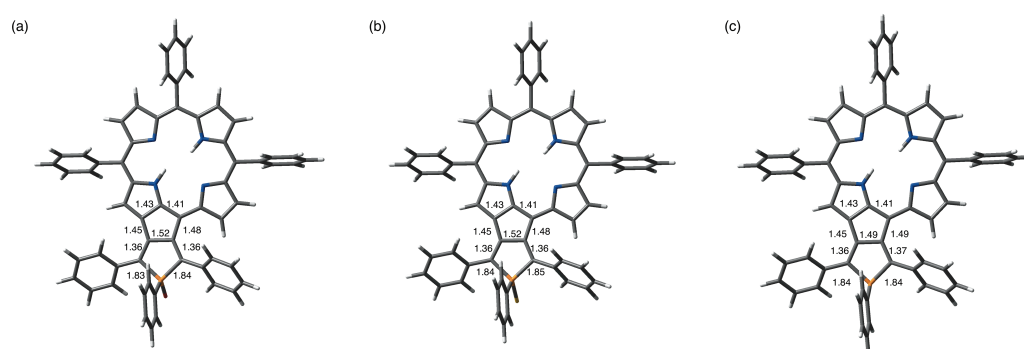
Figure 2-14. Optimized structures of (a) **35H$_2$**, (b) **36H$_2$**, and (c) **37H$_2$**. Selected bond lengths are indicated in Å. *tert*-Butyl groups are omitted for clarity.
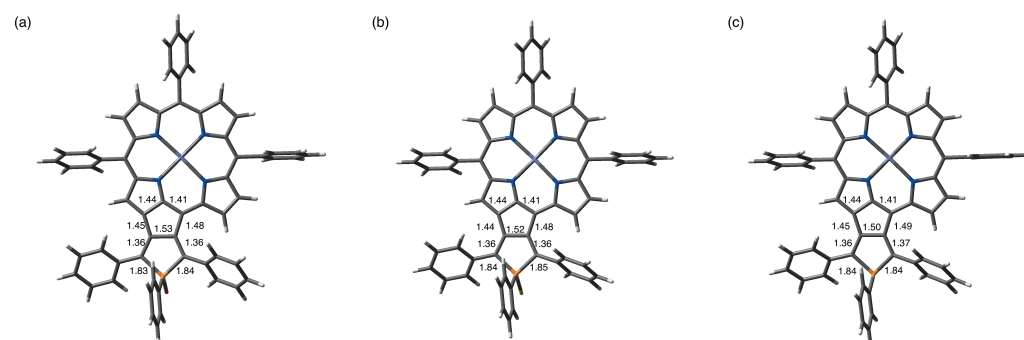
Figure 2-15. Optimized structures of (a) **35Zn**, (b) **36Zn**, and (c) **37Zn**. Selected bond lengths are indicated in Å. *tert*-Butyl groups are omitted for clarity.
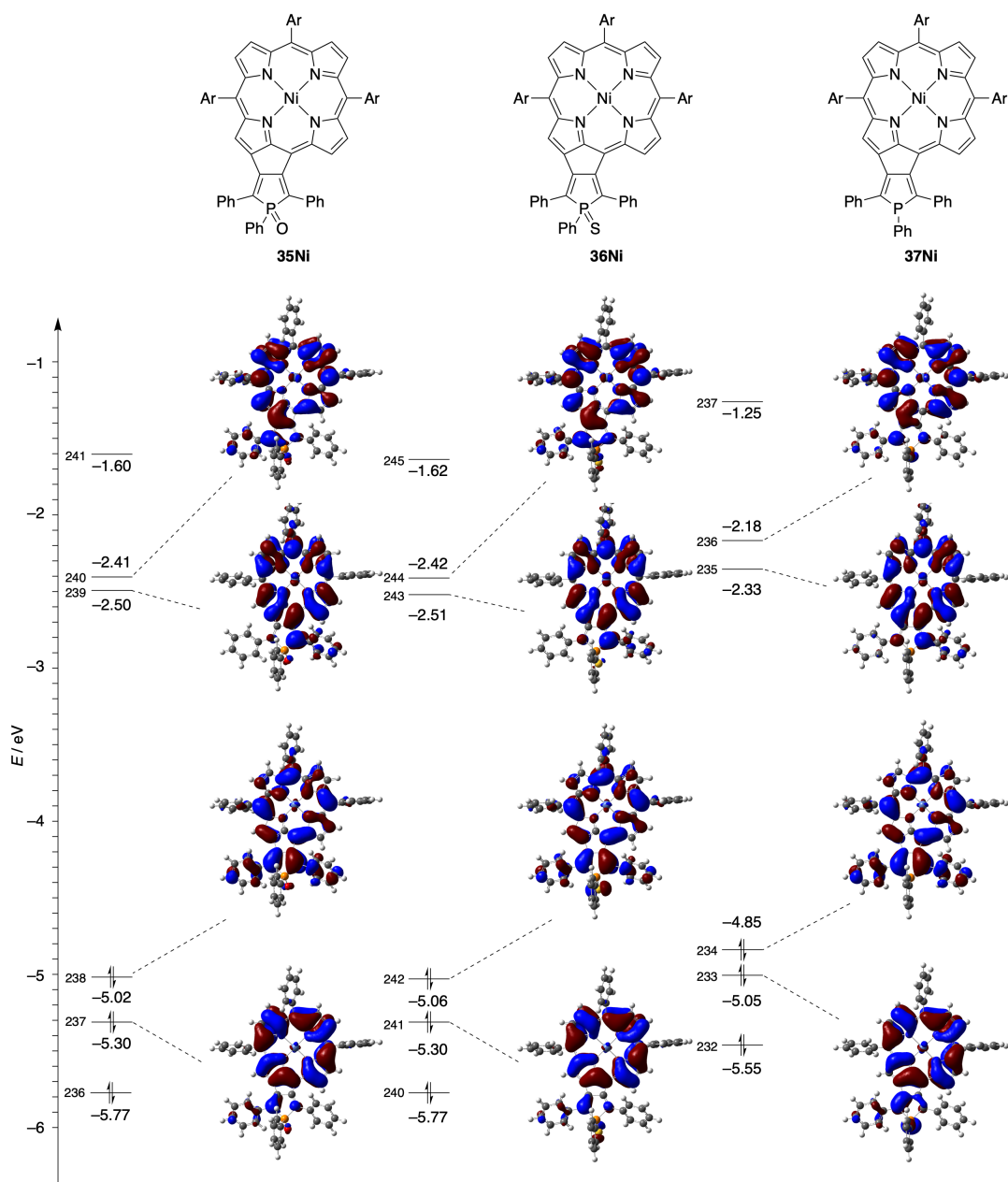
Figure 2-16. Selected Kohn-Sham orbitals of **35Ni**, **36Ni**, and **37Ni**.
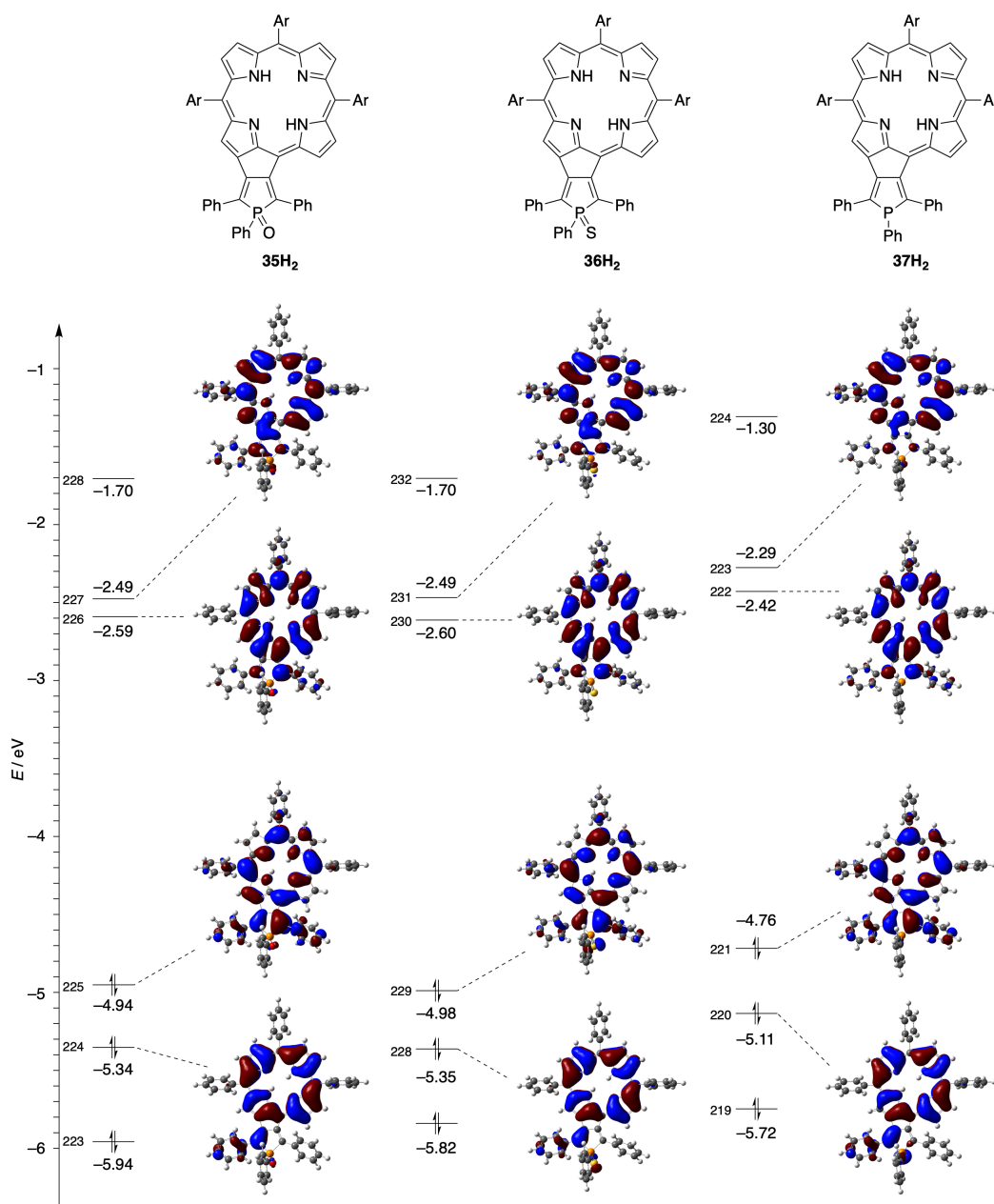
Figure 2-17. Selected Kohn-Sham orbitals of **35H₂**, **36H₂**, and **37H₂**.
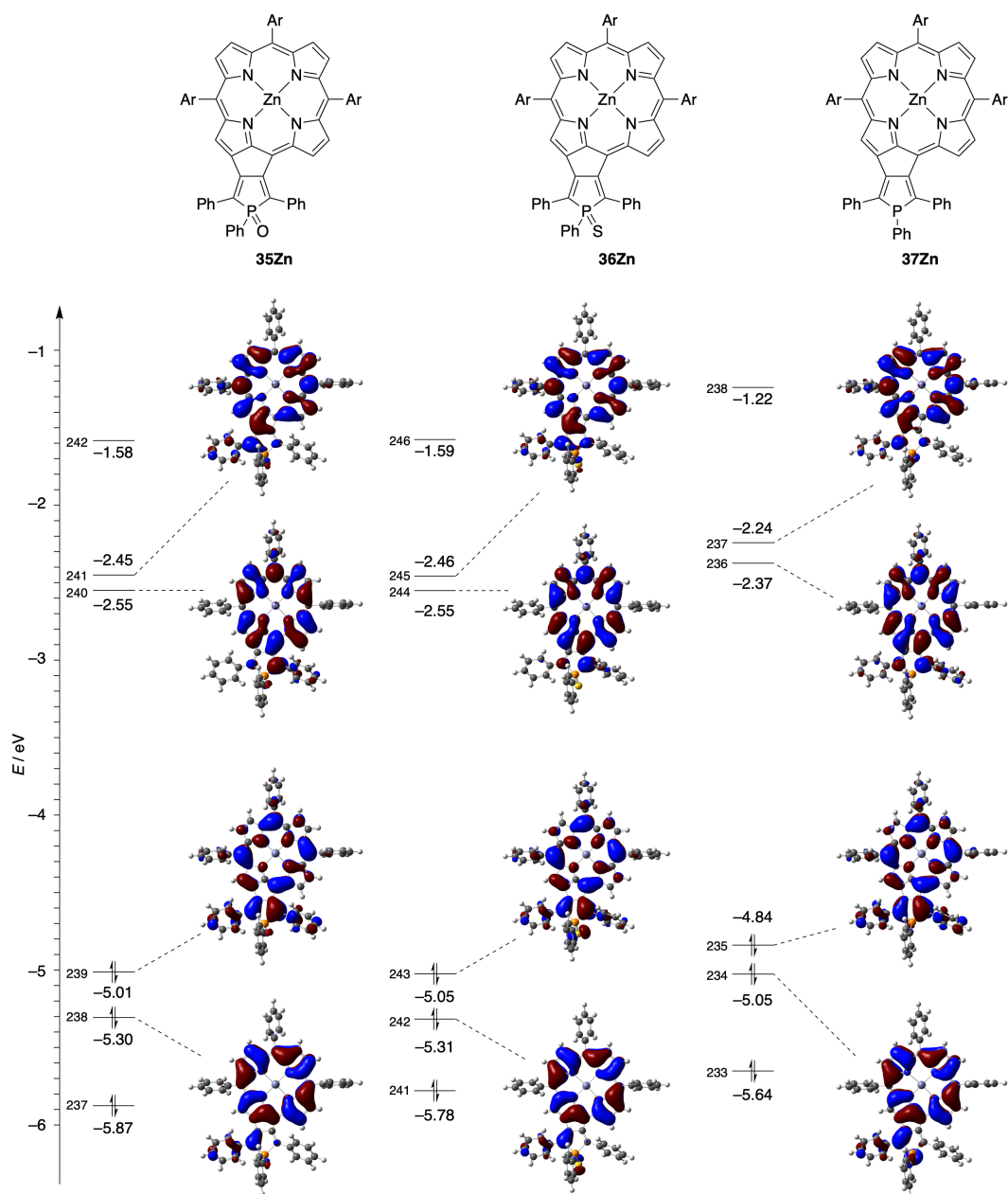
Figure 2-18. Selected Kohn-Sham orbitals of **35Zn**, **36Zn**, and **37Zn**.

(a)

position	NICS (ppm)	1H	δ (ppm)
1	−9.62	2	8.53
2	−1.32	3	9.02
3	2.97	7	9.02
4	−6.68	12	8.89
5	−5.65	13	8.25
6	−5.96	17	8.89
7	−5.96	18	9.02

(b)

position	NICS (ppm)	1H	δ (ppm)
1	−9.61	2	8.53
2	−1.17	3	8.97
3	3.50	7	8.92
4	−6.45	12	8.47
5	−5.78	13	8.20
6	−5.94	17	8.88
7	−6.02	18	8.99

(c)

position	NICS (ppm)	1H	δ (ppm)
1	−9.41	2	8.40
2	−0.42	3	8.83
3	7.44	7	8.56
4	−3.98	12	8.56
5	−5.79	13	8.09
6	−5.85	17	8.74
7	−6.18	18	8.87

(d)

position	NICS (ppm)	1H	δ (ppm)
1	−9.60	2	8.44
2	−0.89	3	8.63
3	3.26	7	9.39
4	−12.83	12	8.54
5	−0.78	13	8.10
6	−12.71	17	8.72
7	−3.18	18	8.76
8	−12.83	22	−2.69
		24	−2.69

(e)

position	NICS (ppm)	1H	δ (ppm)
1	−9.55	2	8.47
2	0.70	3	8.63
3	3.81	7	9.28
4	−12.78	12	8.03
5	−1.12	13	8.09
6	−12.74	17	8.73
7	−3.19	18	8.78
8	−12.97	22	−2.96
		24	−4.47

(f)

position	NICS (ppm)	1H	δ (ppm)
1	−9.41	2	8.34
2	0.00	3	8.52
3	7.76	7	8.98
4	−10.73	12	8.26
5	−1.14	13	7.99
6	−12.57	17	8.59
7	−3.49	18	8.65
8	−12.50	22	−2.57
		24	−3.90

(g)

position	NICS (ppm)	1H	δ (ppm)
1	−9.59	2	8.72
2	−1.23	3	8.87
3	3.14	7	9.40
4	−8.99	12	8.74
5	−6.63	13	8.38
6	−8.20	17	8.75
7	−7.35	18	8.87

(h)

position	NICS (ppm)	1H	δ (ppm)
1	−9.50	2	8.73
2	−1.00	3	8.87
3	3.73	7	9.30
4	−8.81	12	8.13
5	−7.11	13	8.35
6	−8.17	17	8.75
7	−7.32	18	8.87

(i)

position	NICS (ppm)	1H	δ (ppm)
1	−9.39	2	8.58
2	0.08	3	8.71
3	8.02	7	8.90
4	−6.22	12	8.38
5	−6.78	13	8.23
6	−8.08	17	8.61
7	−7.58	18	8.73

Figure 2-19. NICS values and simulated ^{1}H chemical shifts of (a) **35Ni**, (b) **36Ni**, (c) **37Ni**, (d) **35H₂**, (e) **36 H₂**, (f) **37 H₂**, (g) **35Zn**, (h) **36Zn**, and (i) **37Zn**.

2-6. Summary

We established the titanium-mediated [2+2+1] cyclization strategy to obtain versatile phosphole-fused dehydropurpurins **35M**–**37M** as the first example of cyclizations of porphyrins with a large π-system using low-valent metal species. The systematic investigations on the electronic properties of the dehydropurpurins revealed their unique features owing to the oxidation states of the phosphorus atom on the fused phosphole ring. The dehydropurpurins exhibited remarkably broad and red-shifted absorptions because of the perturbation of the electronic structures by the fused phosphole. The phosphole P=O and P=S derivatives **35M** and **36M** were found to possess high electron-accepting character derived from phosphorus(V) centers without the contribution of 24π antiaromatic character, suggesting their potential utility as electron-accepting materials. In contrast, the phosphorus(III) derivatives **37M** revealed different optical and electrochemical properties arising from both 18π aromatic and 24π antiaromatic networks including the lone-pair of the phosphorus(III) atom. Overall, the oxidation state of the phosphorus atom has a clear impact on the electronic properties, demonstrating the advantages of chemical modifications of the phosphorus center for creating an exotic π-system. We believe that application of titanium-mediated [2+2+1] cyclization to porphyrins is highly promising for expanding a world of heterole-fused porphyrinoids as well as phosphole-fused porphyrins.

Chapter 3. Unique Role of Heterole-fused Structures in Aromaticity and Physicochemical Properties of 7,8-Dehydropurpurins

24π weak antiaromatic   *heterole-fused structure*   24π antiaromatic
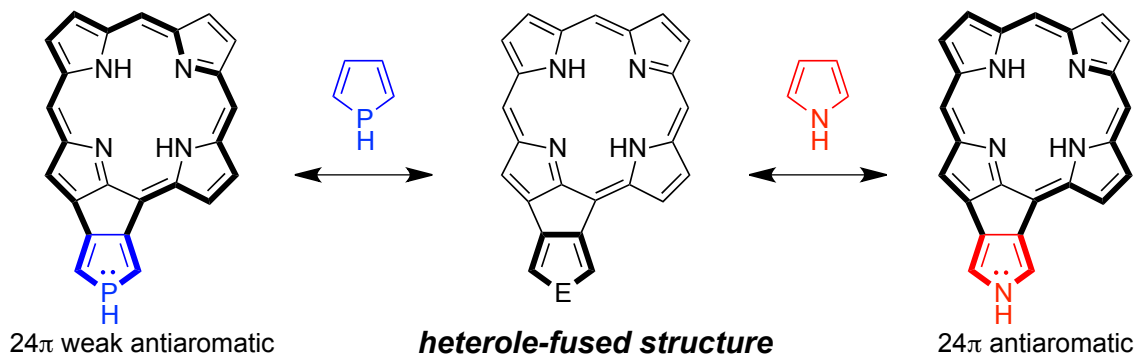
Contents

3-1. Introduction

Aromaticity in organic compounds gives a basis of understanding their energetic stability and electronic properties of cyclic π-conjugated molecules. In particular, porphyrins are 18π-aromatic azaannulenes that have been actively studied in various fields. [32f,74d,90] In recent years, peripherally fused porphyrin derivatives have attracted much attention because of their characteristic physical and electronic properties originated from extended and planar π-conjugations.[34d,63,61,74a–e,83b] Among them, porphyrins with a fused five-membered ring such as 7,8-dehydropurpurins have appeared as an emerging class of unique porphyrinoids. [58,75,76a–f,91] Their altered absorption spectra, relatively short lifetimes of excited states, and small HOMO-LUMO gaps arise from the harmony of antiaromatic 20π-circuit and aromatic 18π-circuit (Figure 3-1a).[75] In this regard, aromatic-fused 7,8-dehydropurpurins have also been synthesized. They exhibited weakened aromatic character caused by the larger contribution of antiaromatic 24π-circuit than aromatic 18π-circuit (Figure 3-1b).[58,76a–f,92] We successfully synthesized phosphole-fused 7,8-dehydropurpurins *via* titanium-mediated [2+2+1] cyclization strategy. The oxidation state of the phosphorus atom was found to have a clear influence on the aromatic character and the resultant whole electronic properties.[93] Namely, phosphorus(III) derivatives **37M** showed both contributions of aromatic 18π-circuit and antiaromatic 24π-circuit in their electronic structures, whereas the corresponding phosphorus(V) (P=O) derivatives **35M** revealed contribution only from aromatic 18π-circuit (Figures 3-1c,d). In this context, we expected that the electronic properties of 7,8-dehydropurpurins could be controlled by modulating the contribution of antiaromatic 24π-circuit. However, it would be difficult to enhance the contribution of antiaromatic 24π-circuit in phosphole-fused 7,8-dehydropurpurins. The lone pair of phosphorus atom in the phosphole system cannot be delocalized efficiently with the cyclopentadiene moiety owing to the pyramidal geometry of the phosphorus atom. [70d–f] Then, we noticed that replacement of the phosphole ring with a pyrrole one in phosphole-fused 7,8-dehydropurpurins would be the best option to achieve this goal. Considering the planar conformation of a pyrrole, the lone pair of the nitrogen atom would interact with the cyclopentadiene moiety effectively, enhancing the contribution of antiaromatic 24π-circuit in the whole electronic structure (Figure 3-1e). Here we report the comparison of pyrrole- and phosphole-fused 7,8-dehydropurpurins in terms of their aromaticity and physicochemical properties. We designed and synthesized pyrrole-fused dehydropurpurins **42M** *via* [2+2+1] cyclization strategy. The systematic investigation on heterole-fused dehydropurpurins **35M**, **37M**, and **42M** together with their theoretical calculations revealed the explicit impact of

heteroatoms in the heterole-fused structures on their aromaticity and physicochemical properties.
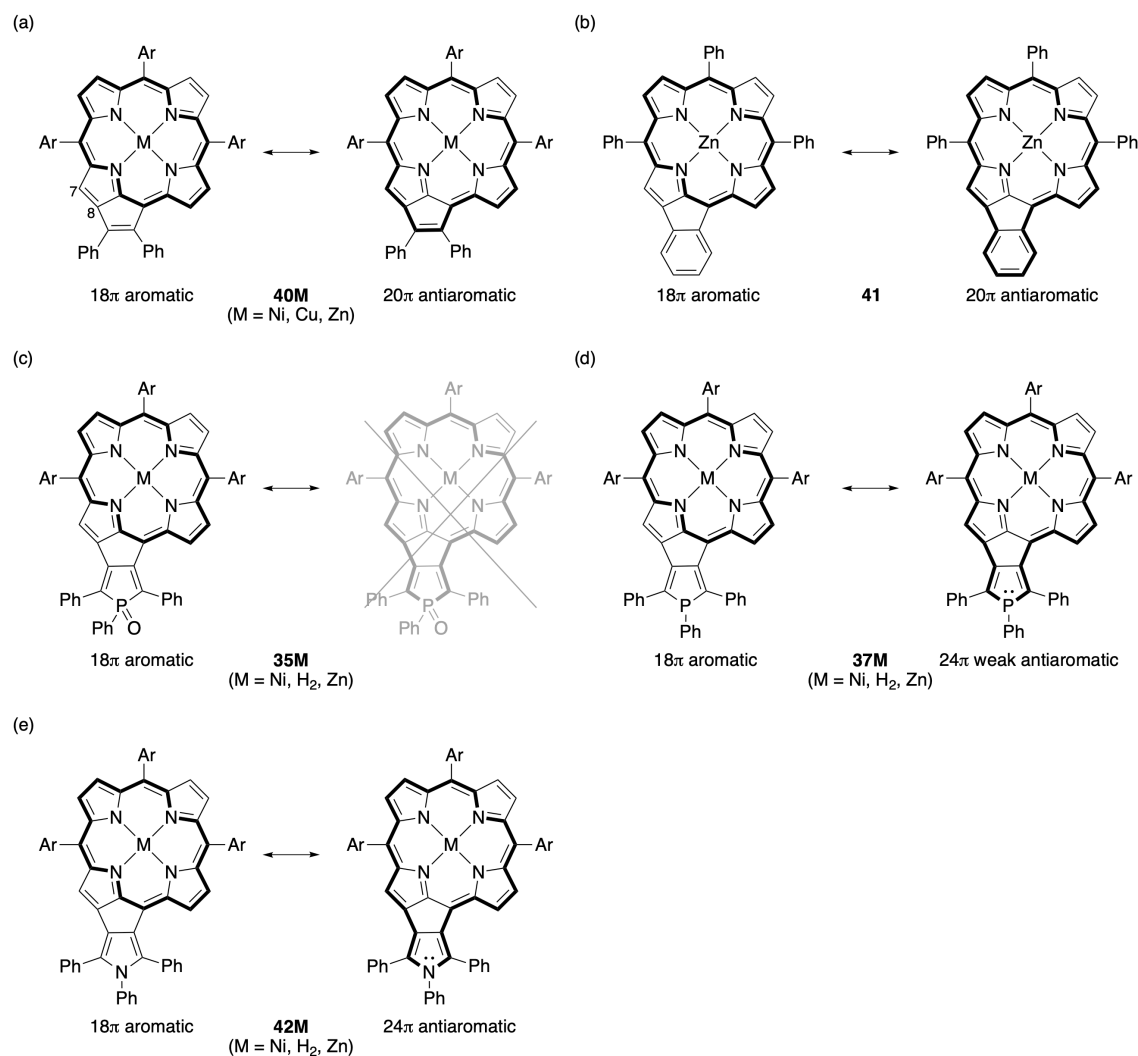
Figure 3-1. Examples of 7,8-dehydropurpurins with resonance structures: (a) 7,8-dehydropurpurins **40M**; (b) benzene-fused 7,8-dehydropurpurin **41**; (c) and (d) phosphole-fused 7,8-dehydropurpurins **35M** and **37M**; (e) pyrrole-fused 7,8-dehydropurpurins **42M**. Ar = 3,5-di-*tert*-butylphenyl.

3-2. Synthesis

The [2+2+1] cyclization of 1,6-diynes are effective means to obtain heteroles with a five-membered ring. In line with this, we attempted the [2+2+1] cyclization of 3,5-bis(phenylethynyl)-porphyrin **34Ni**[93]. The reaction of **34Ni** with aniline in the presence of PdCl₂ and triethylamine under air afforded pyrrole-fused dehydropurpurin **42Ni** in 67% yield (Scheme 3-1).[94] We also tried the same reactions for the corresponding zinc porphyrin **42Zn**, but could not obtain the corresponding pyrrole-fused dehydropurpurin due to instability for **42Zn** under aerobic conditions. Fortunately, demetalation of **34Ni** with sulfuric acid in trifluoroacetic acid provided free-base dehydropurpurin **42H₂**. Then, the treatment of **42H₂** with Zn(OAc)₂·2H₂O under argon atmosphere furnished zinc dehydropurpurin **42Zn**. All the new compounds were fully characterized by using ¹H and ¹³C NMR, high-resolution mass spectrometry, and FT-IR (Experimental Section). Compared to the nickel dehydropurpurin **42Ni**, free-base and zinc dehydropurpurins **42H₂** and **42Zn** are less stable in solution under ambient condition. Although **42H₂** and **42Zn** are stable in the dark under O₂ atmosphere, they gradually decomposed to a complicated mixture under room light and air atmosphere. Osuka and co-workers also reported that non-fused dehydropurpurin **40Zn** could be oxidized under ambient conditions.[75b] To the best of our knowledge, there is no report on decomposition by photochemical oxidation of aromatic-fused dehydropurpurins. The photooxidative decomposition under ambient conditions for **42H₂** and **42Zn** suggests the large contribution of antiaromatic character and electron-donating nature derived from the pyrrole-fused structure.
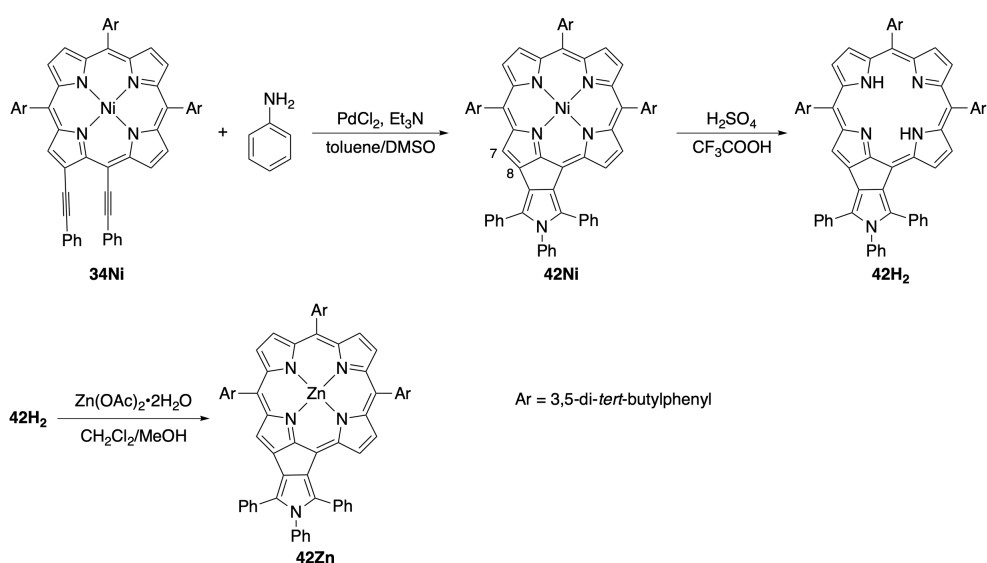
Scheme 3-1. Synthesis of pyrrole-fused dehydropurpurins **42M**.

3-3. X-Ray Crystal Structure

Fortunately, single crystals suitable for X-ray diffraction analysis were obtained by vapor diffusion of acetonitrile into a $CHCl_3$ solution of **42Ni** (Figures 3-2). The crystal structure clearly shows the presence of the pyrrole-fused five-membered ring structure. It is noteworthy that the C8'–C10' bond length (1.447(7) Å) is almost identical to those of benzene-fused dehydropurpurin **41** (ca. 1.44 Å),[76e] but it is still longer than those of non-fused dehydropurpurins **40M** (ca. 1.38 Å).[90a] Nevertheless, it is obviously shorter than that of the phosphorus (V) derivative of phosphole-fused dehydropurpurins (ca. 1.52 Å).[93] The short C8'–C10' bond length suggests a moderate contribution of C=C double bond-like character. Therefore, the fused pyrrole ring affects the structure of the neighboring five-membered ring moiety.
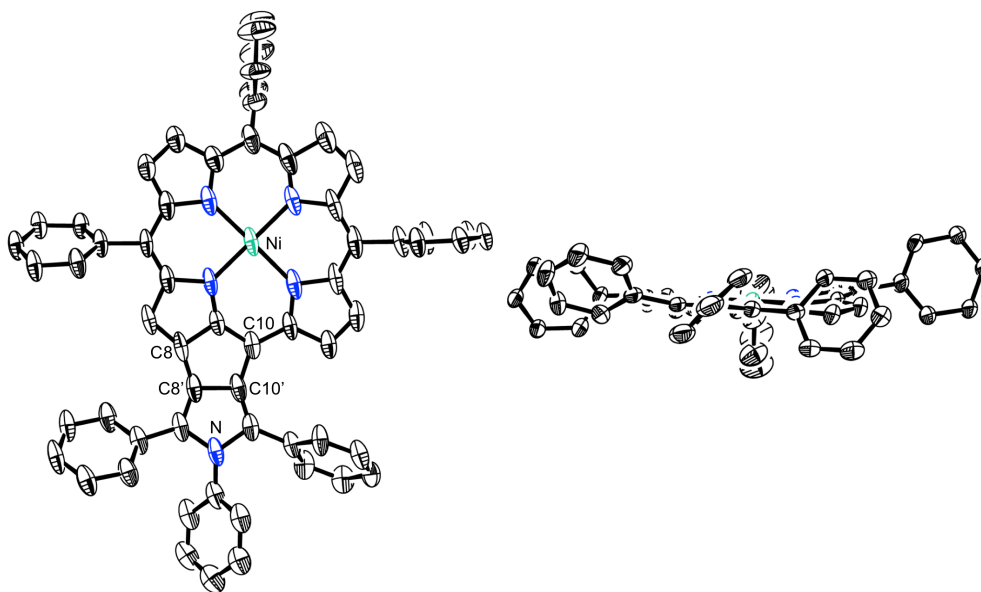
Figure 3-2. X-Ray crystal structure of **42Ni**: top view (left) and side view (right). Thermal ellipsoids represent 50% probability. *tert*-Butyl groups, all hydrogen atoms, solvent molecules, and minor disorder components are omitted for clarity.

3-4. ^{1}H NMR Spectra

The ^{1}H NMR spectroscopy is one of the most useful experimental methods for evaluating aromaticity. The ^{1}H NMR spectra of **42M** display signals from the β-proton at the 7-position in the range of $δ$ = 8.11–7.76 ppm (Experimental Section). These signals are markedly shifted to the upfield region relative to those of phosphole-fused dehydropurpurins **35M** ($δ$ = 9.4–9.2 ppm) and **37M** ($δ$ = 9.0–8.8 ppm).[93] For free-base dehydropurpurins **35H₂**, **37H₂**, and **42H₂**, the signals of the inner NH protons as well as β-protons are the best measure to assess the aromaticity (Figure 3-3). The signals from the inner NH protons of **35H₂**, **37H₂**, and **42H₂** are moved downfield in the order **35H₂** (–1.19 and –2.08 ppm) < **37H₂** (–0.62 and –1.69 ppm) < **42H₂** (0.76 and –0.59 ppm). This tendency is consistent with the upfield shift of the signals of the β-protons in the same order. Therefore, the aromatic diatropic ring current effect on the heterole-fused dehydropurpurins decreases in the order **35M** > **37M** > **42M**. As we expected, the contribution of the antiaromatic 24π-circuit in **42M** is enhanced by effective interaction with the lone-pair of the nitrogen atom, whereas the lone-pair of the phosphorus(III) atom in **37M** cannot interact effectively with the antiaromatic 24π-circuit because of its trigonal geometry. Therefore, these ^{1}H NMR spectroscopic data exemplify that the heteroatoms in the heterole-fused structures have a large impact on the whole aromaticity of dehydropurpurins.
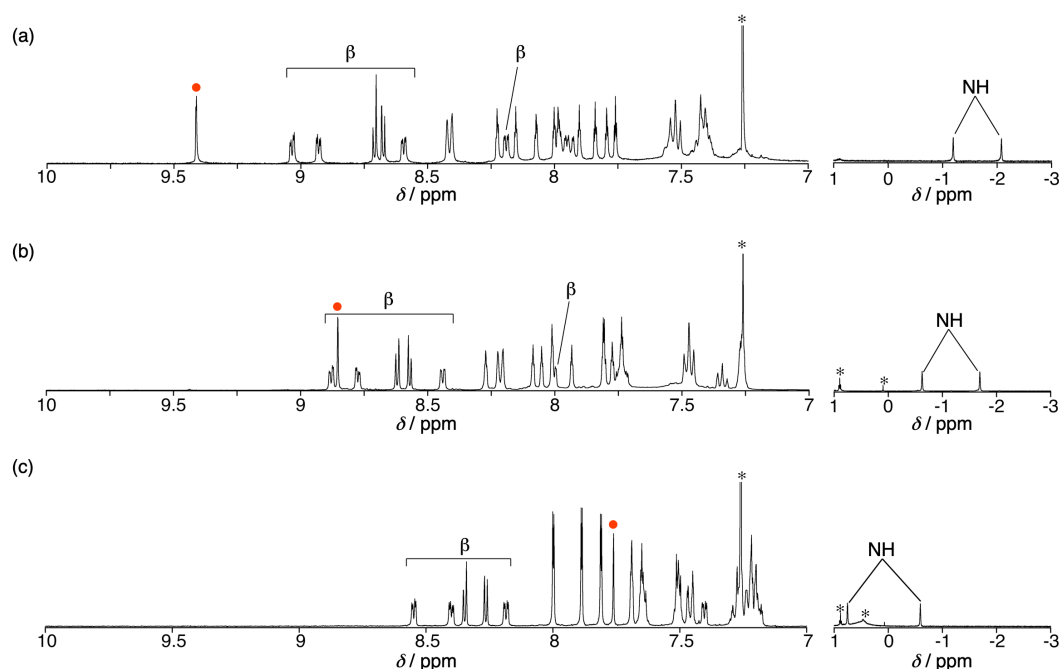
Figure 3-3. The ^{1}H NMR spectra of a) **35H₂**, b) **37H₂**, and c) **42H₂** in CDCl₃ at 25 °C. Red dots represent the signals of the β-protons at the 7-positions. The signals marked with * arise from residual solvents.

3-5. Optical Properties

The UV/vis/NIR absorption spectra and fluorescence spectra of **42M** were measured in CH$_2$Cl$_2$ (Figure 3-4a, Table 3-1) to compare to those of phosphole-fused dehydropurpurins **35H$_2$** and **37H$_2$** (Figure 3-4b). The solutions of **42H$_2$** and **42Zn** were bubbled with argon during the measurements to avoid photooxidative decompositions. The absorption spectra of **42M** exhibit substantially different shape from the phosphole-fused dehydropurpurins as well as typical aromatic porphyrins. They show split Soret bands at 450–500 nm and ill-defined Q bands at 550–800 nm. These spectral features are similar to antiaromatic porphyrinoids,[95] suggesting the considerable contribution of antiaromatic character to the electronic structures. The lowest energy Q-band of **42H$_2$** (751 nm) is shifted to the long wavelength region than those of **35H$_2$** and **37H$_2$** (692 and 705 nm). In addition, **42H$_2$** and **42Zn** show weak fluorescence at 764 and 732 nm. The fluorescence peak of **42H$_2$** (764 nm) is also moved to the long wavelength compared to **35H$_2$** and **37H$_2$** (707 and 719 nm). The fluorescence lifetimes (τ) of the free-base and zinc dehydropurpurins were measured by the time-correlated single photon counting (TCSPC) technique (Figure 3-5). The lifetimes of phosphorus(V) derivatives **35H$_2$** and **35Zn** were determined to be 5.3 and 2.7 ns, respectively, which agree with their moderate fluorescence quantum yields (0.13 for **35H$_2$** and 0.14 for **35Zn**).[93] On the other hand, the lifetimes of phosphorus(III) derivatives **37H$_2$** (τ = 2.6 ns) and **37Zn** (τ = 1.2 ns) were approximately half of those of **35H$_2$** and **35Zn**. Notably, the lifetimes of **42H$_2$** (τ = 0.4 ns) and **42Zn** (τ < 0.2 ns) are one order of magnitude shorter than those of **37H$_2$** and **37Zn**. Overall, the fluorescence lifetime decreases in the order **35M** > **37M** > **42M**. The short-lived excited states of **42M** may reflect the large contribution of antiaromatic 24π-circuit to the electronic structures.
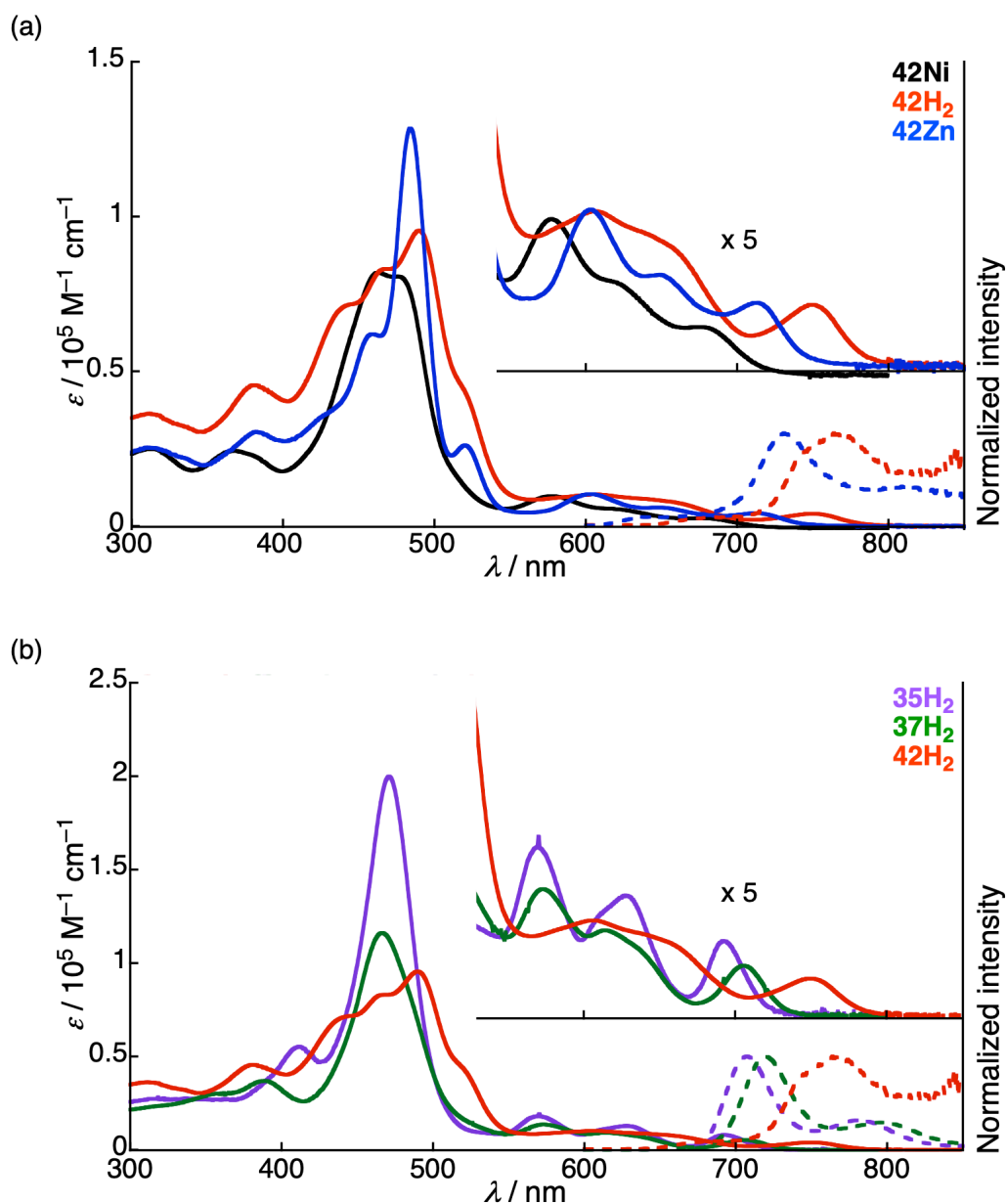
Figure 3-4. UV/Vis/NIR absorption (solid lines) and normalized fluorescence spectra (dashed lines) of (a) **42Ni** (black), **42H$_2$** (red), and **42Zn** (blue) and (b) **35H$_2$** (purple), **37H$_2$** (green), and **42H$_2$** (red) in CH$_2$Cl$_2$.in CH$_2$Cl$_2$. For fluorescence measurements, the samples were excited at wavelengths for Soret band maxima.
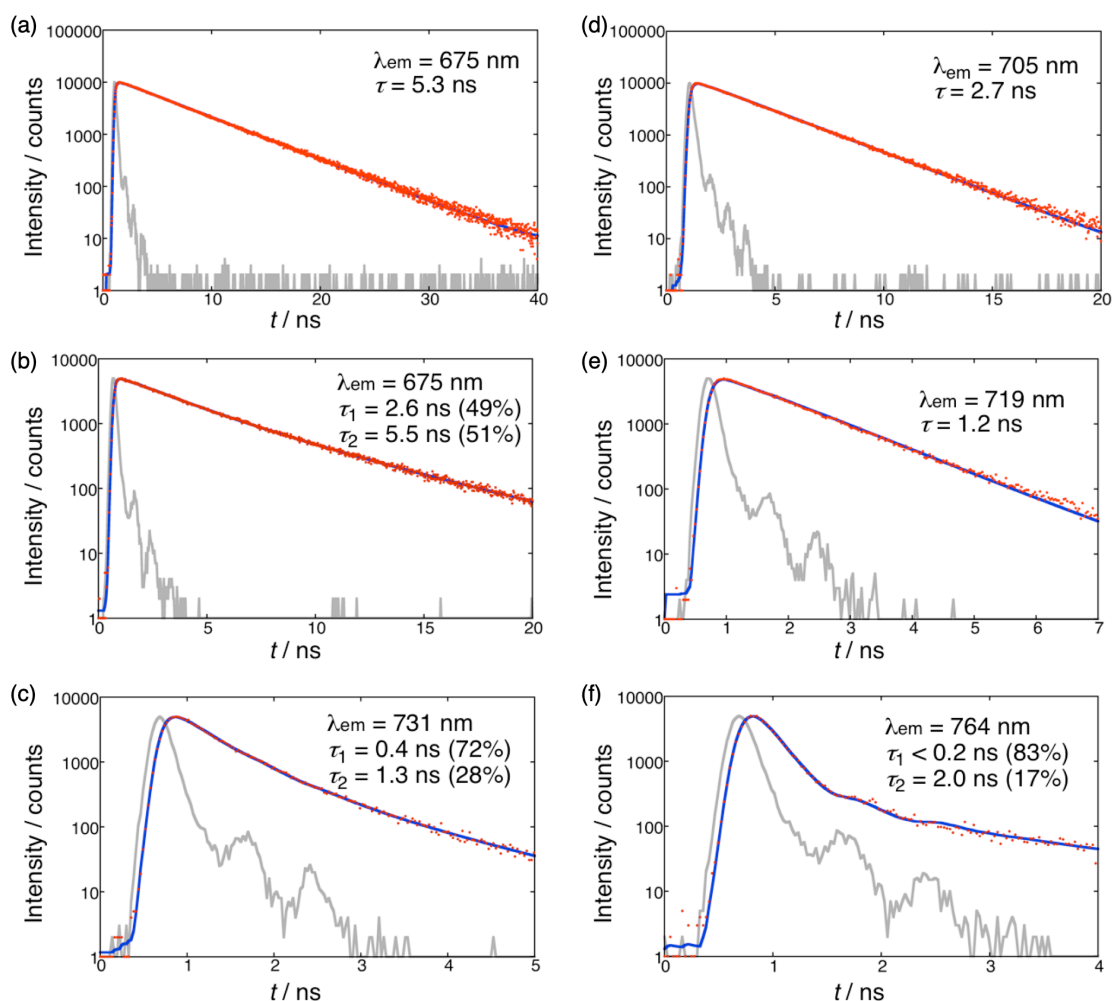
Figure 3-5. Fluorescence decays for (a) **35H₂**, (b) **37H₂**, (c) **42H₂**, (d) **35Zn**, (e) **37Zn**, and (f) **42Zn** in CH₂Cl₂. The samples were excited at wavelengths for Soret band maxima. The solid lines present decay fittings and the gray lines show the instrumental response function. The monitoring wavelengths (λ_{em}) and fluorescence lifetimes (τ) are given in the figures. For **35H₂**, the long-lived component (τ = 5.5 ns) may be attributed to the oxidized compound of **37H₂** (i.e., **35H₂**).

3-6. Electrochemical Properties

The electrochemical properties of **42M** were studied by cyclic voltammetry (CV) and differential pulse voltammetry (DPV) techniques in CH_2Cl_2 with n-Bu_4NPF_6 as an electrolyte (versus ferrocene/ferrocenium ion (Fc/Fc$^+$), (Figure 3-7 and Table 3-1). Irrespective of the metal ions in the cavity, two reversible oxidation peaks and one reversible reduction peak were observed. The first oxidation (E_{ox1}) and reduction (E_{red1}) potentials of **42H$_2$** were determined to be 0.17 and −1.59 V, respectively. These values are shifted to the negative direction compared to those of the corresponding phosphole-fused dehydropurpurins **35H$_2$** (E_{ox1} =0.55 V, E_{red1} = −1.34 V) and **37H$_2$** (E_{ox1} =0.35 V, E_{red1} = −1.49 V),[93] reflecting the electron-donating nature of the fused-pyrrole moiety. The electrochemical HOMO–LUMO gap ($E_g{}^{CV}$ = E_{ox1} − E_{red1}) decreases in the order **35H$_2$** (1.89 eV) > **37H$_2$** (1.84 eV) > **42H$_2$** (1.76 eV), which is in good agreement with the increasing contribution of the antiaromatic 24π-circuit to the electronic structures, as seen in the UV/vis/NIR absorption spectra.
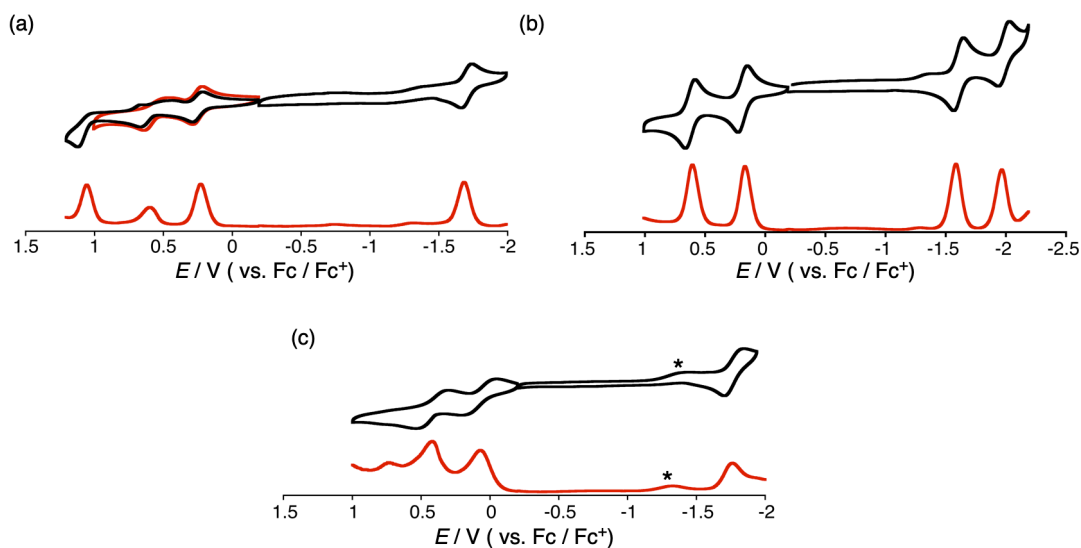
Figure 3-7. Cyclic voltammograms (black) and differential pulse voltammetry (DPV) curves (red) of dehydropurpurins (a) **42Ni**, (b) **42H$_2$**, and (c) **42Zn**. Redox potentials were determined by DPV. Solvent: CH$_2$Cl$_2$; scan rate: 0.05 V s^{-1}; working electrode: glassy carbon; reference electrode: Ag/Ag$^+$ (0.01 M AgNO$_3$); electrolyte: 0.1 M *n*-Bu$_4$NPF$_6$. Peaks marked with ∗ arise from oxygen.

Table 3-1. Electrochemical oxidation and reduction potentials of heterole-fused dehydropurpurins versus Fc/Fc$^+$.

	E_{ox3}	E_{ox2}	E_{ox1}	E_{red1}	E_{red2}	E_g^{CV}
42Ni	1.06	0.60	0.23	−1.67	–	1.91
42H$_2$	–	0.60	0.17	−1.59	−1.96	1.76
42Zn	–	0.42	0.07	−1.76	–	1.83
35H$_2$[a]	–	0.85	0.55	−1.34	−1.67	1.89
37H$_2$[a]	–	–	0.35	−1.49	−1.85	1.84

[a] Taken from ref[93].
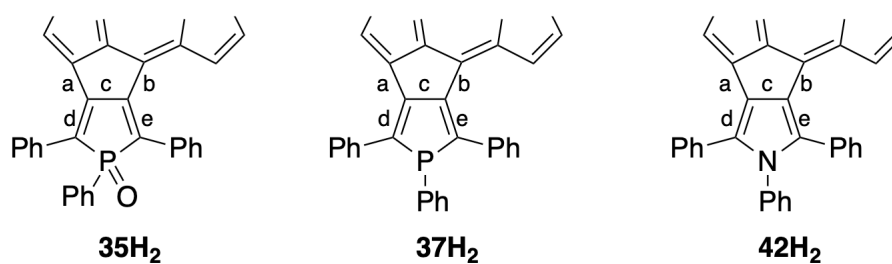
3-7. Theoretical Calculations

We performed density functional theory (DFT) calculations at B3LYP/6-31G(d,p) level to evaluate the effect of heterole-fused structure on the antiaromatic contributions to dehydropurpurins. We obtained the optimized structures of **35H₂**, **37H₂**, and **42H₂** with highly planar conformations. Because the orbital distributions of HOMO/HOMO–1 and LUMO/LUMO+1 for **35H₂**, **37H₂**, and **42H₂** are almost the same, the heteroatom on the heterole moiety has little impact on the molecular orbitals (Figure 3-8). The calculated excitation energies obtained from time-dependent DFT (TD-DFT) calculations on the optimized structures are consistent with the red-shifted absorption of **42H₂** relative to **35H₂** and **37H₂** (Figure 3-9). The selected bond lengths and Wiberg bond indices at the five-membered ring and heterole moieties are summarized in Table 3-2. The C–C bond length of **42H₂** at *c* (1.441 Å) is shorter than those of **35H₂** (1.522 Å) and **37H₂** (1.492 Å), which matches with the trend on the C8'–C10' bond lengths in crystal structures. The Wiberg bond index of C–C bond at *c* of **42H₂** (1.184) is explicitly larger than those of **35H₂** (1.008) and **37H₂** (1.067). In contrast, the C–C bond lengths at *d* and *e* of **42H₂** (1.377–1.380 Å) are longer than those of **35H₂** and **37H₂** (1.356–1.369 Å). The Wiberg bond indices also indicate the decrease of 1,3-butadiene character on the fused-pyrrole moiety. These structural features on the heterole moieties imply that the effective interaction of the fused-heterole moiety with the dehydropurpurin skeleton correlates with the contribution of antiaromatic 24π-circuit to the electronic structures.

We also calculated the ¹H chemical shifts and nucleus-independent chemical shifts (NICS)[89] values on the optimized structures for **35H₂**, **37H₂**, and **42H₂** (Figure 3-10). The calculated ¹H chemical shifts at the 7-position are shifted to upfield region in the order **35H₂** (9.39 ppm) > **37H₂** (8.97 ppm) > **42H₂** (8.03 ppm), which is in parallel with the trend on the ¹H NMR spectra. In addition, the NICS values at the five-membered ring between the porphyrin and fused-heterole moieties for **42H₂** (+14.82 ppm) are larger than those for **37H₂** (+7.76 ppm), which agrees with the enhanced contribution of antiaromatic 24π-circuit to the electronic structures. Consequently, the NICS values at the centers of the porphyrin macrocycles are moved to the positive direction in the order **35H₂** (–12.82 ppm) < **37H₂** (–12.50 ppm) < **42H₂** (–12.13 ppm). The less negative NICS value of **42H₂** indicates that the whole aromaticity is weakened by the increased contribution of antiaromatic 24π-circuit. Furthermore, we estimated the anisotropy of the induced current density (ACID) for **35H₂**, **37H₂**, and **42H₂**.[96] In the ACID plots, aromatic molecules show clockwise current density, whereas antiaromatic molecules exhibit counterclockwise current density. The ACID plots of **35H₂**, **37H₂**, and **42H₂** are depicted

in Figure 3-11. The clockwise current densities on the porphyrin macrocycles of **35H₂**, **37H₂**, and **42H₂** indicate that the heterole-fused dehydropurpurins are aromatic on the whole. It is noteworthy that the counterclockwise current density is evident on the five-membered ring between the porphyrin and fused-pyrrole moieties of **42H₂**. Although the ACID plot of **37H₂** shows the weak counterclockwise current density on the five-membered ring, that of **35H₂** reveals the almost no counterclockwise current density. Moreover, the ACID plot of **42H₂** visualizes the clear current density on the fused-pyrrole moiety, indicating a significant contribution of antiaromatic 24π-circuit to the whole aromaticity. For **37H₂**, the current density on the fused-phosphole moiety is slightly disrupted at the C–P bonds. In contrast, the ACID plot of **35H₂** displays severe disruption of the current density at the C–P bonds. Thus, these ACID plots also verify the contributions of antiaromatic 24π-circuit including the lone pair of the heteroatom in the heterole-fused structure to the whole aromaticity.

Table 3-2. Bond lengths and Wiberg bond indices of **35H₂**, **37H₂**, and **42H₂** on the optimized structures at B3LYP/6-31G(d,p) level.

	a	*b*	*c*	*d*	*e*
			bond length [Å]		
35H₂	1.444	1.479	1.522	1.356	1.360
37H₂	1.452	1.488	1.492	1.364	1.369
42H₂	1.452	1.489	1.441	1.377	1.380
			Wiberg bond index		
35H₂	1.100	1.097	1.008	1.650	1.667
37H₂	1.084	1.078	1.067	1.602	1.617
42H₂	1.078	1.064	1.184	1.459	1.500
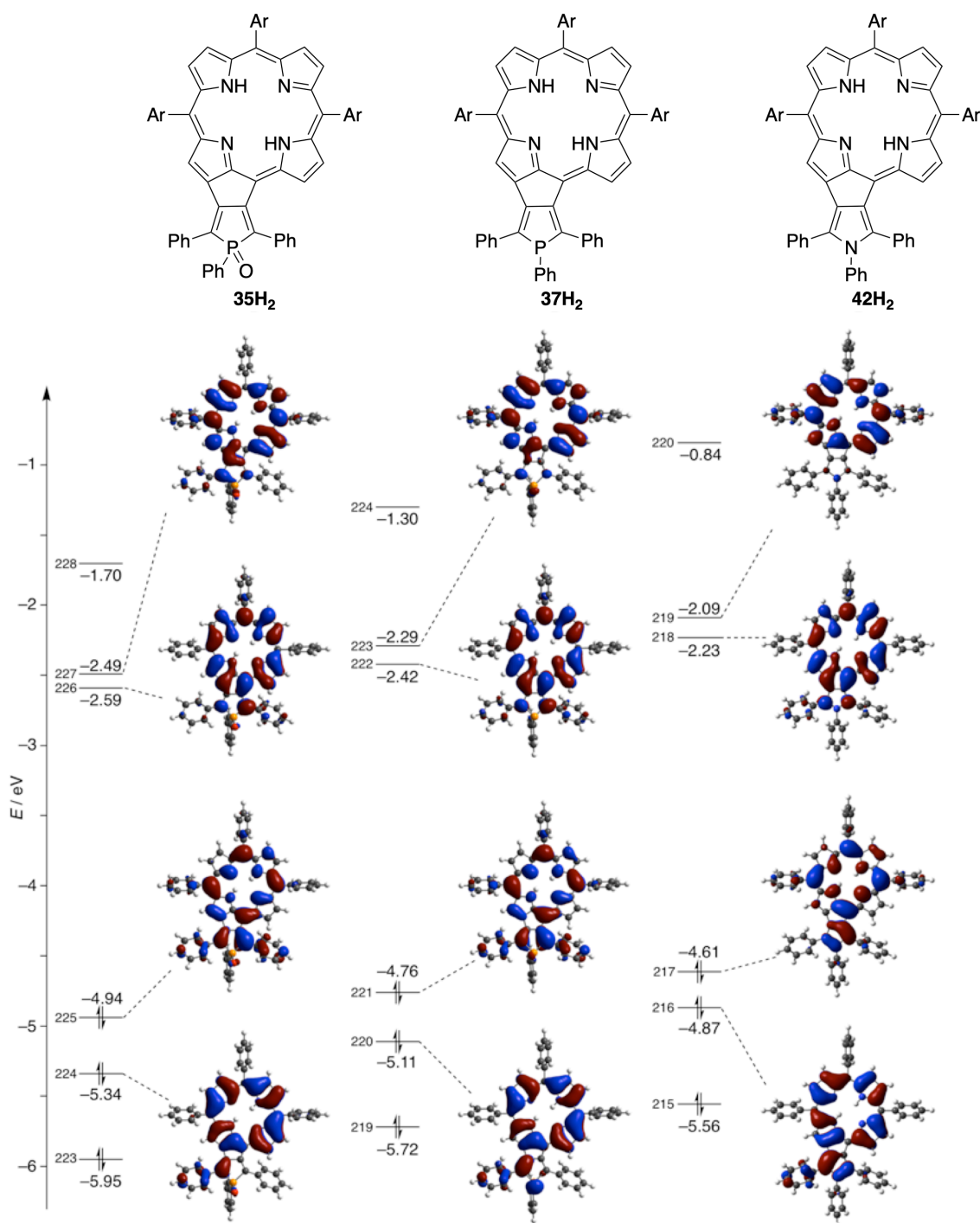
Figure 3-8. Selected Kohn-Sham orbitals of **35H₂**, **37H₂**, and **40H₂**.
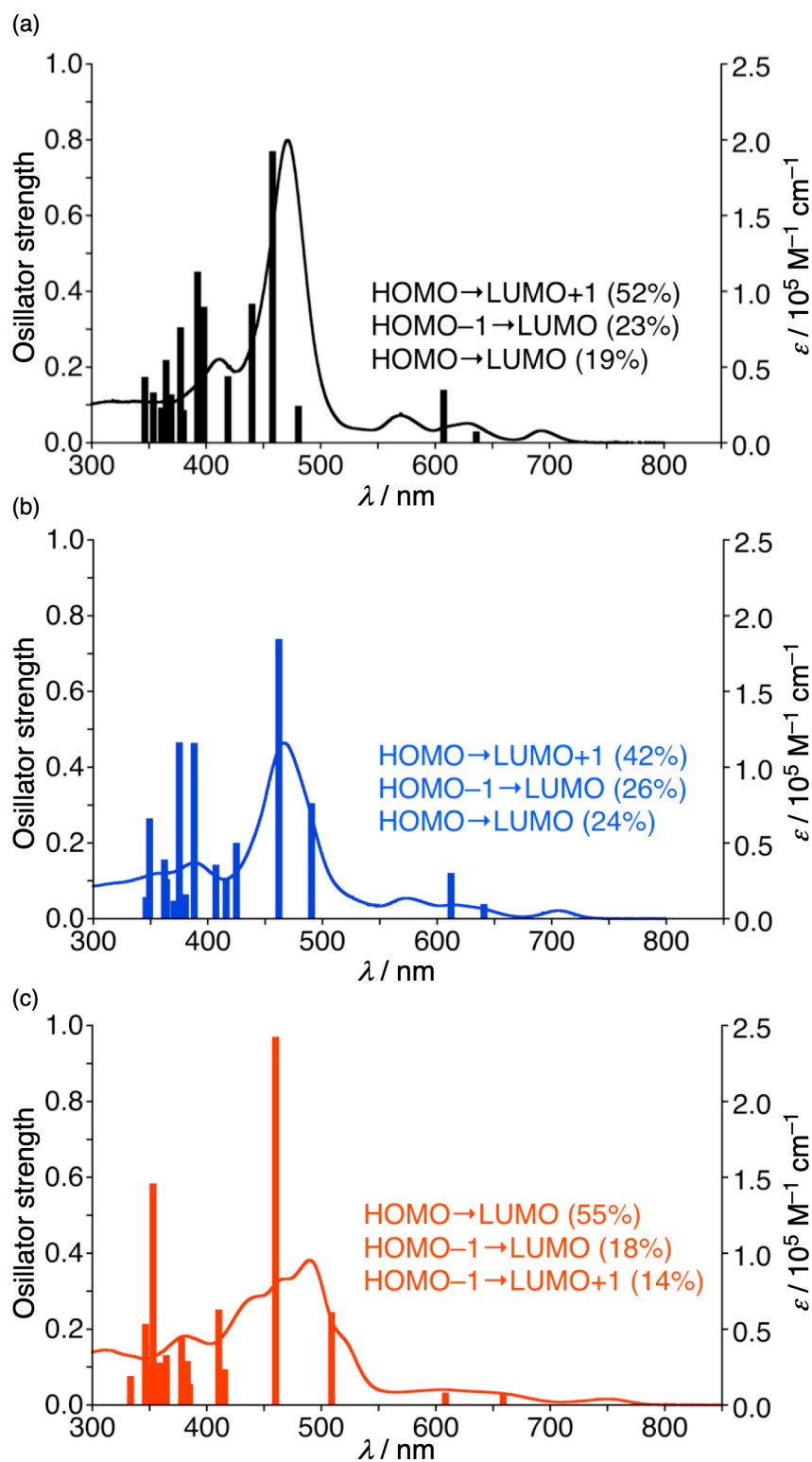
Figure 3-9. Calculated excitation energies with oscillator strengths and absorption spectra of (a) **35H₂**, (b) **37H₂**, and (c) **42H₂**. Excitation weights of the lowest excitation are indicated.

(a)

NICS / ppm	
1	−0.89
2	+3.26
3	−12.83
4	−15.41
5	−3.18
6	−15.69
7	−12.71
8	−15.53
9	−0.78
10	−16.07
11	−12.82
δ_{1H} / ppm	
2	8.44
3	8.63
7	9.39
12	8.54
13	8.10
17	8.72
18	8.76
22	−2.69
24	−4.29

(b)

NICS / ppm	
1	0.00
2	+7.76
3	−10.73
4	−14.97
5	−3.49
6	−15.19
7	−12.57
8	−15.06
9	−1.14
10	−16.06
11	−12.50
δ_{1H} / ppm	
2	8.33
3	8.51
7	8.97
12	8.26
13	7.99
17	8.59
18	8.65
22	−2.57
24	−3.90

(c)

NICS / ppm	
1	+0.19
2	+14.82
3	−6.22
4	−14.49
5	−3.89
6	−14.53
7	−12.34
8	−14.48
9	−2.34
10	−16.09
11	−12.13
δ_{1H} / ppm	
2	8.19
3	8.38
7	8.03
12	7.40
13	7.90
17	8.49
18	8.31
22	−2.28
24	−3.28

Figure 3-10. NICS values and simulated ^{1}H chemical shifts of (a) **35H₂**, (b) **37H₂**, and (c) **42H₂**.
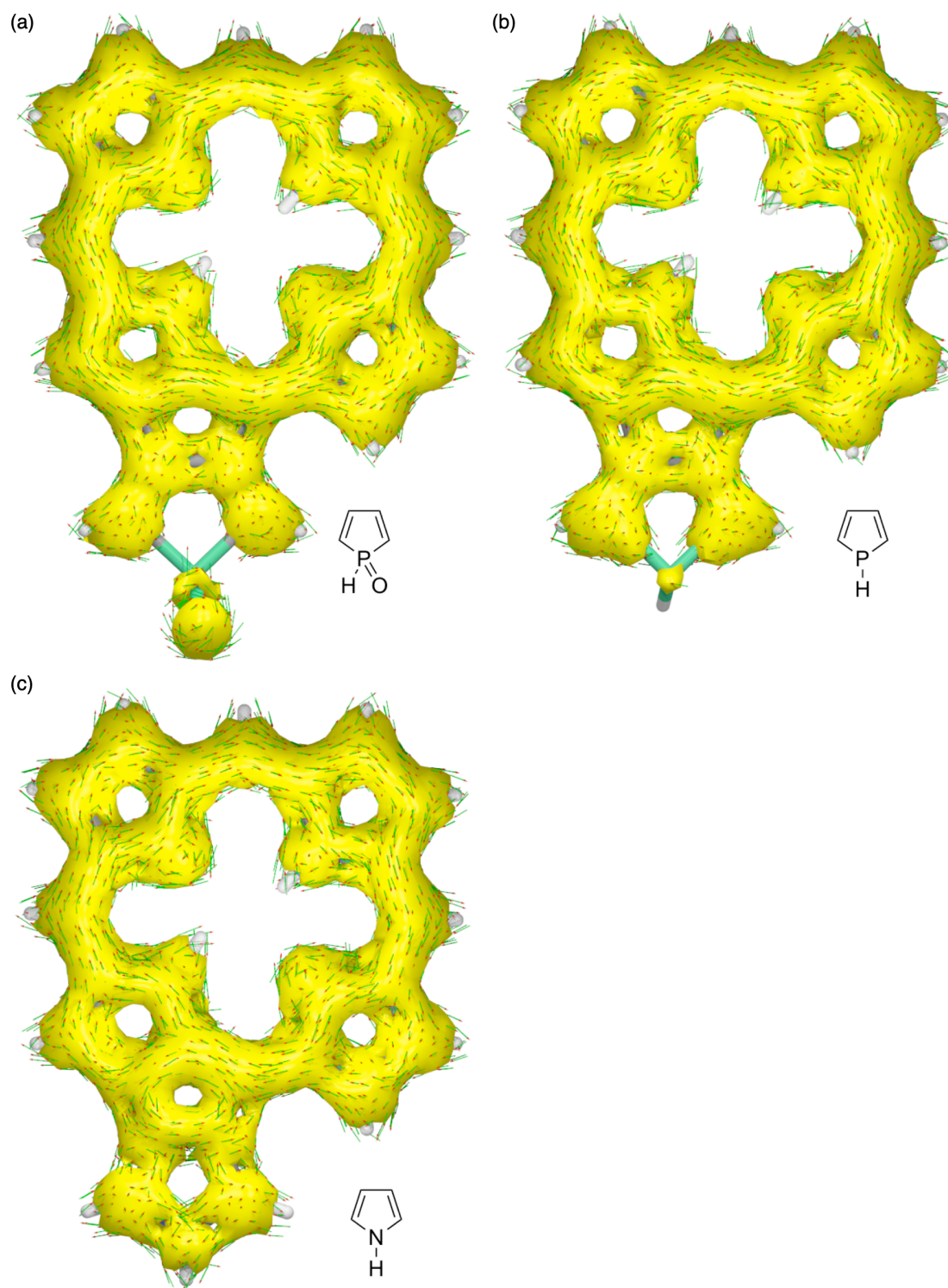
Figure 3-11. ACID plots for (a) **35H₂**, (b) **37H₂**, and (c) **42H₂** at an isosurface value of 0.04. The *meso*-aryl substituents and phenyl groups on the heterole moieties were replaced with hydrogen atoms for clarity.

3-8. Summary

We designed and synthesized pyrrole-fused 7,8-dehydropurpurins **42M** *via* palladium-catalyzed [2+2+1] cyclization and systematically investigated their aromaticity and physicochemical properties in comparison with phosphole-fused 7,8-dehydropurpurins **35M** and **37M**. The ^{1}H NMR spectroscopy revealed that **42M** exhibited upfield-shifted signals of the β-protons and downfield-shifted signals of the inner NH protons. The weakened aromatic diatropic ring current effect on **42M** is attributed to the large contribution of antiaromatic 24π-circuit to the whole electronic structure. The absorption spectra of **42M** showed split Soret bands and ill-defined Q bands, implying the considerable contribution of the antiaromatic character. The short-lived excited states of **42M** also reflected the large contribution of the antiaromatic 24π-circuit. More importantly, the DFT calculations provided the theoretical verification of the aromaticity of the heterole-fused 7,8-dehydropurpurins. The calculated NICS values and ACID plots unambiguously corroborated that the aromaticity of 7,8-dehydropurpurins could be controlled by modulating the contribution of antiaromatic 24π-circuit including the lone-pair of the heteroatom to the whole electronic structures. Consequently, the heteroatoms in the heterole-fused structures have a large impact on the electronic properties of 7,8-dehydropurpurins. Overall, this study demonstrates that the heterole-fused structures on dehydropurpurins can manipulate the whole electronic properties without significant structural change by tuning contribution of antiaromatic 24π-circuit to the whole aromaticity. We believe that the introduction of heterole-fused structures into porphyrinoids is a universal strategy to get new insight into aromaticity and their intrinsic properties in cyclic π-conjugated molecules.

Chapter 4. Synthesis of Thiophene-fused Porphyrin Dimers as Effective π-Extended Helical Chromophores
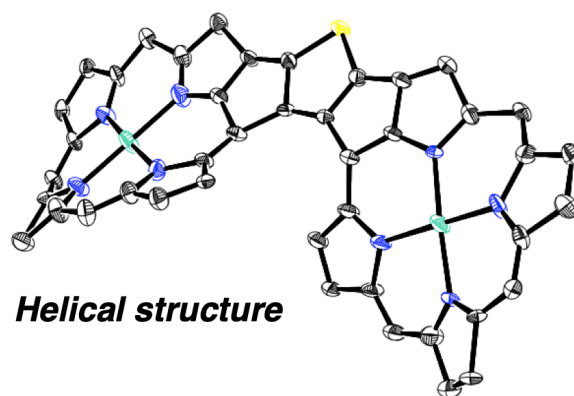
Helical structure

Contents

4-1. Introduction

Porphyrins with π-extended structures have emerged as promising organic functional materials for near infrared (NIR) absorption and emission, solar energy conversion, and nonlinear optical responses.[32a–b,61,74a–b,91a,c,97] Among them, fused porphyrin oligomers have attracted considerable interest because of their fully conjugated π-networks (Figure. 4-1).[32f,34d–f,64,98] The highly π-conjugated nature of the fused porphyrin oligomers gives rise to unusual optical and electronic behavior including extremely red-shifted absorption, large two-photon absorption cross sections, multi-charge storage capabilities, and charge-transporting properties due to effective electronic interactions over the whole molecule.[32f,34d–f,64,98] In recent years, curved π-conjugated molecules with three dimensional (3D) π-systems have attracted attention because they exhibit unique characteristic properties such as flexible conformational change, high solubility, and chiroptical properties.[99,100] Creating 3D π-systems is enabled by the introduction of non-six-membered rings or helical structures. In particular, helical molecules with π-extended structures have been investigated as promising candidates in the field of chiral electronics, and recent examples have revealed inherent chiroptical and electronic responses that are of interest in a variety of applications.[101] Considering the intrinsic optical and electronic properties of fused porphyrin oligomers, we envisioned that small units, *i.e.*, fused porphyrin dimers with helical structures would provide a basis for π-extended helical chromophores with potential applications as chiroptical and electronic materials. Considering that thiophene-fused porphyrinoids can achieve effective π-extension[91d] and thiophene-fused perylene diimide (PDI) derivative can form helical PDI dimers,[102] we designed thiophene-fused porphyrin dimers. Herein, we report the synthesis and structural, optical, and electrochemical properties of helical thiophene-fused porphyrin dimers **43** and **44** (Figure. 4-1).
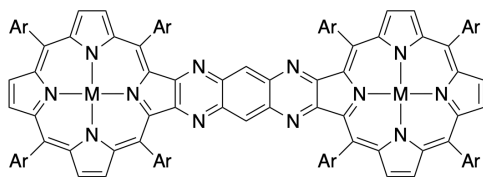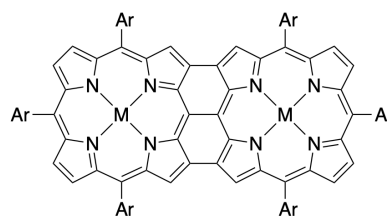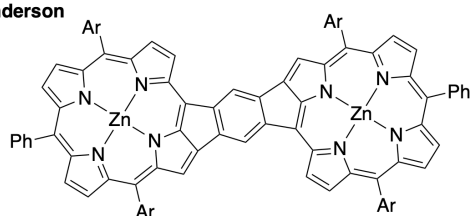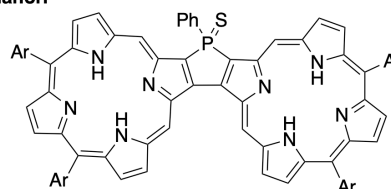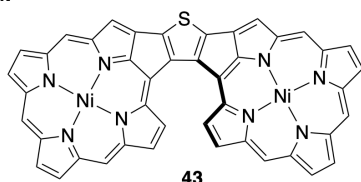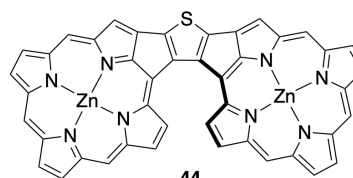
Figure 4-1. Examples of fused porphyrin dimers.

4-2. Synthesis

First, we synthesized thiophene-fused nickel porphyrin dimer **43a** (Scheme 4-1). As previously reported,[69b,80] we obtained the thiophene-bridged porphyrin dimer **29a** in 66% yield by the Suzuki–Miyaura coupling of β-iodoporphyrin **45a** with 2,5-diborylthiophene **46**. The *meso*-position of **29a** was chlorinated with Palau'Chlor (2.2 equiv.) to give porphyrin dimer **47a**, and the subsequent intramolecular Heck reaction of **47a** in the presence of $Pd(OAc)_2$ (20 mol%), PCy_3HBF_4 (40 mol%), and K_2CO_3 (2 equiv.) gave the thiophene-fused porphyrin dimer **43a** in 43% yield over two steps. Porphyrin dimers **29a** and **43a** were fully characterized using high-resolution mass spectrometry (HRMS) and ^1H and ^{13}C NMR spectroscopies (Experimental Section).

It is noteworthy that **43a** is highly soluble in common organic solvents and even in nonpolar *n*-hexane, and is sufficiently stable in solution and in the solid state under ambient conditions. We further designed mesityl-substituted porphyrin dimer **43b**, in which the mesityl groups can be used as labels in ^1H NMR spectroscopy for the determination of the inversion barrier ($\Delta G^{\ddagger}$). Mesityl-substituted porphyrin dimer **43b** was successfully obtained according to Scheme 4-1. In addition, demetallation of **43b** with sulfuric acid in trifluoroacetic acid, followed by treatment of $Zn(OAc)_2·2H_2O$ provided zinc porphyrin dimer **44** in 95% yield (Scheme 4-1). Porphyrin dimers **43b** and **44** were also fully characterized (Experimental Section). The zinc porphyrin dimer **44** is slightly sensitive to light under ambient conditions, but can be stored in the dark for more than two months.
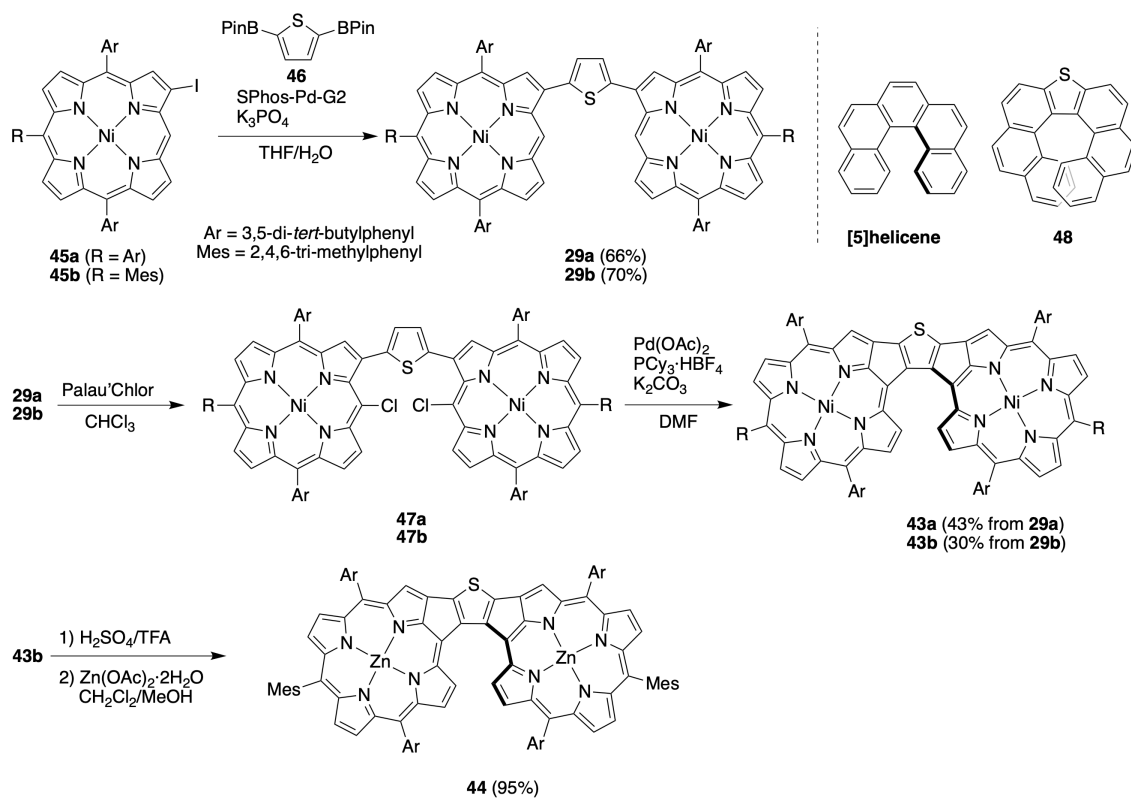
Scheme 4-1. Synthesis of helical thiophene-fused porphyrin dimers **43** and **44**. The chemical structures of [5]helicene and thia[7]helicene **48** are also indicated.

4-3. X-Ray Crystal Structure

Fortunately, single crystals suitable for X-ray diffraction analysis were obtained by vapor diffusion of acetonitrile into a CHCl$_3$ solution of **43a**. The unit cell contained two independent molecules in the unsymmetric unit. As we expected, the structure of **43a** was revealed to be a helical conformation, in which the rings A–G provided a thia[7]helicene-like structure (Figure. 4-2).[103] In the packing structure, no intermolecular π–π interaction was observed due to the steric hindrance of the bulky 3,5-di-*tert*-butylphenyl groups. The mean-plane deviation (MPD) (core 24 atoms) values on each porphyrin macrocycle are 0.339 and 0.296 Å. Since the MPD value of nickel 5,10,15,20- tetraphenylporphyrin is 0.202 Å,[104] the larger MPD values of **43a** are consistent with the helical conformation.

The torsion angle at the central thiophene ring (∠C3–C4–C5–C6) is 22(5)°, which is comparable to that of thia[7]helicene **48** (20.8°).[103] On the other hand, the torsion angles of ∠C2–C3–C4–C5 and ∠C4–C5–C6–C7 are 25(5) and 24(5)°, respectively, which are slightly larger than those of thia[7]helicene **48** (18.6 and 19.2°). In contrast, the torsion angles of ∠C1–C2–C3–C4 (–5(5)°) and ∠C5–C6–C7–C8 (–11(4)°) are smaller than those of thia[7]helicene **48** (14.4 and 15.3°). These structural features are also observed on the other molecule in the unit cell. Overall, the sum of the torsion angles of the inner rims for **43a** is 55°, which is significantly smaller than that of thia[7]helicene **48** (88.3°). The smaller sum of the torsion angles correlates with the larger interplanar angle between the terminal pyrrole rings A and G (70.9°) than that of thia[7]helicene **48** (35.4°). These features suggest that the structural distortion of **43a** is remarkably small compared to that of thia[7]helicene **48**, probably owing to insufficient steric repulsion with a large helical diameter. Since we confirmed the helical structure of thiophene-fused porphyrin dimer **43a**, we evaluated the helical inversion behavior of the thiophene-fused porphyrin dimer.
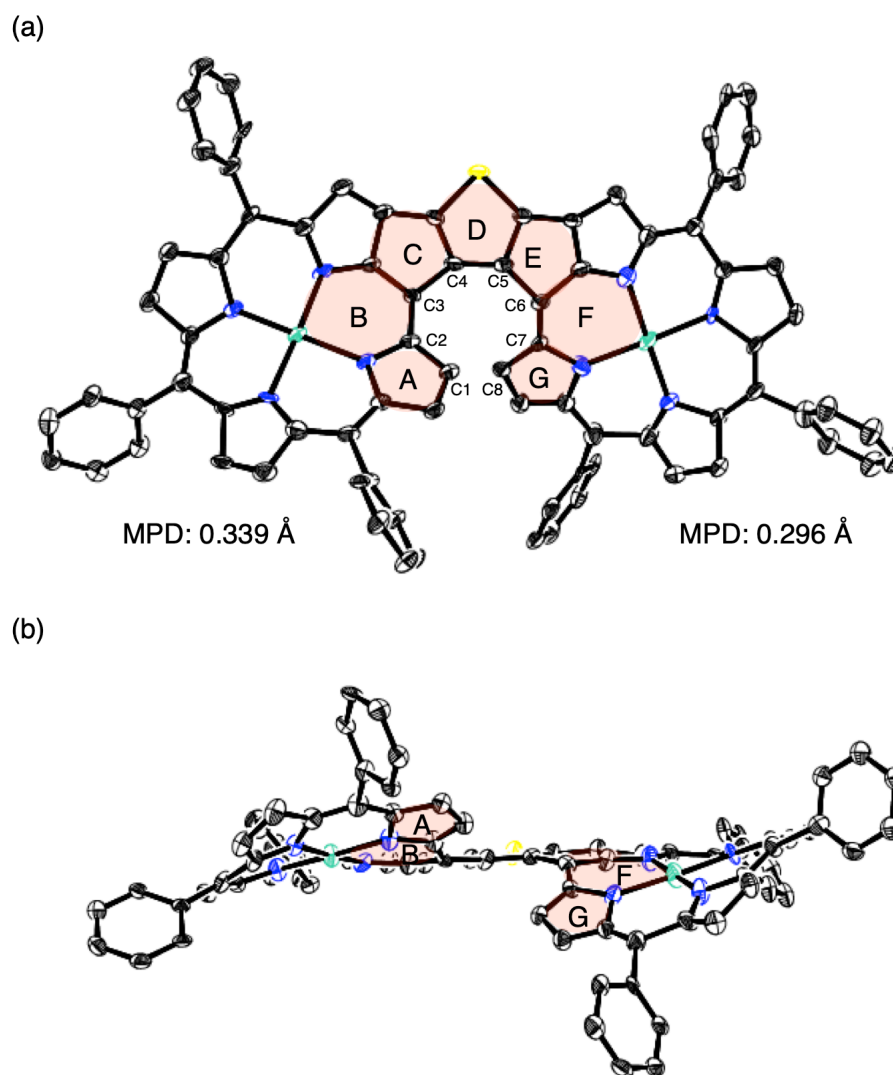
Figure 4-2. X-ray crystal structure of **43a**: (a) top view and (b) side view. One of the two independent molecules in the unit cell is shown. Thermal ellipsoids are shown at 50% probability. Solvent molecules, all hydrogen atoms, and tert-butyl groups are omitted for clarity. The disordered solvent molecules were removed using the PLATON SQUEEZE program.[105]

4-4. ^{1}H NMR Spectra

The ^{1}H NMR spectrum of **43a** in CDCl$_3$ exhibits severely broadened signals at around 8.1, 7.2, and 7.0 ppm, which originated from protons at the *ortho*-positions of the mesoaryl substituents (Figure. 4-3). These broadened signals suggest that the racemic inversion due to the helical structure occurs on the NMR timescale. The optical resolution of **43a** is not possible because of the fast racemic inversion.
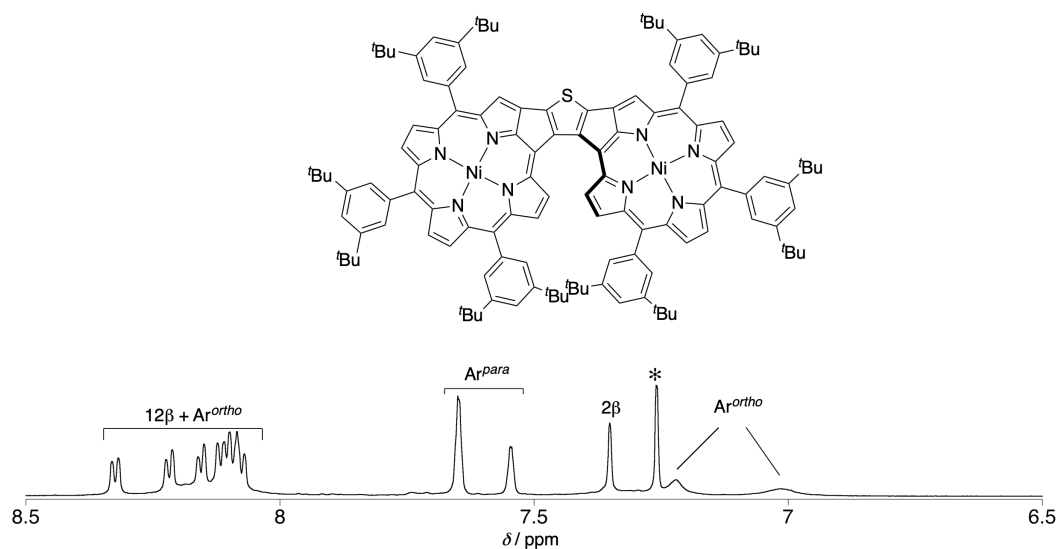
Figure 4-3. ^{1}H NMR spectrum of **43a** in CDCl$_3$ at 25 °C. Peaks marked with ∗ are due to residual solvents.

Although the ^{1}H NMR spectrum of nickel porphyrin dimer **43b** in CDCl$_3$ also exhibits broadened signals originating from the protons at the *ortho*-positions of the 3,5-di-*tert*-butylphenyl groups at around 8.15–8.10 ppm, the signals derived from the protons of the mesityl groups are clearly observed (Figure 4-4a). In contrast, the ^{1}H NMR spectrum of zinc porphyrin dimer **44** in CDCl$_3$ displays six distinct signals of the protons on the 3,5-di-*tert*-butylphenyl groups at 8.11, 8.08, 7.70, 7.67, 7.60, and 7.56 ppm, as well as the signals of the protons on the mesityl groups (Figure 4-4b). Namely, the racemic inversion for nickel porphyrin dimer **44** also takes place on the NMR timescale, while that for zinc porphyrin dimer **44** is slow compared to the NMR timescale.
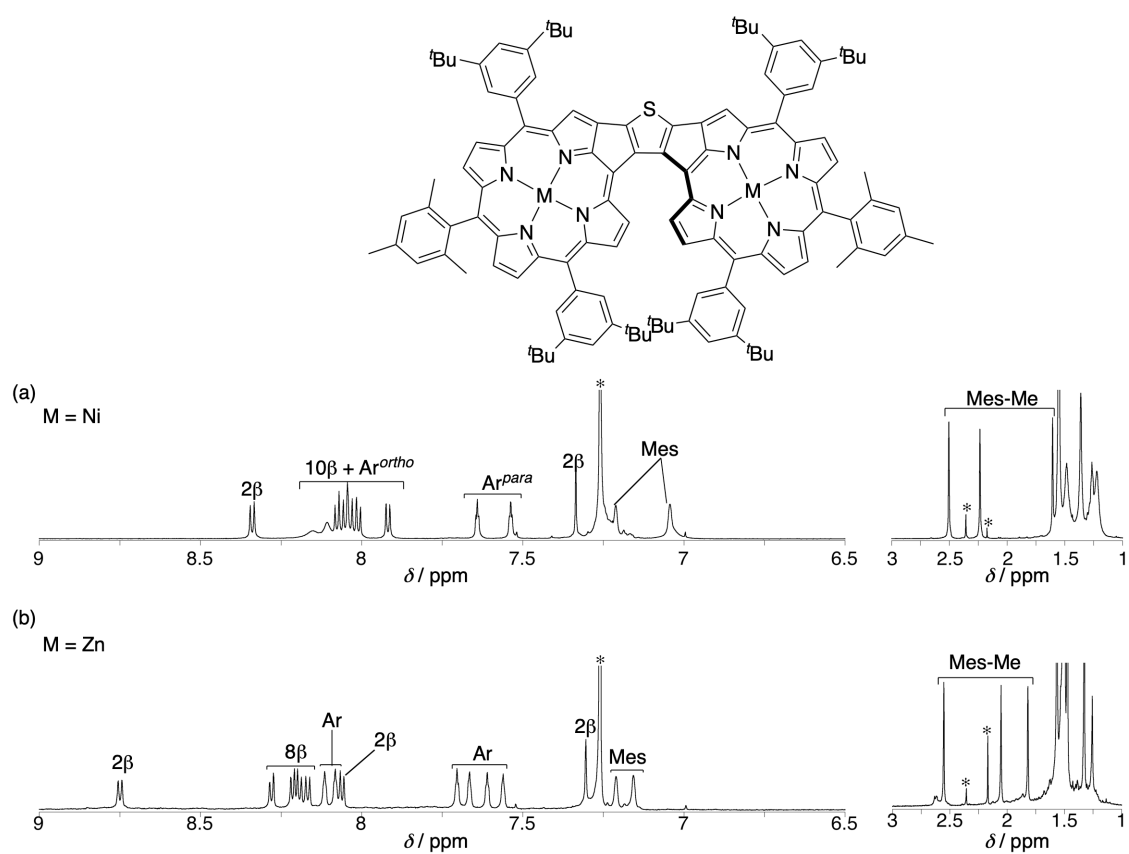
Figure 4-4. ^{1}H NMR spectrum of **43a** and **44** in CDCl$_3$ at 25 ºC. Peaks marked with ∗ are due to residual solvents.

4-5. Racemic Inversion Barriers

To determine the racemic inversion barriers of **43b** and **44**, we probed the temperature-dependent ^{1}HNMR spectra of **44** in C$_2$D$_2$Cl$_4$ (Figure 4-5) and **43b** in toluene-d_8 (Figure 4-6). At 25 ºC, the signals of three methyl groups on the mesityl groups of zinc porphyrin dimer **44** were observed at 2.57, 2.08, and 1.84 ppm, respectively. The signals at 2.08 and 1.84 ppm became broader upon warming, and these two signals were coalesced at 125 ºC. The inversion rate constants (k)[106] for **44** at each temperature were determined using the half-width of the peaks at 1.84 ppm, and then a plot of the $\ln(k/T)$ values versus $1/T$ was fitted into the Eyring equation to give $\Delta H^{\ddagger}$ (18.2 kcal mol^{-1}) and $\Delta S^{\ddagger}$ (-3.1 cal mol^{-1} K^{-1}). In addition, the parameters for nickel porphyrin dimer **43b** were also determined ($\Delta H^{\ddagger}$ = 21.0 kcal mol^{-1} and $\Delta S^{\ddagger}$ = 11.2 cal mol^{-1} K^{-1}). These values gave a racemic inversion barrier $\Delta G^{\ddagger}_{298}$ = 17.7 and 19.1 kcal mol^{-1} for **43b** and **44**, respectively. These $\Delta G^{\ddagger}_{298}$ values are significantly smaller than that of the representative [5]helicene ($\Delta G^{\ddagger}_{293}$ =24.1 kcal mol^{-1}).[107] Namely, the moderate steric repulsion between the two pyrrole rings A and G rationalizes the rapid racemic inversion in solution.
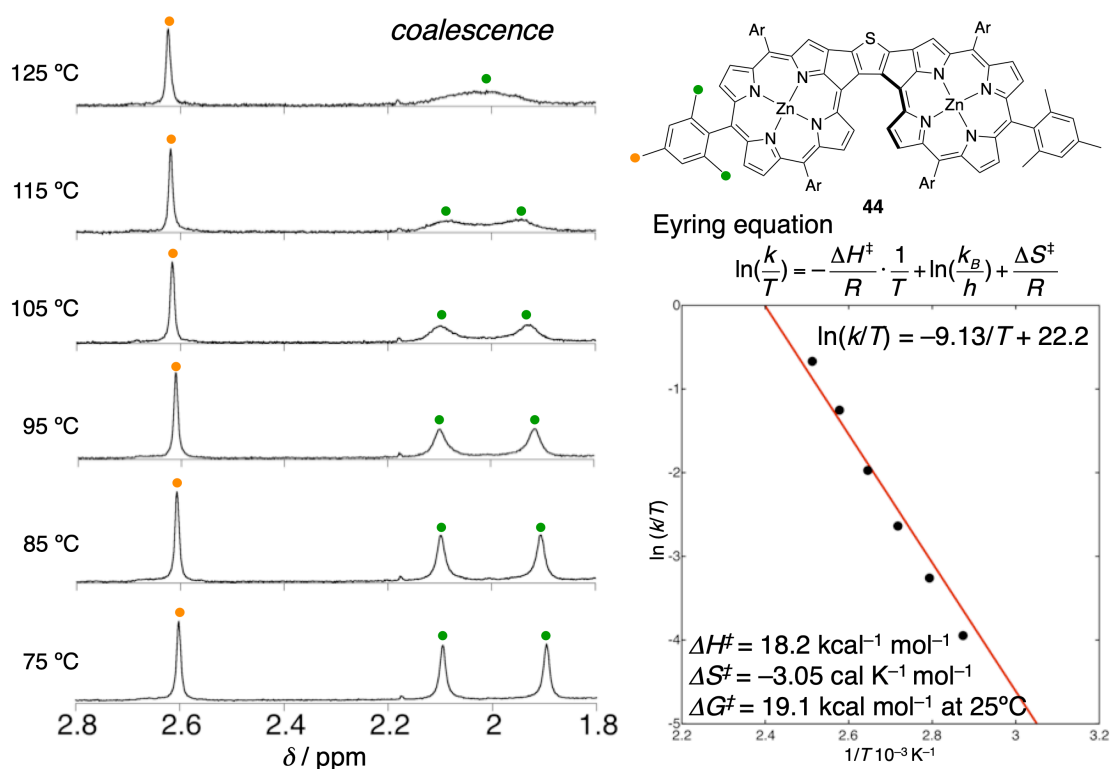
Figure 4-5. Temperature-dependent ^{1}H NMR spectra of **44** in C$_2$D$_2$Cl$_4$ and Eyring plot for the determination of the racemic inversion barrier.
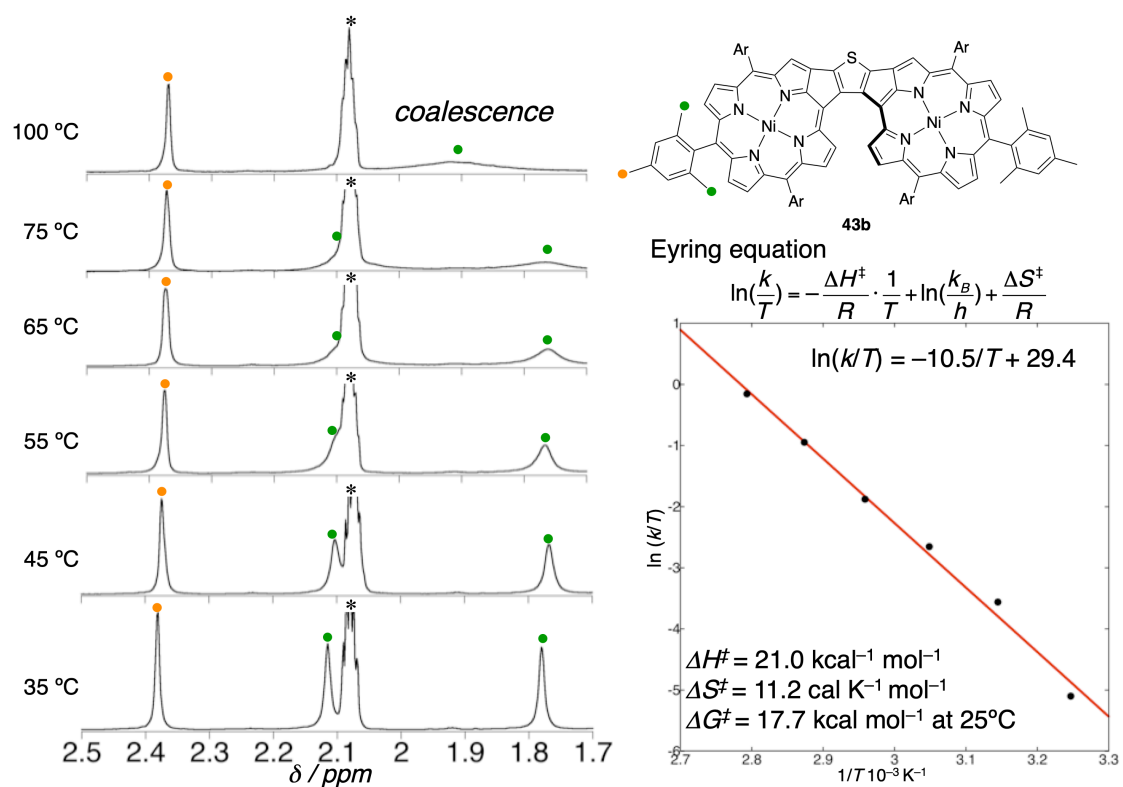
Figure 4-6. Temperature-dependent ^{1}H NMR spectra of **43b** in toluene-d_8 and Eyring plot for the determination of the racemic inversion barrier. Peaks marked with ∗ are due to residual solvents.

4-6. UV/Vis/NIR Absorption Spectra

The UV/Vis/NIR absorption spectra of helical thiophenefused porphyrin dimers **43** and **44** were measured in CH_2Cl_2 (Figure 4-7 and Table 4-1). Since the absorption spectra of **43a** and **43b** are almost the same, the *meso*-substituents have a negligible influence on the absorption properties. Nickel porphyrin dimers **43** exhibit four absorption bands at 417, 458, 559, and 613 nm, and weak absorption peaks are visible up to around 1050 nm. Compared to **43**, zinc porphyrin dimer **44** displays a red-shifted absorption with the edge extending to 1100 nm. Importantly, the lowest energy absorption peaks of **43** (λ = 975 nm) and **44** (λ = 1040 nm) are red-shifted relative to those of the corresponding fused mono-porphyrins (dehydropurpurins) (ca. 720–770 nm).[58,76c,e,108] Moreover, the molar absorption coefficients (ε) of absorption peaks of **43** and **44** at around 600–700 nm (ca. 75 000 M^{-1} cm^{-1}) are one order of magnitude larger than those of the corresponding dehydropurpurins (ca. 2000–4000 M^{-1} cm^{-1}). [58,76c,e,108] The red-shifted peaks and intensified absorption support an effective electronic communication between the two porphyrin moieties through the thiophene-fused structure. It is notable that zinc porphyrin dimer **44** shows no fluorescence. The small absorption coefficient at 1040 nm (ε = 1400 M^{-1} cm^{-1}) indicates that the oscillator strength for fluorescence is small. In addition, the small optical HOMO–LUMO gap leads to fast nonradiative decay, which competes with fluorescence. Consequently, the lack of fluorescence of **44** is related to the weak absorption at 1040 nm.
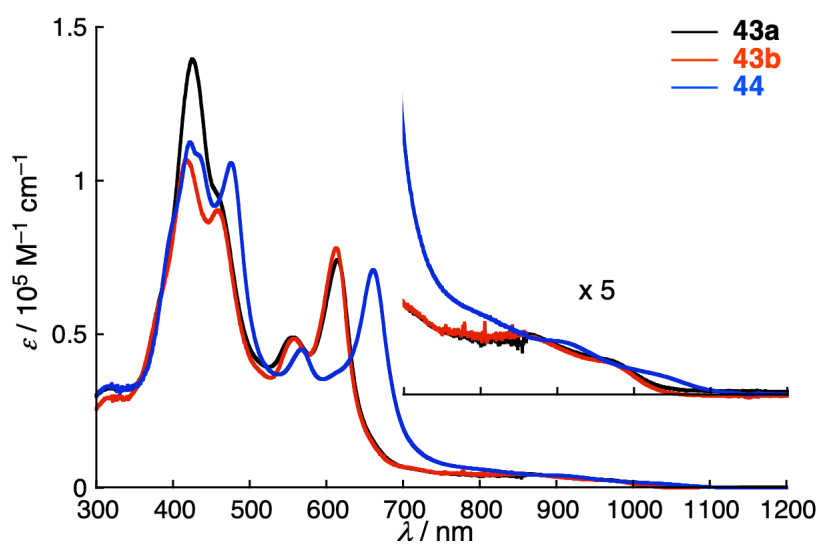
Figure 4-7. UV/Vis/NIR absorption spectra of **43a** (black), **43b** (red), and **44** (blue) in CH_2Cl_2.

Table 4-1. UV/Vis/NIR Absorption properties of porphyrin dimers **43** and **44** in CH_2Cl_2.

porphyrin	λ_{abs} / nm (ε [$10^4 M^{-1} \cdot cm^{-1}$])
43a	426 (14), 462 (9.3), 557 (4.9), 615 (7.4), 864 (0.46), 975 (0.25)
43b	417 (11), 458 (9.1), 559 (4.9), 613 (7.8), 859 (0.47), 975 (0.23)
44	422 (11), 436 (11), 475 (11), 568 (4.5), 661 (7.1), 910 (0.40), 1040 (0.14)

4-7. Electrochemical Properties

The electrochemical properties of **43** and **44** were studied using cyclic voltammetry (CV) and differential pulse voltammetry (DPV) in CH_2Cl_2 (*versus* ferrocene/ferrocenium ions (Fc/Fc^+)) with n-Bu_4NPF_6 as an electrolyte (Figure 4-8 and Table 4-2). Nickel porphyrin dimer **43a** displays three reversible reduction peaks at -1.38, -1.58, and -1.94 V and three oxidation peaks at 0.04, 0.37, and 0.80 V, which are comparable to those of **43b**. Meanwhile, zinc porphyrin dimer **44** reveals three reversible reduction peaks at -1.44, -1.61, and -2.03 V and four oxidation peaks at -0.14, 0.12, 0.47, and 0.62 V. These multiple reduction and oxidation peaks indicate the effective π-communication over the two porphyrins through the thiophene-fused structure.
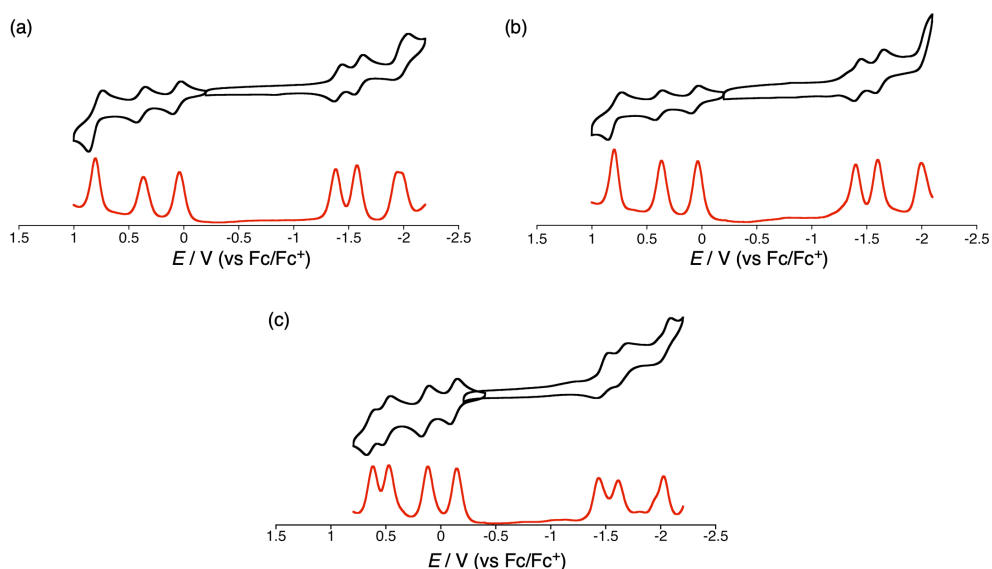
Figure 4-8. Cyclic voltammograms (black) and differential pulse voltammetry (DPV) curves (red) of porphyrin dimers (a) **43a**, (b) **43b**, and (c) **44**. Redox potentials were determined by DPV. Solvent: CH_2Cl_2; scan rate: 0.05 V s^{-1}; working electrode: glassy carbon; reference electrode: Ag/Ag^+ (0.01 M $AgNO_3$); electrolyte: 0.1 M n-Bu_4NPF_6.

Table 4-2. Electrochemical oxidation and reduction potentials of thiophene-fused porphyrin dimers versus Fc/Fc^+.

	E_{ox4}	E_{ox3}	E_{ox2}	E_{ox1}	E_{red1}	E_{red2}	E_{red3}	E_g^{CV}
43a	–	0.80	0.37	0.04	-1.38	-1.58	-1.94	1.42
43b	–	0.80	0.37	0.04	-1.40	-1.60	-2.00	1.44
44	0.62	0.47	0.12	-0.14	-1.44	-1.61	-2.03	1.30

4-8. Theoretical Calculations

To get further insight into the structural and electronic properties of **43** and **44**, we carried out density functional theory (DFT) calculations at the B3LYP/6-31G(d,p) level of theory with C_2 symmetry. The optimized structures support their helical conformations, which are in good agreement with the crystal structure of **43a** (Figure 4-9). The sum of the torsion angles of the inner rims for **43** is 59.5°, which is slightly larger than that for **44** (57.0°) (Table 4-3). The difference in the sum of the torsion angles can be rationalized by distortion of the porphyrin macrocycles by the central metal ions. Namely, the intrinsic ruffled structure of the nickel porphyrin provides the larger torsion angle. The Kohn–Sham frontier orbitals of **43** and **44** are illustrated in Figure 4-10. The HOMOs display large orbital distributions on the thiophene-fused structure, while the LUMOs are well delocalized over the two porphyrin moieties through the thiophene-fused structure. Additionally, the smaller HOMO–LUMO gap of **44** (1.88 eV) than that of **43** (1.94 eV) is consistent with the trend of the optical and electrochemical HOMO–LUMO gaps of **43** and **44**. Then, we assessed the racemization barriers for porphyrin dimers **43** and **44** using the model compounds **43'** and **44'**, in which the *meso*-substituents were replaced with hydrogen atoms to simplify the calculations. From the obtained structures of the ground state (GS) and transition state (TS) for **43'** and **44'**, the computational racemic inversion barriers were calculated to be $\Delta G^{\ddagger} = 16.3$ and 18.7 kcal mol^{-1} at 298.15 K at the B3LYP/ 6-31G(d,p) level of theory, respectively (Figure 4-11). These values are consistent with the experimental values (17.7 and 19.1 kcal mol^{-1} for **43b** and **44**, respectively). It should be noted that the structure of **43'** on the TS state retains the ruffled structure of the nickel porphyrin. Consequently, the distance between the C1 and C8 of **43'** on the TS state (3.40 Å) is larger than that of **44'** (3.27 Å). Therefore, the larger distance for **43'** induces smaller steric repulsion, leading to the smaller racemic inversion barrier of **43'**. These theoretical calculations suggest that distortion of the porphyrin macrocycles by the central metal ions can modulate the racemic inversion barriers of porphyrin-based helical π-conjugated chromophores.

(a)

top view   side view

(b)

top view   side view
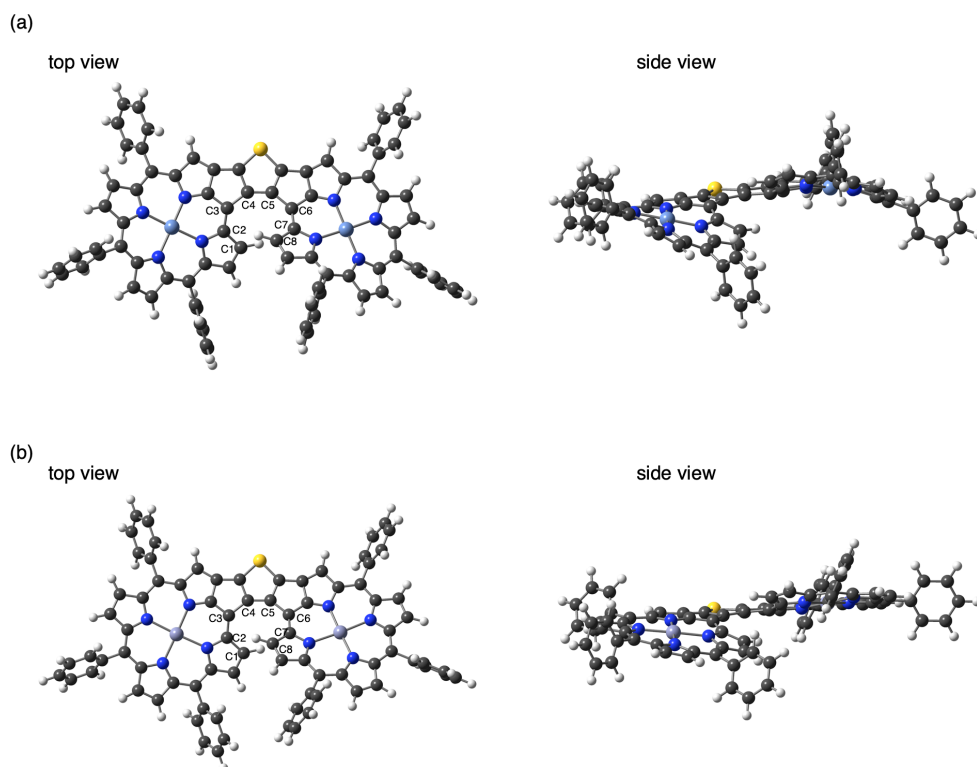
Figure 4-9. Optimized structures of (a) **43** and (b) **44**. Substituents at *meso* positions were replaced with phenyl groups for clarity.

Table 4-3. Selected bond lengths and torsion angles of **43** and **44**.

	43	**44**
C1–C2 / Å	1.440	1.445
C2–C3 / Å	1.387	1.398
C3–C4 / Å	1.492	1.499
C4–C5 / Å	1.412	1.416
C5–C6 / Å	1.492	1.499
C6–C7 / Å	1.387	1.398
C7–C8 / Å	1.440	1.445
∠C1-C2-C3-C4 / °	0.9	2.4
∠C2-C3-C4-C5 / °	26.2	21.8
∠C3-C4-C5-C6 / °	5.3	8.6
∠C4-C5-C6-C7 / °	26.2	21.8
∠C5-C6-C7-C8 / °	0.9	2.4
Sum of torsion angles / °	59.5	57.0
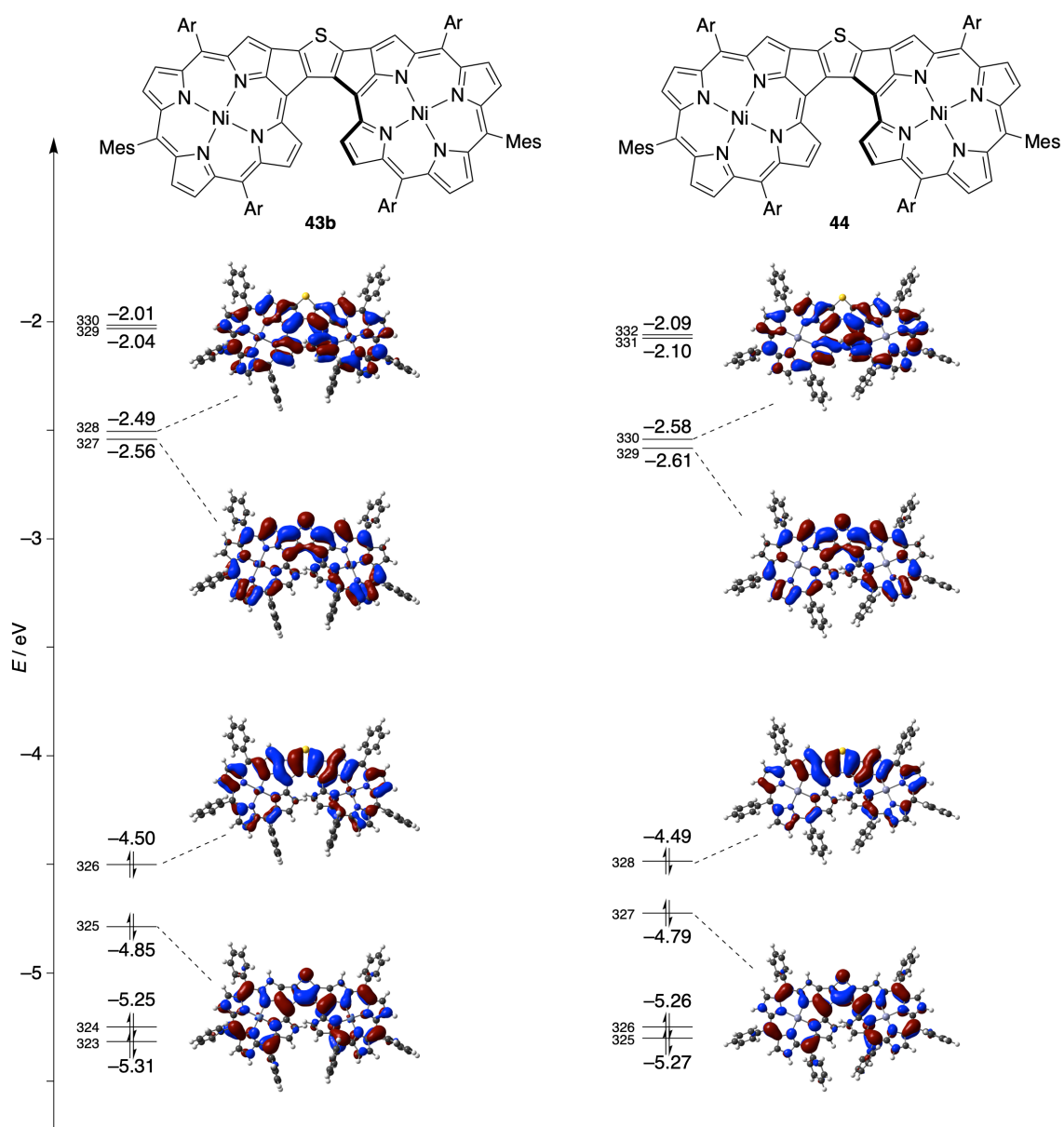
Figure 4-10. Selected Kohn-Sham orbitals of **43b** and **44**. Substituents at *meso* positions were replaced with phenyl groups for clarity.

(a)

(b)
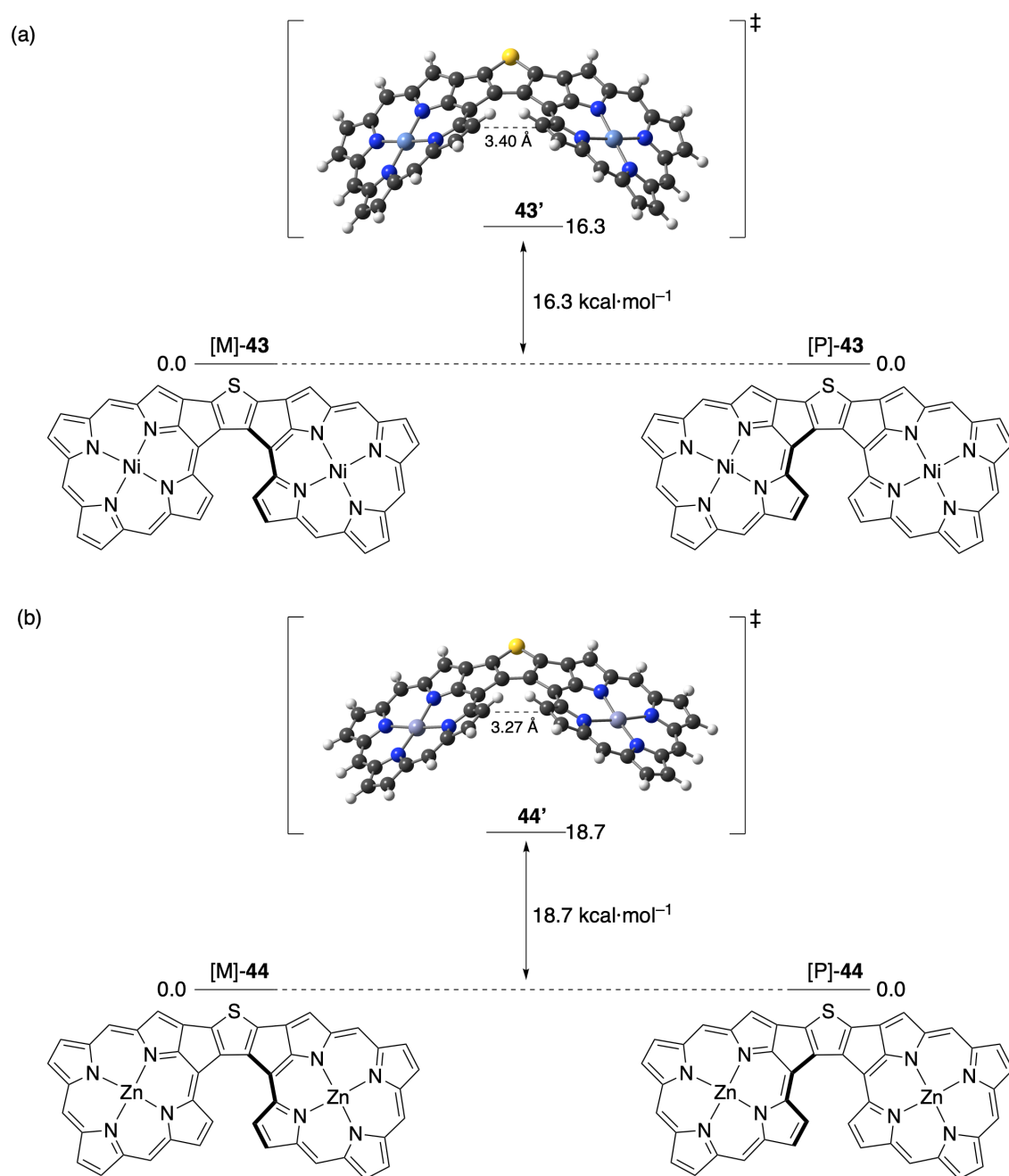
Figure 4-11. Racemization inversion process for (a) **43'** and (b) **44'** the relative Gibbs free energy (kcal mol^{-1}) by DFT calculation with B3LYP/6-31G (d,p). The *meso*-aryl substituents and mesityl groups were replaced with hydrogen atoms to simplify the calculations.

4-9. Summary

In summary, we synthesized thiophene-fused porphyrin dimers as effective π-extended helical chromophores. The helical structure of **43a** was confirmed by its X-ray crystal structure. The optical and electrochemical properties of **43** and **44** exhibit strong electronic communication over the two porphyrin moieties through the thiophene-fused structure. The racemic inversion barriers ($\Delta G^{\ddagger}_{298}$) of **43b** and **44** are significantly smaller than that of the representative [5]helicene. It is striking that the $\Delta G^{\ddagger}_{298}$ values can be modulated by the central metal ions. Although the optical resolution of **43** and **44** is not possible because of the rather small racemic inversion barriers, the introduction of suitable substituents as well as central metal ions may realize optical resolution as a result of the increased racemic inversion barrier. Thus, we believe that this report unveils the potential utility of fused porphyrin oligomers with helical structures as chiroptical and electronic materials.

4-10. Acknowledgement

Summary of This Thesis

In this thesis, synthesis and properties of π-extended porphyrins with heterole structures were described. The author developed synthetic strategies for construction of heterole-linked or -fused structures at peripheral positions in porphyrins and investigated their structural and electronic properties. Furthermore, the authors achieved the modulation of 18π aromaticity by heterole-fused structures.

In Chapter 1, *meso*-to-*meso* or β-to-β phosphole-bridged porphyrin dimers were presented. The author succeeded in synthesis of phosphole-bridged porphyrin dimers by Stille coupling reactions. Notably, phosphole-bridged porphyrin dimers exhibited broadened and red-shifted absorption as well as negative-shifted redox potential derived from phosphole in comparison with those of *p*-phenylene or thienylene-bridged porphyrins, indicating effective interaction between porphyrins through phosphole moiety.

In Chapter 2 and 3, the author established the synthetic method for phosphole- or pyrrole-fused dehydropurpurins by [2+2+1] intramolecular cyclization reactions from bis(alkynyl)porphyrin. A series of phosphole- and pyrrole-fused porphyrins exhibited significantly broadened and red-shifted absorption spectra because of the perturbation to electronic structures of heterole-fused structures through five-membered ring. Phosphole-fused dehydropurpurins with a phosphorus(III) center indicated a weak contribution of 24π antiaromaticity. In addition, pyrrole-fused dehydropurpurins displayed a considerable contributions of 24π antiaromaticity. Consequently, pyrrole-fused dehydropurpurins exhibited small absorption coefficient, red-shifted absorption, and short lifetime in excited states in comparison with those of phosphole-fused dehydropurpurins. Namely, the author accomplished the modulation of the whole aromaticity of porphyrin depending on the oxidation state on phosphorus centers in phosphole and main group elements.

In Chapter 4, thiophene-fused helical porphyrin dimers were mentioned. Fortunately, the author confirmed the helical conformation by X-ray crystal structure. The author investigated their racemic inversion barriers from ^{1}H NMR spectra and found the relatively small racemic inversion. Besides, the author examined their optical and electrochemical properties and revealed the effective electronic interaction between porphyrins through thiophene moiety.

The author demonstrated that the effective synthetic methodologies for novel porphyrinoids with the combination of porphyrins and heteroles enable us to reveal the unique properties of porphyrin with heterole structures for organic functional materials. Therefore, this study will cast light on the chemistry of π-extended porphyrins with main group elements.

Experimental Section

Instrumentation and Materials

Commercially available solvents and reagents were used without further purification unless otherwise mentioned. Silica-gel column chromatography was performed with UltraPure Silica Gel (230-400 mesh, SiliCycle) unless otherwise noted. Thin-layer chromatography (TLC) was performed with Silica gel 60 F_{254} (Merck). UV/Vis/NIR absorption spectra were measured with a Perkin-Elmer Lambda 900 UV/Vis/NIR spectrometer. Steady-state fluorescence spectra were obtained by a HORIBA Nanolog spectrometer. A time-correlated single photon counting (TCSPC) method was employed to measure the fluorescence lifetime using a HORIBA Nanolog-TCSPC. ^{1}H, ^{13}C, and ^{31}P NMR spectra were recorded with a JEOL EX-400 spectrometer (operating at 399.65 MHz for ^{1}H, 100.40 MHz for ^{13}C, and 161.7 MHz for ^{31}P) by using the residual solvent as the internal reference for ^{1}H (CDCl$_3$: δ = 7.26 ppm; CD$_2$Cl$_2$: δ = 5.32 ppm; toluene-d_8: δ = 2.08 ppm; C$_2$D$_2$Cl$_4$: δ = 6.00 ppm) and ^{13}C (CDCl$_3$: δ = 77.16 ppm; CD$_2$Cl$_2$: δ = 53.84 ppm). EXACTIVE Fourier-transform orbitrap mass spectrometer (APCI and ESI) and a Thermo Fisher Scientific LTQ Orbitrap XL spectrometer (MALDI) by using a-cyano-4-hydroxycinnamic acid (CHCA) or 1,8-dihydroxy-9(10*H*)-anthracenone (DIT) as matrix. Attenuated total reflectance-Fourier transform infrared (ATR-FTIR) spectra were taken with the golden gate diamond anvil ATR accessory (NICOLET 6700, Thermo scientific), using typically 64 scans at a resolution of 2 cm^{-1}. All samples were placed in contact with the diamond window using the same mechanical force. Single-crystal X-ray diffraction analysis data were collected at –180 ºC with a Rigaku XtaLAB P200 apparatus using two-dimensional detector PILATUS 100K/R with Cu-Ka radiation (1.54187 Å) for **36Zn**, at –120 °C on a Rigaku Saturn724+ CCD diffractometer with graphite monochromated Mo*K*a radiation (0.71075 Å) for **37Ni**, and at monochromated Mo*K*$_a$ radiation (0.71075 Å) for **43a**. The structures were solved by direct method (SHELXS-2014). Redox potentials were measured by cyclic voltammetry and differential pulse voltammetry method on an ALS electrochemical analyzer model 660A.

Density Functional Theory (DFT) Calculations.

All calculations were carried out using the *Gaussian 09* program. All structures were fully optimized without any symmetry restriction. The optimization were performed using the density functional theory (DFT) method with restricted B3LYP (Becke's three-parameter hybrid exchange functionals and the Lee-Yang-Parr correlation functional) level, employing a basis set

Experimental Section

6-31G(d,p) for C, H, N, O, P, S, Ni, and Zn. The absolute ^{1}H shielding values were obtained using the GIAO method at the B3LYP/6-31G(d,p) level. The ^{1}H chemical shifts were calculated relative to CHCl$_3$ (δ = 7.26 ppm, absolute shielding: 24.96 ppm). Excitation energies and oscillator strengths were calculated with the TD-SCF method at B3LYP/6-31G(d,p) level. Anisotropy of the induced current density (ACID) plots were obtained by employing the CSGT method to calculate the current densities.

Chapter 1

meso-Phosphole-bridged Porphyrin Dimer (*meso*-28):

A flask containing **31** (100 mg, 100 mmol), **32** (40 mg, 50 mmol), Pd(PPh$_3$)$_4$ (15 mg, 25 mmol), CuI (5.4 mg, 30 mmol), and CsF (30 mg, 200 mmol) was purged with argon, and then charged with DMF (3.0 mL). The mixture was stirred at 115 °C for 11 h. The reaction mixture was cooled to room temperature. The reaction mixture was quenched by water and extracted with CH$_2$Cl$_2$, dried over Na$_2$SO$_4$. After removal of the solvent, the residue was separated by silica gel chromatography using a 2:1 mixture of *n*-hexane and CH$_2$Cl$_2$ as eluent to afford *meso*-28 as a red solid (43 mg, 21 mmol, 41%).

meso-28: ^{1}H NMR (399.65 MHz, CDCl$_3$, 25 °C): δ = 10.16 (d, J = 4.8 Hz, 2H, β), 9.12 (d, J = 4.8 Hz, 2H, β), 8.91 (d, J = 4.8 Hz, 2H, β), 8.82 (d, J = 4.8 Hz, 2H, β), 8.80–8.70 (m, 8H, β), 8.15–7.56 (m, 20H, Ar + Ph), 7.03–6.96 (m, 1H, Ph), 6.94–6.86 (m, 2H, Ph), 3.19–3.03 (m, 2H, CH$_2$), 2.80–2.66 (m, 2H, CH$_2$), 2.46–2.33 (m, 1H, CH$_2$), 2.20–2.09 (m, 1H, CH$_2$), and 1.65–1.38 (m, 108H, *tert*-Butyl) ppm. ^{13}C NMR (100.40 MHz, CDCl$_3$, 25 °C): δ = 148.93, 148.89, 142.9, 142.8, 142.44, 142.38, 142.1, 141.14, 141.07, 139.90, 139.88, 139.79, 133.9, 133.5, 132.6, 132.5 (J = 12 Hz), 132.23, 132.24 (J = 18 Hz), 131.6, 131.5, 131.4, 128.8, 128.6, 128.2, 128.1, 121.0, 120.5, 35.01, 34.95, 31.70, and 31.65 ppm. ^{31}P NMR (161.7 MHz, CDCl$_3$, 25 °C): δ = 54.9 ppm. UV/Vis (CH$_2$Cl$_2$): λ (ε, M^{-1}·cm^{-1}) = 420 (220000), 534 (32000), and 581 (10000) nm. HRMS (APCI) calcd. for C$_{137}$H$_{154}$N$_8$O$_1$Ni$_2$P$_1$; [M+H]$^+$: 2074.0685; found 2074.0726. FT-IR (ATR): ν = 3900, 3894, 3747, 3649, 2955, 2911, 2865, 2356, 2162, 1593, 1541, 1363, 1352, 1247, 1010, 798, 712, 454, 406, and 401 cm^{-1}. m.p.: >300 °C.

meso-Thienylene-bridged Porphyrin Dimer (*meso*-29):

A flask containing **34** (50 mg, 50 mmol), 2,5-dibromothiophene (2.25 mL, 20 mmol), Pd(PPh$_3$)$_4$ (2.2 mg, 2.0 mmol), and Cs$_2$CO$_3$ (62 mg, 200 mmol) was purged with argon, and then charged with toluene (2.0 mL). The mixture was stirred at 120 °C for 54 h. The reaction mixture was cooled to room temperature. The reaction mixture was quenched by water and extracted with

CH$_2$Cl$_2$, and dried over Na$_2$SO$_4$. After removal of the solvent, the residue was separated by silica gel chromatography using a 6:1 mixture of *n*-hexane and CH$_2$Cl$_2$ as eluent to afford ***meso*-29** as a red solid (19 mg, 9.8 mmol, 49%).

***meso*-29**: ^{1}H NMR (399.65 MHz, CDCl$_3$, 25 °C): δ = 9.43 (d, J = 4.8 Hz, 4H, β), 8.95(d, J = 4.8 Hz, 4H, β), 8.84–8.81 (m, 8H, β), 8.05 (s, 2H, Thienyl), 7.92 (d, J = 2.0 Hz, 8H, Ar), 7.89 (d, J = 2.0 Hz, 4H, Ar), 7.76 (t, J = 2.0 Hz, J = 1.6 Hz, 4H, Ar), 7.76–7.73 (t, J = 2.0 Hz, J = 1.6 Hz, 2H, Ar), and 1.55–1.47 (m, 108H, *tert*-Butyl) ppm. ^{13}C NMR (100.40 MHz, CDCl$_3$, 25 °C): δ = 149.0, 148.9, 144.0, 143.5, 143.1, 142.9, 142.8, 139.9, 132.9, 132.5, 132.3, 132.0, 131.9, 130.5, 128.8, 128.6, 127.7, 121.2, 120.9, 120.6, 109.5, 35.0, and 31.7 ppm. UV/Vis (CH$_2$Cl$_2$): λ (ε, M^{-1}·cm^{-1}) = 427 (350000) and 532 (41000) nm. HRMS (MALDI) calcd. for C$_{128}$H$_{144}$N$_8$Ni$_2$S$_1$; [M]$^{\bullet+}$: 1940.9936; found 1940.9937. FT-IR (ATR): ν = 3853, 3839, 3751, 3741, 2953, 1684, 1591, 1362, 997, 929, 795, and 710 cm^{-1}. m.p.: >300 °C.

meso-Phenylene-bridged Porphyrin Dimer (*meso*-30):

A flask containing **34** (50 mg, 50 mmol), 1,4-dibromobenzene (4.46 mg, 20 mmol), Pd(PPh$_3$)$_4$ (2.2 mg, 2 mmol), and Cs$_2$CO$_3$ (62 mg, 200 mmol) was purged with argon, and then charged with toluene (2.0 mL). The mixture was stirred at 120 °C for 18 h. The reaction mixture was cooled to room temperature. The reaction mixture was quenched by water and extracted with CH$_2$Cl$_2$, and dried over Na$_2$SO$_4$. After removal of the solvent, the residue was separated by silica gel chromatography using a 6:1 mixture of *n*-hexane and CH$_2$Cl$_2$ as eluent to afford **27** as a red solid (12 mg, 6.2 mmol, 32%).

***meso*-30**: ^{1}H NMR (399.65 MHz, CDCl$_3$, 25 °C): δ = 9.12 (d, J = 4.8 Hz, 4H, β), 8.94 (d, J = 4.8 Hz, 4H, β), 8.86–8.83 (m, 8H, β), 8.35 (s, 2H, Ph), 7.95 (d, J = 1.6 Hz, 4H, Ar), 7.90 (d, J = 1.2 Hz, 4H, Ar), 7.76 (t, J = 2.0 Hz, 1.6 Hz, 4H, Ar), 7.73 (t, J = 2.0Hz, 1.6 Hz, 2H, Ar), and 1.52–1.47 (m, 108H, *tert*-Butyl) ppm. ^{13}C NMR (100.40 MHz, CDCl$_3$, 25 °C): δ = 148.98, 148.93, 142.88, 142.86, 142.79, 142.6, 140.6, 140.0, 132.6, 132.42, 132.39, 132.2, 131.9, 128.9, 128.7, 121.1, 120.28, 120.24, 118.2, 35.0, and 31.7 ppm. UV/Vis (CH$_2$Cl$_2$): λ (ε, M^{-1}·cm^{-1}) = 423 (420000) and 529 (42000) nm. HRMS (MALDI) calcd. for C$_{130}$H$_{146}$N$_8$Ni$_2$; [M]$^{\bullet+}$: 1935.0372; found 1935.0379. FT-IR (ATR): ν = 3853, 3749, 3736, 3689, 2966, 2365, 2356, 2056, 2004, 1474, 1007, 797, and 710 cm^{-1}. m.p.: >300 °C.

β-Phosphole-bridged Porphyrin Dimer (β-28):

A flask containing **33** (100 mg, 100 mmol), **32** (40 mg, 50 mmol), Pd(PPh$_3$)$_4$ (15 mg, 25 mmol), CuI (5.4 mg, 30 mmol), and CsF (30 mg, 200 mmol) was purged with argon, and then charged

with DMF (3.0 mL). The mixture was stirred at 115 °C for 21 h. The reaction mixture was cooled to room temperature. The reaction mixture was quenched by water and extracted with hexane/AcOEt, washed with water, and dried over Na_2SO_4. After removal of the solvent, the residue was separated by silica gel chromatography using a 2:1 mixture of *n*-hexane and CH_2Cl_2 as eluent to afford ***β*-28** as a brown solid (10 mg, 5.0 mmol, 10%).

***β*-28**: ^{1}H NMR (399.65 MHz, CDCl$_3$, 25 °C): δ = 10.53 (s, 2H, *meso*), 9.18 (d, *J* = 4.8 Hz, 2H, β), 9.02 (s, 2H, β), 8.91 (d, *J* = 4.8 Hz, 2H, β), 8.87–8.73 (m, 8H, β), 8.12–7.61 (m, 20H, Ar+Ph), 7.20–7.05 (m, 3H, Ph), 3.26–3.15 (m, 4H, CH$_2$), 2.50–2.36 (m, 1H, CH$_2$), 2.25–2.13 (m, 1H, CH$_2$), and 1.70–1.36 (m, 108H, *tert*-Butyl) ppm. ^{13}C NMR (100.40 MHz, CDCl$_3$, 25 °C): δ = 148.96, 148.87, 143.10, 143.06, 143.03, 142.91, 142.88, 142.71, 142.66, 141.9, 141.0, 140.0, 139.8 (*J* = 8.0 Hz), 132.6, 132.4, 131.0 (*J* = 10.0 Hz), 128.9, 128.7 (*J* = 9.0 Hz), 121.2, 121.12, 121.05, 120.4, 119.90, 119.84, 104.6 (*J* = 4.0 Hz), 35.0, 31.76, 31.69, and 31.66 ppm. ^{31}P NMR (161.7 MHz, CDCl$_3$, 25 °C): δ = 57.2 ppm. UV/Vis (CH$_2$Cl$_2$): λ (ε, $M^{-1} \cdot cm^{-1}$) = 414 (130000), 530 (25000), and 589 (20000) nm. HRMS (APCI) calcd. for $C_{137}H_{153}N_8O_1Ni_2P_1$; $[M]^{\bullet+}$: 2073.0634; found 2073.0606. FT-IR (ATR): ν = 3801, 3675, 3618, 2921, 2898, 2889, 2365, 2335, 2173, 2049, 2039, 2027, 1958, 1592, 1473, 1458, 1361, 1245, 1006, and 713 cm^{-1}. m.p.: >300 °C.

β-Thienylene-bridged Porphyrin Dimer (*β*-29):

A flask containing **35** (70 mg, 66 mmol), 2,5-dibromothiophene (2.50 mL, 22 mmol), Pd(PPh$_3$)$_4$ (2.54 mg, 2.2 mmol), and Cs$_2$CO$_3$ (72 mg, 220 mmol) was purged with argon, and then charged with toluene (0.85 mL). The mixture was stirred at 110 °C for 15 h. The reaction mixture was cooled to room temperature. The reaction mixture was filtered through a small plug of silica gel with copious washings (CH$_2$Cl$_2$). After removal of the solvent, the residue was separated by silica gel chromatography using a 6:1 mixture of *n*-hexane and CH$_2$Cl$_2$ as eluent to afford ***β*-29** as a red solid (18.5 mg, 9.5 mmol, 43%).

***β*-29**: ^{1}H NMR (399.65 MHz, CDCl$_3$, 25 °C): δ = 10.37 (s, 2H, *meso*), 9.21 (d, *J* = 4.8 Hz, 2H, β), 9.16 (s, 2H, β), 8.95 (d, *J* = 4.8 Hz, 2H, β), 8.88–8.82 (m, 8H, β), 8.15 (s, 2H, Thienyl), 7.99 (d, *J* = 2.0 Hz, 4H, Ar), 7.93 (d, *J* = 2.0 Hz, 4H, Ar), 7.90 (d, *J* = 2.0 Hz, 4H, Ar), 7.79 (t, *J* = 2.0 Hz, 1.6 Hz, 2H, Ar), 7.76 (t, *J* = 2.0 Hz, 1.6 Hz, 2H, Ar), 7.73 (t, *J* = 2.0 Hz, 1.6 Hz, 2H, Ar) and 1.57–1.46 (m, 108H, *tert*-Butyl) ppm. ^{13}C NMR (100.40 MHz, CDCl$_3$, 25 °C): δ = 149.1, 149.0, 148.9, 134.3, 143.2, 143.1, 134.0, 142.9, 142.8, 141.5, 140.04, 140.00, 139.90, 139.6, 129.0, 128.8, 128.7, 127.7, 121.22, 121.17, 121.11, 120.6, 120.1, 119.9, 103.9, 35.07, 35.01, 31.74, and 31.70 ppm. UV/Vis (CH$_2$Cl$_2$): λ (ε, $M^{-1} \cdot cm^{-1}$) = 418 (250000), 531 (39000), and 576

(30000) nm. HRMS (MALDI) calcd. for $C_{128}H_{144}N_8Ni_2S_1$; $[M]^{•+}$: 1940.9936; found 1940.9944. FT-IR (ATR): ν = 3651, 3591, 3586, 2956, 2903, 2869, 2360, 2022, 1592, 1245, 1007, 826, 795, and 714 cm^{-1}. m.p.: >300 °C.

β-Phenylene-bridged Porphyrin Dimer (*β*-30):

A flask containing **35** (50 mg, 50 mmol), 1,4-dibromobenzene (4.0 mg, 17 mmol), Pd(PPh$_3$)$_4$ (2.0 mg, 1.7 mmol), and Cs$_2$CO$_3$ (55 mg, 170 mmol) was purged with argon, and then charged with toluene (0.85 mL). The mixture was stirred at 120 °C for 23 h. The reaction mixture was cooled to room temperature. The reaction mixture was filtered through a small plug of silica gel with copious washings (CH$_2$Cl$_2$). After removal of the solvent, the residue was separated by silica gel chromatography using a 5:1 mixture of *n*-hexane and CH$_2$Cl$_2$ as eluent to afford *β*-30 as a red solid (3.0 mg, 1.5 mmol, 9%).

β-30: ^{1}H NMR (399.65 MHz, CDCl$_3$, 25 °C): δ = 10.14 (s, 2H, *meso*), 9.19 (d, *J* = 4.8 Hz, 2H, β), 9.13 (s, 2H, β), 8.96 (d, *J* = 4.8 Hz, 2H, β), 8.91–8.84 (m, 8H, β), 8.48 (s, 4H, Ph), 8.00 (d, *J* = 2.0 Hz, 4H, Ar), 7.93 (d, *J* = 2.0 Hz, 4H, Ar), 7.92 (d, *J* = 2.0 Hz, 4H, Ar), 7.79 (t, *J* = 2.0 Hz, 1.6 Hz, 2H, Ar), 7.76 (t, *J* = 2.0 Hz, 1.6 Hz, 2H, Ar), 7.74 (t, *J* = 2.0 Hz, 1.6 Hz, 2H, Ar) and 1.57–1.46 (m, 108H, *tert*-Butyl) ppm. ^{13}C NMR (100.40 MHz, CDCl$_3$, 25 °C): δ = 149.04, 148.99, 148.9, 145.1, 143.2, 143.04, 142.99, 142.8, 142.7, 142.6, 141.5, 140.6, 140.08, 140.05, 139.93, 135.8, 132.8, 132.5, 132.4, 132.3, 132.22, 132.15, 131.2, 130.7, 128.8, 128.7, 121.2, 121.14, 121.08, 120.6, 120.0, 119.6, 104.2, 35.1, 35.01, 34.99, 31.8, and 31.7 ppm. UV/Vis (CH$_2$Cl$_2$): λ (ε, M^{-1}·cm^{-1}) = 417 (330000), 527 (39000), and 562 (18000) nm. HRMS (MALDI) calcd. for $C_{130}H_{146}N_8Ni_2$; $[M]^{•+}$: 1935.0372; found 1935.0379. FT-IR (ATR): ν = 3865, 3841, 3797, 3649, 3567, 2958, 2450, 2359, 2342, 2005, 1559, 1522, 1004, and 718 cm^{-1}. m.p.: >300 °C.

Chapter 2

[3,5-Bis(phenylethynyl)-10,15,20-tris(3,5-di-*tert*-butylphenyl)Porphyrinato]Nickel(II) (34Ni):

A flask containing *meso*, β-dichloro nickel porphyrin[67c] (20 mg, 20 μmol), Pd$_2$(dba)$_3$ (3.7 mg, 4.0 μmol), and SPhos (3.3 mg, 8.0 μmol) was purged with argon, and then charged with toluene (2.0 mL) and phenylethynyltributylstannane (35 μL, 100 μmol). The mixture was stirred at 110 °C for 1 h. After cooling to room temperature, the reaction mixture was filtered through a small plug of silica gel with copious washings with CH$_2$Cl$_2$. After removal of the solvent, the

Experimental Section

residue was separated by silica gel chromatography using a 1:7 mixture of CH_2Cl_2 and *n*-hexane as eluent to afford **34Ni** (15.1 mg, 13.4 μmol, 67%) as a purple solid.

34Ni: ^{1}H NMR (399.65 MHz, CD_2Cl_2, 25 °C): δ = 9.72 (d, *J* = 4.8 Hz, 1H, β), 9.04 (s, 1H, β), 8.84 (d, *J* = 4.8 Hz, 1H, β), 8.71 (m, 4H, β), 7.89 (d, *J* = 1.8 Hz, 2H, Ar), 7.87 (d, *J* = 1.8 Hz, 2H, Ar), 7.86 (d, *J* = 1.8 Hz, 2H, Ar), 7.81 (m, 2H, Ph), 7.77 (m, 3H, Ar), 7.51 (m, 2H, Ph), 7.35–7.25 (m, 6H, Ar), and 1.50 (m, 54H, *tert*-Butyl) ppm. ^{13}C NMR (100.40 MHz, CD_2Cl_2, 25 °C): δ = 149.71, 149.67, 146.1, 143.9, 143.7, 143.5, 142.8, 141.3, 140.7, 139.72, 139.65, 139.1, 133.6, 133.3, 133.1, 132.98, 132.94, 132.89, 132.3, 132.1, 129.1, 128.93, 128.89, 128.82, 128.7, 128.6, 125.1, 124.2, 124.1, 122.2, 122.0, 121.7, 121.4, 102.5, 98.6, 98.4, 90.0, 87.0, 35.3, and 31.8 ppm. HRMS (MALDI) calcd. for $C_{78}H_{80}N_4Ni_1$; $[M]^{•+}$: 1130.5731; found 1130.5742. m.p.: >300 °C.

Phosphole-fused Nickel Dehydropurpurin (35Ni):

A flask containing **34Ni** (62.3 mg, 55.0 μmol), $Ti(O^iPr)_4$ (0.16 mL, 0.55 mmol) purged with argon, and then charged with Et_2O (55 mL). A solution of ^iPrMgCl in Et_2O (1.0 M, 2.2 mL, 2.2 mmol) was added to the mixture at –70 °C, and the reaction mixture was stirred for 2 h at –50 °C. Then $PhPCl_2$ (0.37 mL, 2.75 mmol) was added to the mixture at –50 °C. The mixture was stirred for 1 h at –50 °C, and then warmed to room temperature. After the mixture was stirred for 1 h, the reaction was quenched by water and filtered through a Celite bed, and the Celite bed was washed with CH_2Cl_2 several times. The aqueous phase was extracted with CH_2Cl_2, and the combined organic extracts were dried over Na_2SO_4. After the solvent was removed, the residue was dissolved in CH_2Cl_2 and H_2O_2 (30 wt%) was added to the mixture. After stirring for 30 min at room temperature, the reaction was quenched with water. The product was extracted with CH_2Cl_2, and dried over Na_2SO_4. After removal of the solvent, the residue was separated by silica gel column chromatography using a 1:2 mixture of EtOAc and *n*-hexane as eluent to afford **35Ni** (43 mg, 34 μmol, 62%) as a green solid.

35Ni: ^{1}H NMR (399.65 MHz, $CDCl_3$, 25 °C): δ = 9.32 (s, 1H, β), 8.87 (d, *J* = 4.8 Hz, 1H, β), 8.80 (d, *J* = 4.8 Hz, 1H, β), 8.77–8.73 (m, 2H, β), 8.50 (d, *J* = 4.8 Hz, 1H, β), 8.38 (d, *J* = 7.6 Hz, 2H, Ph), 8.30 (d, *J* = 4.8 Hz, 1H, β), 8.14 (bs, 1H, Ar), 8.00–7.92 (m, 6H, Ph+Ar), 7.81–7.69 (m, 6H, Ar), 7.54 (m, 2H, Ph), 7.46–7.40 (m, 7H, Ph), and 1.57–1.46 (m, 54H, *tert*-Butyl) ppm. ^{13}C NMR (100.40 MHz, $CDCl_3$, 25 °C): δ = 157.8, 152.3, 152.0, 150.0, 149.9, 149.2, 149.1, 145.2, 144.4, 144.3, 144.0, 143.8, 143.5, 141.8, 141.5, 140.9, 139.7, 139.0, 138.9, 138.4, 138.2 (*J* = 18.3 Hz), 134.8, 134.4, 134.3, 134.1 (*J* = 10.6 Hz), 133.1, 132.8, 131.9, 131.3, 131.2, 130.2, 129.5, 129.2, 129.1, 129.0, 128.9, 128.8, 128.7, 128.6, 128.3, 128.2, 127.8, 126.7,

125.7, 123.1, 122.9, 122.3, 121.7, 121.6, 121.5, 107.7 (J = 19.3 Hz), 35.3, 35.1, 31.9, 31.8 ppm. ^{31}P NMR (161.7 MHz, CDCl$_3$, 25 °C): δ = 58.2 ppm. UV/Vis (CH$_2$Cl$_2$): λ (ε, M^{-1}·cm^{-1}) = 332 (27400), 409 (43700), 469 (144000), 578 (19300), 620 (8900) nm. HRMS (MALDI) calcd. for C$_{84}$H$_{85}$N$_4$O$_1$P$_1$Ni$_1$; [M]$^{•+}$: 1254.5809; found 1254.5811. FT-IR (ATR): v = 1199 cm^{-1} (P=O). m.p.: 280–290 °C.

Phosphole-fused Nickel Dehydropurpurin (36Ni):

A flask containing **34Ni** (182.4 mg, 0.16 mmol), Ti(O^{i}Pr)$_4$ (0.48 mL, 1.6 mmol) purged with argon, and then charged with Et$_2$O (160 mL). A solution of ^{i}PrMgCl in Et$_2$O (1.0 M, 6.4 mL, 6.4 mmol) was added to the mixture at −70 °C, and the reaction mixture was stirred for 2 h at −50 °C. Then PhPCl$_2$ (1.08 mL, 8.0 mmol) was added to the mixture at −50 ºC. The mixture was stirred for 30 min at −50 °C, and then warmed to room temperature. After the mixture was stirred for 1 h, S powder (excess) was added to the mixture. Then, the reaction was quenched with water. The product was extracted with CH$_2$Cl$_2$, and dried over Na$_2$SO$_4$. After removal of the solvent, the residue was separated by silica gel column chromatography using a 1:4 mixture of CH$_2$Cl$_2$ and *n*-hexane as eluent to afford **36Ni** (161.4 mg, 0.13 mmol, 79%) as a green solid.

36Ni: ^{1}H NMR (399.65 MHz, CDCl$_3$, 25 °C): δ = 9.22 (s, 1H, β), 8.85 (d, J = 5.2, Hz, 1H, β), 8.77 (d, J = 4.8 Hz, 1H, β), 8.74 (d, J = 4.8 Hz, 1H, β), 8.71 (d, J = 4.8 Hz, 1H, β), 8.46 (d, J = 5.2 Hz, 1H, β), 8.30 (d, J = 8.4 Hz, 2H, Ph), 8.14 (m, 3H, Ph), 8.10 (d, J = 4.8 Hz, 1H, β), 8.00 (m, 2H, Ph+Ar), 7.87 (bs, 2H, Ar), 7.79–7.75 (m, 5H, Ar), 7.70 (m, 1H, Ar), 7.52–7.39 (m, 9H, Ph), and 1.61–1.46 (m, 54H, *tert*-Butyl) ppm. ^{13}C NMR (100.40 MHz, CDCl$_3$, 25 °C): δ = 158.1, 152.5 (J = 26.9 Hz), 149.8, 149.2, 149.0, 145.8, 145.2, 144.4, 143.9 (J = 17.3 Hz), 134.8, 134.1, 134.0, 133.7, 133.6, 133.1, 133.0, 132.9, 131.89, 131.86, 131.7, 131.4 (J= 11.5 Hz), 131.1, 131.0, 130.2, 130.0, 129.4, 129.2, 129.0, 128.9, 128.8, 128.7, 128.4, 128.3, 127.6, 123.3, 122.9, 122.8, 122.2, 121.7, 121.52, 121.48, 108.1 (J = 18.3 Hz), 35.2, 35.14, 35.09, 31.9, 31.8, and 29.9 ppm. ^{31}P NMR (161.7 MHz, CDCl$_3$, 25 °C): δ = 74.2 ppm. UV/Vis (CH$_2$Cl$_2$): λ (ε, M^{-1}·cm^{-1}) = 334 (27500), 408 (37900), 468 (158000), 576 (20800), and 613 (10000) nm. HRMS (MALDI) calcd. for C$_{84}$H$_{85}$N$_4$O$_1$P$_1$Ni$_1$; [M]$^{•+}$: 1270.5581; found 1270.5585. FT-IR (ATR): v = 688 cm^{-1} (P=S). m.p.: 280–298 °C.

Phosphole-fused Dehydropurpurin (35H$_2$):

Conc. H$_2$SO$_4$ (0.06 mL) was slowly added to a mixture of **35Ni** (7.8 mg, 6.2 μmol) and trifluoroacetic acid (0.6 mL) at 0 °C. The reaction mixture was stirred at 0 °C for 1 h, and then poured into water at 0 °C. After neutralization by KOH aq. at 0 °C, the product was extracted

with CH_2Cl_2, and dried over Na_2SO_4. After removal of the solvent, the mixture was filtered through a small plug of silica gel with copious washings with CH_2Cl_2 as eluent to afford **35H₂** (6.8 mg, 5.7 µmol, 91%) as a green solid.

35H₂: ^1H NMR (399.65 MHz, $CDCl_3$, 25 °C): δ = 9.41 (d, J = 1.2 Hz, 1H, β), 9.04 (dd, J = 2.0 Hz, 4.8 Hz, 1H, β), 8.93 (dd, J = 2.0 Hz, 4.8 Hz, 1H, β), 8.71 (d, J = 4.8 Hz, 1H, β), 8.68 (d, J = 4.4 Hz, 1H, β), 8.59 (dd, J = 2.0 Hz, 4.8 Hz, 1H, β), 8.41 (d, J = 8.0 Hz, 2H, Ph), 8.22 (m, 1H, Ar), 8.19 (dd, J = 2.0 Hz, 4.8 Hz, 1H, β), 8.15 (m, 1H, Ar), 8.07 (m, 1H, Ar), 8.00 (d, J = 6.4 Hz, 2H, Ar), 7.94 (m, 2H, Ph), 7.91 (m, 1H, Ar), 7.84 (m, 1H, Ar), 7.79 (m, 1H, Ar), 7.76 (m, 1H, Ar), 7.54–7.50 (m, 5H, Ph), 7.43–7.38 (m, 6H, Ph), 1.61–1.45 (m, 54H, *tert*-Butyl), −1.19 (s, 1H, NH), and −2.08 (s, 1H, NH) ppm. ^{13}C NMR (100.40 MHz, $CDCl_3$, 25 °C): δ = 166.5, 160.5, 156.4 (J = 25.8 Hz), 153.5, 153.2, 149.9 (J = 15.3), 148.99, 148.96, 148.90, 141.6, (J = 30.5 Hz), 133.1, 132.2, 135.6, 135.4, 135.22, 135.15, 135.12, 134.4 (J = 10.5 Hz), 133.1, 132.2, 131.8, 131.4, 131.3, 130.4, 130.3, 129.8, 129.72, 129.66, 129.2, 129.0, 128.9, 128.81, 128.75, 128.6, 128.52, 128.45, 128.2, 127.8, 126.5, 126.1, 125.6, 124.6 (J = 5.7 Hz), 124.2, 124.1, 121.7, 121.51, 121.47, 107.5 (J = 19.1 Hz), 35.3, 35.20, 35.15, 31.97, 31.93, and 31.8 ppm. ^{31}P NMR (161.7 MHz, $CDCl_3$, 25 °C): δ = 60.3 ppm. UV/Vis (CH_2Cl_2): λ (ε, $M^{-1} \cdot cm^{-1}$) = 412 (55300), 471 (200000), 570 (19200), 628 (12900), and 692 (8000) nm. Fluorescence (CH_2Cl_2, λ_{ex} = 471 nm): λ_{max} = 707 and 780 nm (Φ_F = 0.13). HRMS (MALDI) calcd. for $C_{84}H_{87}N_4O_1P_1$; $[M]^{\bullet+}$: 1198.6612.; found 1198.6617. FT-IR (ATR): ν = 1199 cm^{-1} (P=O). m.p.: 277–288 °C.

Phosphole-fused Dehydropurpurin (36H₂):

Conc. H_2SO_4 (0.45 mL) was slowly added to a mixture of **36Ni** (58 mg, 45.6 µmol) and Trifluoroacetic acid (4.5 mL) at 0 °C. The reaction mixture was stirred at 0 °C for 1 h, and then poured into water at 0 °C. After neutralization by KOH aq. at 0 °C, the product was extracted with CH_2Cl_2, and dried over Na_2SO_4. After removal of the solvent, the mixture was filtered through a small plug of silica gel with copious washings with CH_2Cl_2 as eluent to afford **36H₂** (51.6 mg, 42.4 µmol, 93%) as a green solid.

36H₂: ^1H NMR (399.65 MHz, $CDCl_3$, 25 °C): δ = 9.34 (s, 1H, β), 9.04 (dd, J = 1.2 Hz, 4.8 Hz, 1H, β), 8.93 (dd, J = 1.2 Hz, 4.8 Hz, 1H, β), 8.72 (d, J = 4.8 Hz, 1H, β), 8.67 (d, J = 4.8 Hz, 1H, β), 8.59 (dd, J = 1.6 Hz, 4.8 Hz, 1H, β), 8.38 (d, J = 8.0 Hz, 2H, Ph), 8.29 (d, J = 6.8 Hz, 1H, Ph), 8.19 (m, 2H, Ar), 8.14 (m, 2H, Ph), 8.05–8.03 (m, 3H, β + Ar), 7.98 (m, 1H, Ar), 7.94 (m, 1H, Ar), 7.85 (m, 1H, Ar), 7.81 (m, 1H, Ar), 7.78 (m, 1H, Ar), 7.73 (m, 1H, Ph), 7.60 (m, 1H, Ph), 7.55–7.50 (m, 2H, Ph), 7.46–7.39 (m, 5H, Ph), 7.16 (d, J = 7.2 Hz, 1H, Ph), 1.67–1.47 (m, 54H, *tert*-Butyl), −1.12 (s, 1H, NH), and −2.05 (s, 1H, NH) ppm. ^{13}C NMR (100.40 MHz,

CDCl$_3$, 25 °C): δ = 167.0, 160.2, 156.4 (J = 39.1 Hz), 153.6 (J = 26.7 Hz), 149.9, 149.8, 148.96, 148.94, 148.89, 148.85, 142.7, 135.5, 135.4, 135.1, 134.8, 134.7, 134.0, 133.9, 132.0, 131.78, 131.75, 131.5 (J = 11.4 Hz), 131.3, 130.93, 130.89, 130.4, 130.2, 130.1, 129.9, 129.8, 129.7, 129.6, 129.42, 129.40, 129.18, 129.16, 129.0, 128.9, 128.79, 128.76, 128.6, 128.5, 128.24, 128.17, 127.4, 125.9, 124.6, 124.3, 124.2, 124.1, 121.7, 121.5, 108.0, 107.8, 35.31, 35.28, 35.17, 35.15, 31.9, 31.86, and 31.84 ppm. ^{31}P NMR (161.7 MHz, CDCl$_3$, 25 °C): δ = 75.0 ppm. UV/Vis (CH$_2$Cl$_2$): λ (ε, M^{-1}·cm^{-1}) = 411 (47700), 471 (200000), 568 (19400), 612 (11600), 628 (11900), and 692 (7800) nm. Fluorescence (CH$_2$Cl$_2$, λ_{ex} = 471 nm): λ_{max} = 703 and 778 nm (Φ_F = 0.01). HRMS (MALDI) calcd. for C$_{84}$H$_{87}$N$_4$S$_1$P$_1$; [M]$^{•+}$: 1214.6384; found 1214.6385. FT-IR (ATR): ν = 694 cm^{-1} (P=S). m.p.: 266–278 °C.

Phosphole-fused Zinc Dehydropurpurin (35Zn):

A solution of Zn(OAc)$_2$· 2H$_2$O (66 mg, 0.3 mmol) in MeOH (1.5 mL) was added to the mixture of **35H$_2$** (37.0 mg, 30 μmol) in CH$_2$Cl$_2$ (3.0 mL). The reaction mixture was stirred for 1h at room temperature. After removal of the solvent, the mixture was filtered through a small plug of silica gel with copious washings with EtOAc as eluent to afford **35Zn** (38.4 mg, 29.3 μmol, 98%)as a green solid.

35Zn: ^{1}H NMR (399.65 MHz, CDCl$_3$/C$_5$D$_5$N, 25 °C): δ = 9.42 (s, 1H, β), 8.95 (d, 1H, J = 4.4 Hz, β), 8.84, (d, J = 5.2 Hz, 2H, β), 8.77 (d, J = 4.4 Hz, 1H, β), 8.49 (d, J = 4.8 Hz, 1H, β), 8.46 (d, J = 7.6 Hz, 2H, Ph), 8.23 (s, 1H, Ar), 8.15 (s, 1H, Ar), 8.12 (d, J = 4.8 Hz, 1H, β), 8.08 (m, 1H, Ar), 8.01–7.97 (m, 3H, Ar+Ph), 7.93 (m, 3H, Ar+Ph), 7.83 (m, 1H, Ar), 7.79 (m, 1H, Ar), 7.75 (m, 1H, Ar), 7.55–7.51 (m, 5H, Ph), 7.42–7.38 (m, 5H, Ph), and 1.63–1.50 (m, 56H, *tert*-Butyl) ppm. ^{13}C NMR (100.40 MHz, CDCl$_3$/C$_5$D$_5$N, 25 °C): δ = 164.2, 154.6 (J = 28.9 Hz), 154.3, 152.5, 151.1, 150.7 (J = 26.0 Hz), 150.5, 149.9, 149.3, 149.2, 1490.0, 148.7, 148.6, 148.5, 148.4, 148.3, 143.4 (J = 29.9 Hz), 142.1, 142.0, 141.0, 136.9, 136.7, 135.8, 135.7, 135.64, 135.58, 135.3, 134.6 (J = 10.6 Hz), 134.0, 133.3, 132.9, 132.53, 132.48, 132.4, 132.3, 131.6, 131.4 (J = 10.6 Hz), 130.51, 130.48, 129.8, 129.64, 129.60, 129.5, 129.3, 129.1, 128.8, 128.7, 128.6, 128.3, 128.2, 126.6, 125.6 (J = 18.3 Hz), 125.2, 125.0 (J = 12.5 Hz), 124.5, 123.4, 123.1, 122.9, 121.0, 120.9, 119.5, 108.1 (J = 19.3 Hz), 35.2, 35.74, 35.07, 31.96, 31.92, 31.88, and 31.82 ppm. ^{31}P NMR (161.7 MHz, CDCl$_3$/C$_5$D$_5$N, 25 °C): δ = 59.1 ppm. UV/Vis (pyridine/CH$_2$Cl$_2$ = 1/99): λ (ε, M^{-1}·cm^{-1}) = 312 (28500), 481 (238000), 611 (19700), and 663 (15200) nm. Fluorescence (pyridine/CH$_2$Cl$_2$ = 1/99, λ_{ex} = 482 nm): λ_{max} = 692 nm (Φ_F = 0.14). HRMS (MALDI) calcd. for C$_{84}$H$_{85}$N$_4$O$_1$P$_1$Zn$_1$; [M]$^{•+}$: 1260.5747; found 1260.5751. FT-IR (ATR): ν = 1171 cm^{-1} (P=O). m.p.: >300 °C.

Experimental Section

Phosphole-fused Zinc Dehydropurpurin (36Zn):

A solution of $Zn(OAc)_2 \cdot 2H_2O$ (93 mg, 4.2 mmol) in MeOH (2.1 mL) was added to the mixture of **36H₂** (51.6 mg, 42.4 µmol) in CH_2Cl_2 (4.2 mL). The reaction mixture was stirred for 1h at room temperature. After removal of the solvent, the mixture was filtered through a small plug of silica gel with copious washings with CH_2Cl_2 as eluent to afford **36Zn** (51.1 mg, 39 µmol, 92%) as a green solid.

36Zn: ^{1}H NMR (399.65 MHz, CDCl₃, 25 °C): δ = 9.38 (s, 1H, β), 9.04 (d, J = 4.4 Hz, 1H, β), 8.92 (d, J = 4.4 Hz, 2H, β), 8.84 (d, J = 5.2 Hz, 1H, β), 8.92 (d, J = 4.8 Hz, 1H, β), 8.32 (m, 2H, Ar), 8.21 (m, 1H, Ar), 8.15 (m, 1H, Ar), 8.09–8.04 (m, 5H, Ar+Ph), 8.00 (d, J = 4.8 Hz, 1H, β), 7.98 (m, 1H, Ph), 7.94 (m, 1H, Ar), 7.84 (m, 1H, Ar), 7.80 (m, 1H, Ar), 7.77 (m, 1H, Ar), 7.70 (t, J = 7.2 Hz, 1H, Ph), 7.57 (t, J = 7.2 Hz, 1H, Ph), 7.52–7.48 (m, 2H, Ph), 7.44–7.35 (m, 5H, Ph), 7.10 (d, J = 7.6 Hz, 1H, Ph), and 1.63–1.49 (m, 54H, *tert*-Butyl) ppm. ^{13}C NMR (100.40 MHz, CDCl₃, 25 °C): δ = 164.3, 154.2, 153.8, 152.4, 151.2 (J = 45.8 Hz), 150.7, 150.1, 149.5 (J = 10.5 Hz), 148.9, 148.8, 148.7, 148.6, 148.4, 143.7, 143.4, 141.5, 141.4, 140.5, 137.3 (J = 16.2 Hz), 134.7, 134.5, 133.9, 133.1, 133.0, 132.7, 131.7, 131.5, 131.4, 130.9, 130.3, 129.89, 129.82, 129.63, 129.57, 129.43, 129.36, 129.0, 128.9, 128.7, 128.3 (J = 48.6 Hz), 124.8, 122.0, 121.4, 121.2, 109.3, 109.1, 35.31, 35.28, 35.17, 35.1, 32.0, and 31.9 ppm. ^{31}P NMR (161.7 MHz, CDCl₃, 25 °C): δ = 75.2 ppm. UV/Vis (pyridine/CH_2Cl_2 = 1/99): λ (ε, $M^{-1} \cdot cm^{-1}$) = 319 (31500), 482 (269000), 610 (23000), and 663 (18600) nm. Fluorescence (pyridine/CH_2Cl_2 = 1/99, λ_{ex} = 482 nm): λ_{max} = 688 nm (Φ_F = 0.03). HRMS (MALDI) calcd. for $C_{84}H_{85}N_4S_1P_1Zn_1$; $[M]^{\bullet+}$: 1276.5519; found 1276.5509. FT-IR (ATR): ν = 695 cm^{-1} (P=S). m.p.: >300 °C.

Phosphole-fused Nickel Dehydropurpurin (37Ni):

A flask containing **36Ni** (13.6 mg, 10.7 µmol) was purged with argon, and then charged with toluene (1.1 ml). To the mixture was added $P(NMe_2)_3$ (0.05 mL), and the reaction mixture was stirred for 1 h at 90 °C. After removal of the solvent, the mixture was filtered through a small plug of silica gel with copious washings with CH_2Cl_2 as eluent to afford **37Ni** (12.8 mg, 10.3 µmol, 96%) as a green solid.

37Ni: ^{1}H NMR (399.65 MHz, CDCl₃, 25 °C): δ = 8.84 (s, 1H, β), 8.67 (d, J = 4.8 Hz, 1H, β), 8.63–8.59 (m, 3H, β), 8.35 (d, J = 5.2 Hz, 1H, β), 8.28 (br, 1H, Ar), 8.16 (d, J = 8.8 Hz, 2H, Ar), 8.13 (d, J = 4.8 Hz, 1H, β), 8.08 (br, 2H, Ar), 7.74–7.65 (m, 7H, Ar+Ph), 7.59 (br, 2H, Ar), 7.47–7.43 (m, 3H, Ar), 7.36–7.29 (m, 4H, Ar+Ph), 7.21 (m, 3H, Ph), and 1.63–1.26 (m, 54H, *tert*-Butyl) ppm. ^{13}C NMR (100.40 MHz, CDCl₃, 25 °C): δ = 158.9, 150.4 (J = 13.5 Hz), 149.6, 149.1, 149.0, 145.3, 144.7, 144.1, 143.49, 143.47, 143.3, 142.3, 142.2, 141.20, 141.17, 140.8 (J

= 5.8 Hz), 140.5, 140.1, 140.0 (J = 4.8 Hz), 139.1, 137.6, 137.5, 137.2, 137.0, 134.3, 134.1 (J = 12.5 Hz), 133.8, 132.5, 132.3, 132.2, 132.0, 129.7, 129.6, 129.3, 128.9, 129.1, 129.0, 128.9, 128.81, 128.76, 128.69, 128.2, 127.7, 127.5, 127.4, 122.6 (J = 45.3 Hz), 121.7, 121.4, 121.3, 121.2, 120.8, 110.0, 35.1, and 31.8 ppm. ^{31}P NMR (161.7 MHz, CDCl$_3$, 25 °C): δ = 47.6 ppm. UV/Vis (CH$_2$Cl$_2$): λ (ε, M^{-1}·cm^{-1}) = 330 (26400), 384 (29400), 472 (104000), 580 (15100), and 623 (8500) nm. HRMS (MALDI) calcd. for C$_{84}$H$_{85}$N$_4$PNi$_1$; [M]$^{•+}$: 1238.5860; found 1238.5875.

Phosphole-fused Dehydropurpurins (37H$_2$):

A flask containing **36H$_2$** (30.0 mg, 25 μmol) was purged with argon, and then charged with toluene (2.5 mL). To the mixture was added to P(NMe$_2$)$_3$ (0.1 mL), and the reaction mixture was stirred for 1 h at 90 °C. After removal of the solvent, the mixture was filtered through a small plug of silica gel with copious washings with CH$_2$Cl$_2$ as eluent to afford **37H$_2$** (29.6 mg, 25 μmol, quant.) as a dark green solid.

37H$_2$: ^{1}H NMR (399.65 MHz, CDCl$_3$, 25 °C): δ = 8.89 (dd, J = 1.8 Hz, 4.8 Hz, 1H, β), 8.85 (s, 1H, β), 8.78 (dd, J = 1.8 Hz, 4.8 Hz, 1H, β), 8.62 (d, J = 4.0 Hz, 1H, β), 8.57 (d, J = 4.0 Hz, 1H, β), 8.44 (dd, J = 1.2 Hz, 5.6 Hz, 1H, β), 8.27 (m, 1H, Ar), 8.21 (d, J = 8.4 Hz, 2H, Ph), 8.09 (m, 1H, Ar), 8.05 (m, 1H, Ar), 8.01 (m, 2H, β+Ar), 7.93 (m, 1H, Ar), 7.81 (m, 3H, Ar), 7.77–7.72 (m, 5H, Ar+Ph), 7.47 (t, J = 8.0 Hz, 5H, Ph), 7.34 (m, 1H, Ph), 7.28 (m, 3H, Ph), 1.66–1.43 (m, 54H, *tert*-Butyl), –0.62 (s, 1H, inner NH), and –1.69 (s, 1H, inner NH) ppm. ^{31}P NMR (161.7 MHz, CDCl$_3$, 25 °C): δ = 51.1 ppm. UV/Vis (CH$_2$Cl$_2$): λ (ε, M^{-1}·cm^{-1}) = 387 (36600), 466 (116000), 573 (13600), 613 (9100), and 705 (5400) nm. Fluorescence (CH$_2$Cl$_2$, λ_{ex} = 465 nm): λ_{max} = 719 and 797 nm (Φ_F = 0.07). HRMS (MALDI) calcd. for C$_{84}$H$_{88}$N$_4$P$_1$; [M+H]$^+$: 1183.6741; found 1183.6698. Because **37H$_2$** is oxidized to **35H$_2$** during the ^{13}C NMR measurement, we could not obtain the ^{13}C NMR spectrum.

Phosphole-fused Zinc Dehydropurpurins (37Zn):

A flask containing **36Zn** (30.0 mg, 23 μmol) was purged with argon, and then charged with toluene (2.3 mL). To the mixture was added to P(NMe$_2$)$_3$ (0.1 mL), and the reaction mixture was stirred for 1 h at 90 °C. After removal of the solvent, the mixture was filtered through a small plug of silica gel with copious washings with CH$_2$Cl$_2$ as eluent to afford **37Zn** (28.7 mg, 23 μmol, quant.) as a green solid.

37Zn: ^{1}H NMR (399.65 MHz, CDCl$_3$, 25 °C): δ = 8.96 (s, 1H, β), 8.94 (d, J = 4.4 Hz, 1H, β), 8.83 (d, J = 4.8 Hz, 1H, β), 8.81 (d, J = 4.8 Hz, 1H, β), 8.75 (d, J = 4.4 Hz, 1H, β), 8.44 (d, J = 4.8 Hz, 1H, β), 8.26 (br, 1H, Ar), 8.10–8.05 (m, 5H, Ar+Ph), 8.02 (d, J = 4.8 Hz, 1H, β), 8.00

(m, 1H, Ar), 7.97 (m, 1H, Ar), 7.88 (m, 1H, Ar), 7.80 (m, 1H, Ar), 7.77 (m, 1H, Ar), 7.74 (m, 1H, Ar), 7.62 (m, 3H, Ph), 7.45 (t, J = 6.7, 7.3 Hz, 2H, Ph), 7.38 (t, J = 7.3 Hz, 3H, Ph), 7.29 (m, 1H, Ph), 7.22 (m, 3H, Ph), and 1.68–1.48 (m, 54H, *tert*-Butyl) ppm. ^{31}P NMR (161.7 MHz, CDCl$_3$, 25 °C): δ = 50.1 ppm. UV/Vis (pyridine/CH$_2$Cl$_2$ = 1/99): λ (ε, M^{-1}·cm^{-1}) = 331 (33900), 398 (40900), 482 (212000), 612 (17300), and 675 (16200) nm. Fluorescence (pyridine/CH$_2$Cl$_2$ = 1/99, λ_{ex} = 483 nm): λ_{max} = 694 nm (Φ_F = 0.07). HRMS (MALDI) calcd. for C$_{84}$H$_{85}$N$_4$P$_1$Zn$_1$; [M]$^{+\bullet}$: 1244.5798; found 1244.5784. Because **37Zn** is oxidized to **35Zn** during the ^{13}C NMR measurement, we could not obtain the ^{13}C NMR spectrum.

Chapter 3

Pyrrole-fused Nickel Dehydropurpurin (42Ni):

A flask containing **34Ni** (10 mg, 8.8 µmol), PdCl$_2$ (0.16 mg, 0.9 µmol), PhNH$_2$ (4 µL, 44 µmol) and Et$_3$N (6 µL, 44 µmol) was charged with a 4:1 mixture of DMSO and toluene (1.5 mL). The mixture was stirred at 100 °C for 20 h under air. After cooling to ambient temperature, the reaction mixture was quenched with water, extracted with toluene, and dried over Na$_2$SO$_4$. After removal of solvent, the crude product was purified with silica gel column chromatography using a 4:1 mixture of CH$_2$Cl$_2$ and *n*-hexane to afford **42Ni**. Reprecipitation from CH$_2$Cl$_2$ and methanol gave **42Ni** (7.2 mg, 5.9 µmol, 67%) as a green solid.

42Ni: ^{1}H NMR (399.65 MHz, CDCl$_3$, 25 °C): δ = 8.54 (d, J = 4.9 Hz, 1H, β), 8.44 (d, J = 4.9 Hz, 1H, β), 8.41 (d, J = 4.3 Hz, 1H, β), 8.37 (d, J = 4.9 Hz, 1H, β), 8.23 (d, J = 4.9 Hz, 1H, β), 8.00 (s, 1H, β), 7.88 (d, J = 1.8 Hz, 2H, Ar), 7.79 (d, J = 1.8 Hz, 2H, Ar), 7.71 (d, J = 1.8 Hz, 2H, Ar), 7.67 (m, 2H, Ar), 7.64 (m, 2H, Ar+β), 7.57 (m, 2H, Ph), 7.47–7.43 (m, 5H, Ph), 7.30–7.17 (m, 8H, Ph), 1.51 (brs, 18H, *tert*-Butyl), and 1.44 (brs, 36H, *tert*-Butyl) ppm. ^{13}C NMR (100.40 MHz, CD$_2$Cl$_2$, 25 °C): δ = 157.9, 149.8, 149.5, 149.4, 146.9, 145.3, 144.8, 144.4, 143.7, 142.2, 140.9, 140.6, 140.4, 139.33, 139.28, 134.9, 134.7, 133.8, 133.3, 132.7, 132.5, 132.4, 132.2, 131.7, 131.2, 130.7, 129.6, 129.5, 129.3, 128.64, 128.57, 128.1, 127.9, 127.5, 124.1, 123.6, 122.9, 121.7, 121.6, 121.5, 119.1, 112.1, 35.4, 35.3, 35.2, 31.82, and 31.78 ppm. UV/Vis (CH$_2$Cl$_2$): λ (ε, M^{-1}·cm^{-1}) = 318 (24700), 368 (24300), 464 (81900), 474 (80600), 578 (9700), 619 (5500), and 679 (2500). HRMS (APCI) calcd. for C$_{84}$H$_{86}$N$_5$Ni$_1$; [M+H]$^+$: 1222.6231; found 1222.6211. FT-IR (ATR): ν = 3613, 2953, 2900, 2866, 2364, 1591, 1476, 1424, 1287, 1245, 1068, 996, 935, 712, and 444 cm^{-1}. m.p.: >300 °C.

Pyrrole-fused Dehydropurpurin (42H₂):

Conc. H_2SO_4 (0.25 mL) was slowly added to a mixture of **42Ni** (30 mg, 0.025 mmol) and trifluoroacetic acid (2.5 mL) at 0 °C. The reaction mixture was stirred at 0 °C for 1 h under dark, and then poured into water at 0 °C. After neutralization by KOH aq. at 0 °C, the product was extracted with CH_2Cl_2 and dried over Na_2SO_4. After removal of solvent, the product was reprecipitated from CH_2Cl_2 and methanol gave **42H₂** (24.3 mg, 0.021 mmol, 83%) as a blown solid.

42H₂: ^{1}H NMR (399.65 MHz, CDCl₃, 25 °C): δ = 8.55 (dd, J = 4.8 Hz, 1.8 Hz, 1H, β), 8.40 (dd, J = 4.8 Hz, 1.8 Hz, 1H, β), 8.35 (d, J = 4.8 Hz, β), 8.27 (d, 4.2 Hz, 1H, β), 8.19 (dd, J = 4.8 Hz, 1.8 Hz, β), 8.00 (d, J = 1.8 Hz, 2H, Ar), 7.89 (d, J = 1.8 Hz, 2H, Ar), 7.81 (d, J = 1.8 Hz, 2H, Ar), 7.76 (s, 1H, β), 7.69 (m, 2H, Ar), 7.64 (m, 3H, Ar+Ph), 7.51 (m, 3H, Ph), 7.47 (m, 1H, Ph), 7.45 (m, 1H, Ph), 7.40 (dd, J = 1.8 Hz, 4.8 Hz, 1H, β), 7.29-7.18 (m, 8H, Ph), 1.54 (s, 18H, *tert*-Butyl), 1.45 (brs, 1H, *tert*-Butyl), 0.76 (brs, 1H, NH), and −0.59 (brs, 1H, NH) ppm. ^{13}C NMR (100.40 MHz, CDCl₃, 25 °C): δ = 157.4, 149.3, 148.8, 148.7, 144.4, 141.6, 140.9, 139.6, 139.5, 139.0, 138.9, 136.8, 135.0, 134.6, 134.2, 133.5, 132.0, 131.8, 130.3, 129.3, 129.16, 129.13, 129.0, 129.2, 128.3, 128.0, 127.5, 127.2, 127.1, 125.8, 124.4, 124.1, 121.0, 120.93, 120.95, 120.8, 119.79, 119.85, 119.82, 110.8, 35.2, 35.1, and 31.9 ppm. UV/Vis (CH_2Cl_2): λ (ε, $M^{-1} \cdot cm^{-1}$) = 313 (36300), 383 (45500), 439 (70500), 468 (83100), 490 (95500), 607 (10200), 658 (7700), and 751 (4000) nm. Fluorescence (CH_2Cl_2, λ_{ex} = 490 nm): λ_{max} = 764 nm. HRMS (MALDI) calcd. for $C_{84}H_{87}N_5$; $[M]^{\cdot+}$: 1165.6956; found 1165.6956. FT-IR (ATR): ν = 2951, 2902, 2867, 1591, 1476, 1444, 1393, 1362, 1246, 1233, 910, 801, 711, and 694 cm^{-1}. m.p.: >300 °C.

Pyrrole-fused Zinc Dehydropurpurin (42Zn):

A flask containing **42H₂** (11.7 mg, 0.01 mmol) and $Zn(OAc)_2 \cdot 2H_2O$ (21.8 mg, 0.1 mmol) was purged with argon, and then charged with a degassed 1:1 mixture of CH_2Cl_2 and methanol (2 mL). The reaction mixture was stirred at room temperature for 3 h under dark. After removal of solvent, the mixture was filtered through a small plug of silica gel with copious washing with a 1:2 mixture of CH_2Cl_2 and *n*-hexane as eluent to afford **42Zn** (12.3 mg, 0.01 mmol, quant.) as a green solid.

42Zn: ^{1}H NMR (399.65 MHz, CDCl₃, 25 °C): δ = 8.74 (d, J = 4.9 Hz, 1H, β), 8.63 (d, J = 4.3 Hz, 1H, β), 8.58 (d, J = 4.9 Hz, 1H, β), 8.53 (d, J = 4.9 Hz, 1H, β), 8.35 (d, J = 4.3 Hz, 1H, β), 8.11 (s, 1H, β), 8.08 (d, J = 1.2 Hz, 2H, Ar), 7.96 (d, J = 1.2 Hz, 2H, Ar), 7.89 (2H, J = 1.8 Hz, 2H, Ar), 7.73 (m, 2H, Ph), 7.69 (m, 3H, Ar), 7.61 (d, J = 4.9 Hz, 1H, β), 7.56 (m, 1H, Ph), 7.53

(m, 4H, Ph), 7.34–7.27 (m, 3H, Ph), 7.24 (m, 5H, Ph), 1.58 (s, 18H, *tert*-Butyl), and 1.49 (brs, 36H, *tert*-Butyl) ppm. ^{13}C NMR (100.40 MHz, CDCl$_3$, 25 °C): δ = 164.7, 154.8, 151.4, 150.75, 150.67, 150.5, 149.8, 149.0, 148.7, 148.6, 147.5, 141.8, 141.7, 141.4, 140.5, 139.1, 136.5, 134.6, 133.8, 133.6, 132.6, 132.3, 132.1, 131.8, 131.2, 130.9, 130.4, 129.2, 129.1, 129.0, 128.9, 128.4, 127.9, 125.6, 124.8, 124.3 121.3, 120.84, 120.78, 120.6, 118.8, 112.6, 35.2, 35.12, 35.10, and 31.9 ppm. UV/Vis (CH$_2$Cl$_2$): λ (ε, M^{-1}·cm^{-1}) = 313 (25300), 380 (30000), 459 (62000), 484 (129000), 520 (26000), 603 (10300), 649 (6000), and 713 (4100) nm. Fluorescence (CH$_2$Cl$_2$, λ_{ex} = 484 nm): λ_{max} = 732 and 815 nm. HRMS (ESI) calcd for C$_{84}$H$_{85}$N$_5$Zn$_1$; [M]$^{\bullet+}$: 1227.6091; found 1227.6120. FT-IR (ATR): ν = 2951, 2902, 2867, 1590, 1492, 1476, 1423, 1361, 1331, 1268, 1218, 1071, 1054, 999, 935, 899, 881, 707, and 698 cm^{-1}. m.p.: > 300 °C.

Chapter 4

Thiophene-bridged Porphyrin Dimer (29a (β-29)):

A flask containing **45a** (211 mg, 0.2 mmol), thiophene **46** (33.6 mg, 0.1 mmol), SPhos-Pd-G2 (7.2 mg, 0.01 mmol) and K$_3$PO$_4$ (106 mg, 0.5 mmol) was purged with argon, and charged with THF (8 mL) and H$_2$O (2 mL). After stirring for 3 h at 65 °C, the reaction mixture was cooled to room temperature, quenched with water, extracted with CH$_2$Cl$_2$, and dried over Na$_2$SO$_4$. After removal of solvent, the crude product was purified with silica gel column chromatography using a 8:1 mixture of *n*-hexane and CH$_2$Cl$_2$ to afford **29a**. Reprecipitation from CH$_2$Cl$_2$ and MeOH gave **29a** (128.9 mg, 0.0663 mmol, 66%) as a red solid.

29a:[80] ^{1}H NMR (399.65 MHz, CDCl$_3$, 25 °C): δ = 10.36 (s, 2H, *meso*), 9.20 (d, *J* = 4.3 Hz, 2H, β), 9.14 (s, 2H, β), 8.95 (d, *J* = 4.9 Hz, 2H, β), 8.50–8.83 (m, 8H, β), 8.14 (s, 2H, Thienyl), 7.98 (d, *J* = 1.8 Hz, 4H, Ar-*ortho*), 7.91 (d, *J* = 1.8 Hz, 4H, Ar-*ortho*), 7.89 (d, *J* = 1.8 Hz, 4H, Ar-*ortho*), 7.78–7.77 (m, 2H, Ar-*para*), 7.75–7.74 (m, 2H, Ar-*para*), 7.72 (m, 2H, Ar-*para*), 1.52 (s, 36H, *tert*-Butyl), 1.50 (s, 36H, *tert*-Butyl), and 1.48 (s, 36H, *tert*-Butyl) ppm.

Thiophene-bridged Porphyrin Dimer (29b):

A flask containing **45b** (41.7 mg, 0.042 mmol), thiophene **46** (7.09 mg, 0.021 mmol), SPhos-Pd-G2 (1.5 mg, 0.0021 mmol) and K$_3$PO$_4$ (22.3 mg, 0.11 mmol) was purged with argon, and charged with THF (1.6 mL) and H$_2$O (0.4 mL). After stirring for 13 h at 65 °C, the reaction mixture was cooled to room temperature, quenched with water, extracted with CH$_2$Cl$_2$, and dried over Na$_2$SO$_4$. After removal of solvent, the crude product was purified with silica gel column chromatography using a 6:1 mixture of *n*-hexane and CH$_2$Cl$_2$. Reprecipitation from CH$_2$Cl$_2$ and MeOH gave **29b** (26.6 mg, 0.0147 mmol, 70%) as a red solid.

29b: ^{1}H NMR (399.65 MHz, CDCl$_3$, 25 °C): δ = 10.36 (s, 2H, *meso*), 9.20 (d, *J* = 4.9 Hz, 2H, β), 9.13 (s, 2H, β), 8.94 (d, *J* = 4.9 Hz, 2H, β), 8.84 (d, *J* = 4.9 Hz, 2H, β), 8.81 (d, *J* = 4.9 Hz, 2H, β), 8.63 (d, *J* = 4.9 Hz, 4H, β), 8.13 (s, 2H, Thienyl), 7.99 (d, *J* = 1.8 Hz, 4H, Ar-*ortho*), 7.93 (d, *J* = 1.8 Hz, 4H, Ar-*ortho*), 7.77 (m, 2H, Ar-*para*), 7.75 (m, 2H, Ar-*para*), 7.21 (s, 4H, Mes), 2.57 (s, 6H, Methyl), 1.84 (s, 12H, Methyl), 1.53 (s, 36H, *tert*-Butyl), and 1.50 (s, 36H, *tert*-Butyl) ppm. ^{13}C NMR (100.40 MHz, CDCl$_3$, 25 °C): δ = 149.3, 149.2, 143.5, 143.4, 143.3, 143.2, 142.7, 142.6, 141.7, 140.1, 140.0, 139.8, 139.1, 137.8, 137.6, 137.5, 133.1, 133.0, 132.4, 131.4, 131.3, 130.7, 129.5, 129.3, 129.1, 127.9, 121.33, 121.29, 120.2, 119.9, 117.7, 104.2, 35.23, 35.19, 31.90, 31.87, 21.59, and 21.55 ppm. HRMS (APCI) calcd for C$_{118}$H$_{124}$N$_8$Ni$_2$S$_1$; [M+H]$^+$: 1801.8449; found 1801.8446. FT-IR (ATR): ν = 2953, 2867, 1592, 1461, 1427, 1382, 1362, 1334, 1298, 1246, 1202, 1069, 1001, 974, 928, 900, 883, 827, 814, 796, and 714 cm^{-1}. m.p.: > 300 °C.

Thiophene-fused Helical Porphyrin Dimer (43a):

A flask containing **29a** (100 mg, 0.0514 mmol) was purged with argon, and then charged with CHCl$_3$ (10.3 mL). Palau'Chlor (23.7 mg, 0.113 mmol) was added to the mixture at 0 °C. The reaction mixture was stirred at 0 °C for 30 min, and then stirred at room temperature for 13 h. The mixture was diluted with CH$_2$Cl$_2$, and then filtered through a small plug of silica gel with copious washing with CH$_2$Cl$_2$. After removal of solvent, the crude product of **47a** was using for next step without further purification. A flask containing **47a**, Pd(OAc)$_2$ (2.3 mg, 0.0103 mmol), PCy$_3$·HBF$_4$ (7.6 mg, 0.0206 mmol), and K$_2$CO$_3$ (14.2 mg, 0.103 mmol) was purged with argon, and charged with DMF (2.6 mL). The mixture was heated to reflux with stirring for 3.5 h, and then cooled to ambient temperature. The mixture was extracted with toluene, and dried over Na$_2$SO$_4$. After removal of solvent, the crude product was purified with silica gel column chromatography using a 10:1 mixture of *n*-hexane and CH$_2$Cl$_2$ to afforded **1a**. Recrystallization from CH$_2$Cl$_2$ and MeOH gave **43a** (43.4 mg, 0.0224 mmol, 43%) as a dark solid.

43a: ^{1}H NMR (399.65 MHz, CDCl$_3$, 25 °C): δ = 8.33 (d, *J* = 5.4 Hz, 2H, β), 8.22-8.07 (m, 14H, β + Ar-*ortho*), 7.65 (m, 4H, Ar-*para*), 7.55 (m, 2H, Ar-*para*), 7.35 (s, 2H, β), 7.22 (br, 4H, Ar-*ortho*), 7.01 (br, 4H, Ar-*ortho*), and 1.56–1.23 (m, 108H, *tert*-Butyl) ppm. ^{13}C NMR (100.40 MHz, CDCl$_3$, 25 °C): δ = 158.6, 149.7, 149.41, 149.37, 149.3, 146.9, 145.9, 145.3, 144.8, 143.2, 143.0, 142.9, 141.0, 140.9, 139.2, 139.1, 138.0, 133.8, 133.4, 131.3, 130.7, 129.9, 129.7, 128.7, 128.0, 125.9, 125.7, 121.6, 121.4, 121.1, 120.4, 119.9, 109.3, 35.1, and 31.8 ppm. UV/Vis/NIR (CH$_2$Cl$_2$): λ (ε, M^{-1}·cm^{-1}) = 426 (139000), 462 (93200), 557 (49000), 615 (74300), 864 (4600), and 975 (2500) nm. HRMS (APCI) calcd for C$_{128}$H$_{140}$N$_8$Ni$_2$S$_1$; [M+H]$^+$: 1937.9701; found

1937.9672. FT-IR (ATR): ν = 2953, 2904, 2867, 1592, 1461, 1425, 1393, 1361, 1298, 1247, 1072, 1012, 994, 974, 938, 900, 882, 861, 825, 715, and 693 cm^{-1}. m.p.: > 300 °C.

Thiophene-fused Helical Porphyrin Dimer (43b):

A flask containing **29b** (175.7 mg, 0.0974 mmol) was purged with argon, and then charged with CHCl$_3$ (19.5 mL). Palau'Chlor (44.9 mg, 0.214 mmol) was added to the mixture at 0 °C. The reaction mixture was stirring at 0 °C for 30 min, and then stirred at room temperature for 13 h. The mixture was diluted with CH$_2$Cl$_2$, and then filtered through a small plug of silica gel with copious washing with CH$_2$Cl$_2$. After removal of solvent, the crude product of **47b** was using for next step without further purification. A flask containing **47b**, Pd(OAc)$_2$ (4.4 mg, 0.0195 mmol), PCy$_3$·HBF$_4$ (14.3 mg, 0.0390 mmol), and K$_2$CO$_3$ (26.9 mg, 0.195 mmol) was purged with argon, and charged with DMF (4.9 mL). The mixture was heated to reflux with stirring for 4.5 h, and then cooled to ambient temperature. The mixture was extracted with toluene, and dried over Na$_2$SO$_4$. After removal of solvent, the crude product was purified with silica gel column chromatography using a 8:1 mixture of *n*-hexane and CH$_2$Cl$_2$ to afforded **43b**. Recrystallization from CH$_2$Cl$_2$ and MeOH gave **43b** (52.7 mg, 0.0293 mmol, 30%) as a dark solid.

43b: ^{1}H NMR (399.65 MHz, CDCl$_3$, 25 °C): δ = 8.34 (d, *J* = 4.9 Hz, 2H, β), 8.15–8.00 (m, 12H, β + Ar-*ortho*), 7.92 (d, *J* = 4.3 Hz, 2H, β), 7.65–7.64 (m, 2H, Ar-*para*), 7.54–7.53 (m, 2H, Ar-*para*), 7.33 (s, 2H, β), 7.22 (brs, 2H, Mes), 7.04 (brs, 2H, Mes), 2.50 (s, 6H, Methyl), 2.24 (s, 6H, Methyl), and 1.61-1.22 (m, 78H, *tert*-Butyl and Methyl) ppm. ^{13}C NMR (100.40 MHz, CDCl$_3$, 25 °C): δ = 158.6, 149.7, 149.4, 149.3, 147.0, 146.0, 145.4, 144.9, 142.8, 142.7, 142.4, 141.0, 140.9, 139.1, 138.7, 138.6, 138.0, 137.8, 136.3, 133.8, 132.1, 131.8, 131.1, 129.8, 128.8, 128.1, 128.0, 125.5, 122.9, 121.6, 121.1, 120.5, 120.0, 109.5, 35.2, 35.0, 31.9, 31.7, 31.6, 29.9, 21.5, 21.4, and 21.0 ppm. UV/Vis/NIR (CH$_2$Cl$_2$): λ (ε, M^{-1}·cm^{-1}) = 417 (107000), 458 (90500), 559 (48600), 613 (78100), 859 (4700), and 975 (2300) nm. HRMS (APCI) calcd for C$_{118}$H$_{120}$N$_8$Ni$_2$S$_1$; [M+H]$^+$: 1797.8136; found 1797.8126. FT-IR (ATR): ν = 2951, 2865, 1590, 1458, 1393, 1351, 1296, 1240, 1201, 1069, 1008, 991, 972, 935, 899, 882, 855, 825, 796, 741, 716, 697, and 685 cm^{-1}. m.p.: > 300 °C.

Thiophene-fused Helical Porphyrin Dimer (44):

Conc. H$_2$SO$_4$ (0.22 mL) was added to the mixture of **43b** (40 mg, 0.0222 mmol) and trifluoroacetic acid (2.2 mL) at 0 °C. The reaction mixture was stirring for 2 h at 0 °C under dark condition. After neutralization by KOH aq. at 0 °C, the product was extracted with CH$_2$Cl$_2$ and dried over Na$_2$SO$_4$. After removal of solvent, a solution of Zn(OAc)$_2$·2H$_2$O (97.6 mg, 0.445

mmol) in MeOH (1.1 mL) was added to the crude product in CH_2Cl_2 (1.1 mL). The reaction mixture was stirring for 1h at room temperature under dark condition. After removal of solvent, the mixture was diluted with a 1:1 mixture of *n*-hexane and CH_2Cl_2 and filtered through a small plug of silica gel with copious washings with a 1:1 mixture of *n*-hexane and CH_2Cl_2 as eluent to afford **44** (38.4 mg, 0.0212 mmol, 95%) as a dark solid.

44: ^{1}H NMR (399.65 MHz, CDCl$_3$, 25 °C): δ = 8.75 (d, J = 4.9 Hz, 2H, β), 8.28 (d, J = 4.3 Hz, 2H, β), 8.21 (d, J = 4.3 Hz, 2H, β), 8.19 (d, J = 4.9 Hz, 2H, β), 8.17 (d, J = 4.9 Hz, 2H, β), 8.11 (m, 2H, Ar), 8.08 (m, 2H, Ar), 8.06 (d, J = 4.3 Hz, 2H, β), 7.70–7.69 (m, 2H, Ar), 7.67 (m, 2H, Ar), 7.61–7.60 (m, 2H, Ar), 7.56 (m, 2H, Ar), 7.31 (s, 2H, β), 7.21 (brs, 2H, Mes), 7.15 (brs, 2H, Mes), 2.56 (s, 6H, Methyl), 2.05 (s, 6H, Methyl), 1.81 (s, 6H, Methyl), 1.57 (s, 18H, *tert*-Butyl), 1.50 (s, 18H, *tert*-Butyl), 1.47 (s, 18H, *tert*-Butyl), and 1.33 (s, 18H, *tert*-Butyl) ppm. ^{13}C NMR (100.40 MHz, CDCl$_3$, 25 °C): δ = 167.7, 154.3, 153.9, 153.3, 152.4, 151.6, 150.2, 149.2, 149.1, 148.9, 148.5, 142.8, 141.5, 140.8, 139.7, 138.9, 138.7, 138.3, 137.5, 132.4, 131.8, 131.5, 131.3, 130.8, 130.1, 129.6, 129.2, 129.1, 127.9, 127.8, 124.8, 121.8, 121.3, 120.6, 118.3, 112.1, 35.20, 35.15, 35.1, 35.0, 31.94, 31.90, 31.86, 31.7, 29.9, 21.6, 21.5, and 21.4 ppm. UV/Vis/NIR (CH$_2$Cl$_2$): λ (ε, M^{-1}·cm^{-1}) = 422 (113000), 436 (108000), 475 (106000), 568 (45100), 661 (71000), 910 (4000), and 1040 (1400) nm. HRMS (APCI) calcd for $C_{118}H_{120}N_8Zn_2S_1$; [M+H]$^+$: 1809.8012; found 1809.7994. FT-IR (ATR): ν = 2952, 2862, 1589, 1475, 1458, 1424, 1392, 1360, 1335, 1285, 1243, 1200, 1063, 1007, 984, 966, 934, 881, 820, 795, 738, 727, and 715 cm^{-1}. m.p.: > 300 °C.

Crystal Data

Table 1. Crystal data and structure refinement for compounds in Chapters 2–4.

	36Zn[a]	**42Ni**	**43a**[a]
formula	$C_{84}H_{85}N_4PSZn$	$C_{84}H_{85}N_5Ni \cdot CHCl_3$	$2(C_{128}H_{140}N_8Ni_2S_1) \cdot$ $7(CHCl_3)$
M_r	1278.95	1342.64	4715.48
T [K]	93(2)	153(2)	153
crystal system	triclinic	triclinic	triclinic
space group	P-1 (No.2)	P-1 (No.2)	P1 (No.1)
a [Å]	13.3527(5)	9.3913(18)	19.992(4)
b [Å]	14.3734(9)	15.731(3)	20.190(5)
c [Å]	20.6744(9)	26.057(5)	21.414(3)
a [°]	80.374(4)	78.511(8)	69.720(15)
b [°]	76.560(4)	86.633(9)	63.048(12)
g [°]	73.856(5)	75.626(7)	80.939(17)
V [Å^3]	3684.6(3)	3654.1(12)	7202(3)
Z	2	2	1
ρ_{calcd} [g cm^{-3}]	1.153	1.220	1.087
F [000]	1356	1420	2478
crystal size [mm^3]	0.39×0.09×0.03	0.20×0.10×0.01	0.10×0.05×0.03
$2\theta_{max}$ [°]	126.00	52.5	50.0
reflections collected	41566	27140	48710
independent reflections	11469	14281	35758
parameters	838	1068	2611
R_1 ($I > 2.0s(I)$)	0.0666	0.0997	0.1317
wR_2 (all data)	0.1854	0.3200	0.3652
GOF	1.051	1.071	1.047
CCDC umber	1907852	1990845	2093263

[a] These values have been obtained by removal of the solvent molecules by using the PLATON SQUEEZE program.

Reference

[1] K. M. Kadish, K. M. Smith, R. Guilard, *The Porphyrin Handbook,* Academic Press, San Diego, **2000**.

[2] (a) Storm, C. B.; Teklu, Y. *J. Am. Chem. Soc.* **1972**, 94, 1745. (b) Storm, C. B.; Teklu, Y.; Sokoloski, E. A. *Ann. N. Y. Acad. Sci.* **1973**, *206*, 631. (c) Abraham, R. J.; Hawkes, G. E.; Smith, K. M. *Tetrahedron Lett.* **1974**, *16*, 1483. (d) Eaton, S. S.; Eaton, G. R. *J. Am. Chem. Soc.* **1977**, *99*, 1601. (e) Limbach, H. H.; Hennig; J.; Kendrick, R.; Yannoni, C. S. *J. Am. Chem. Soc.* **1984**, *106*, 4059.

[3] (a) Gouterman, M.; Dolphin, D., Ed.; Academic Press: New York, **1978**; *Vol. III*, Part A, 1. (b) Gouterman, M. *J. Mol. Spectrosc.* **1961**, *6*, 138. (c) Gouterman, M. *J. Chem. Phys.* **1959**, *30*, 1139. (d) McHugh, A. J.; Gouterman, M.; Weiss, C. *Theoret. Chim. Acta* **1972**, *24*, 346.

[4] (a) Kim, D.; Kirmaier, C.; Holten, D. *Chem. Phys.* **1983**, *75*, 305. (b) Rodriguez, J.; Kirmaier, C.; Holten, D. *J. Am. Chem. Soc.* **1989**, *111*, 6500.

[5] (a) Fischer H.; Zeile, K. *Ann. Chem.*, **1929**, *468*, 98. (b) Fischer H.; Orth, H. *Die Chemie des Pyrrols*: Akademische Verlag., Leipzig, **1937**, vol. II, part i. (c) Arsenault, G. P.; Bullock E.; MacDonald S. F. *J. Am. Chem. Soc.*, **1960**, *82*, 4384.

[6] Rothemund, P. *J. Am. Chem. Soc.* **1935**, *57*, 2010.

[7] Rothemund, P.; Menotti, A. R. *J. Am. Chem. Soc.* **1941**, *63*, 267.

[8] Adler, A. D.; Longo, F. R.; Shergalis, W. *J. Am. Chem. Soc.* **1964**, *86*, 3145. (b) Adler, A. D.; Longo, F. R.; Finarelli, J. D.; Goldmacher, J.; Assour, J.; Korsakoff, L. *J. Org. Chem.* **1967**, 32, 476. (c) Kim, J. B.; Adler, A. D.; Longo, F. R. *In The Porphyrins*; Dolphin, D., Ed.; Academic Press: New York, **1978**; Vol. *1*, pp 85.

[9] (a) Lindsey, J. S.; Hsu, H. C.; Schreiman, I. C. *Tetrahedron Lett.* **1986**, *27*, 4969. (b) Lindsey, J. S.; Schreiman, I. C.; Hsu, H. C.; Kearney, P. C.; Marguerettaz, A. M. *J. Org. Chem.* **1987**, *52*, 827. (c) Lindsey, J. S.; Wagner, R. W. *J. Org. Chem.* **1989**, *54*, 828. (d) Lindsey, J. S.; MacCrum, K. A.; Tyhonas, J. S.; Chuang, Y. Y. *J. Org. Chem.* **1994**, *59*, 579.

[10] d'A. Rocha Gonsalves, A.; Pereira, M. M.; Serra, A. C.; Johnstone, R. A. W.; Nunes, M. L. P. *J. Chem. Soc. Perkin 1* **1994**, 2053.

[11] Mandal, A. K.; Taniguchi, M.; Diers, J. R.; Niedzwiedzki, D. M.; Kirmaier, C.; Lindsey, J. S.; Bocian, D. F.; Holten, D. *J. Phys. Chem. A* **2016**, *120*, 9719.

[12] (a) Wiehe, A.; Ryppa, C.; Senge, M. O. A. *Org. Lett.* **2002**, *4*, 3807. (b) Ryppa, C.; Senge, M. O.; Hatscher, S. S.; Kleinpeter, E.; Wacker, P.; Schilde, U.; Wiehe, A. *Chem. Eur. J.* **2005**, *11*, 3427.

[13] Taniguchi, M.; Balakumar, A.; Fan, D.; McDowell, B. E.; Lindsey, J. S. *J. Porphyr. Phthalocyanines* **2005**, *09*, 554.

[14] Treibs, A.; Häberle, N. *Justus Liebigs Ann. Chem.* **1968**, *718*, 183.

[15] Manka S. J.; Lawrence, S. D. *Tetrahedron Lett.* **1989**, *30*, 6989.

[16] Bruckner, C.; Posakony, J. J.; Johnson, C. K.; Boyle, R. W.; James, B. R.; Dolphin, D. *J. Porphyr. Phthalocyanines* **1998**, *2*, 455.

[17] Yoshida, N.; Shimizu, H.; Osuka, A. *Chem Lett.* **1998**, *27*, 55.

[18] Shultz, D. A.; Gwaltney, K. P.; Lee, H. *J. Org. Chem.* **1998**, *63*, 769.

[19] (a) Wiehe, A.; Ryppa, C.; Senge, M. O. A. *Org. Lett.* **2002**, *4*, 3807. (b) S. Hatscher; Senge, M. O. A. *Tetrahedron Lett.* **2003**, *44,* 157.

[20] (a) Neya, S.; Funasaki, N. *Tetrahedron Lett.* **2002**, *43*, 1057. (b) Neya, S.; Quan, J. S.; Hoshino, T.; Hata, M.; Funasaki, N. *Tetrahedron Lett.* **2004**, *45*, 8629.

[21] Hiroto, S.; Miyake, Y.; Shinokubo, H. *Chem. Rev.* **2017**, *117*, 2910.

[22] DiMagno, S. G.; Lin, V. S. Y.; Therien, M. J. *J. Org. Chem.* **1993**, *58*, 5983.

[23] Screen, T. E. O.; Lawton, K. B.; Wilson, G. S.; Dolney, N.; Ispasoiu, R.; Goodson, T., III; Martin, S. J.; Bradley, D. D. C.; Anderson, H. L. *J. Mater. Chem.* **2001**, *11*, 312.

[24] (a) Schlözer, R.; Fuhrhop, J.-H. *Angew. Chem. Int. Ed Engl.* **1975**, *14*, 363. (b) Shi, D. F.; Wheelhouse, R. T.; *Tetrahedron Lett.* **2002**, *43*, 9341.

[25] Guo, C.-C.; Chen, Q.-Y.; Jin, L.-M.; Yin, J.-J.; Chen, L. *Synlett* **2005**, *2005*, 2893.

[26] Boyle, R. W.; Johnson, C. K.; Dolphin, D. *J. Chem. Soc. Chem. Commun.* **1995**, 527.

[27] Nakano, A.; Shimizu, H.; Osuka, A. *Tetrahedron Lett.* **1998**, *39*, 9489.

[28] (a) Rumyantseva, V. D.; Aksenova, E. A.; Ponamoreva, O. N.; Mironov, A. F. *Russ. J. Bioorganic Chem.* **2000**, *26*, 423. (b) Chumakov , D. E.; Khoroshutin, A. V.; Anisimov, A. V.; Kobrakov, K. I. *Chem. Heterocycl Compd.* **2009**, *45*, 259.

[29] Schlözer, R.; Fuhrhop, J.-H. *Angew. Chem. Int. Ed Engl.* **1975**, *14*, 363.

[30] Hata, H.; Shinokubo, H.; Osuka, A. *J. Am. Chem. Soc.* **2005**, *127*, 8264.

[31] Fujimoto, K.; Yorimitsu, H.; Osuka, A. *Org. Lett.* **2014**, *16*, 972.

[32] (a) Anderson, H. L. *Chem. Commun.* **1999**, 2323. (b) Vicente, M. G. H.; Jaquinod, L.; Smith, K. M. *Chem. Commun.* **1999**, 1771. c) Arnold, D. P. *Synlett* **2000**, 296. (d)

Aratani, N.; Osuka, A. *Bull. Chem. Soc. Jpn.* **2001**, *74*, 1361. (e) Burrell, A. K.; Officer, D. L.; Plieger, P. G.; Reid, D. C. W. *Chem. Rev.* **2001**, *101*, 2751. (f) Tanaka, T.; Osuka, A. *Chem. Soc. Rev.* **2015**, *44*, 943.

[33] (a) Crossley, M. J.; Burn, P. L. *J. Chem. Soc., Chem. Commun.* **1991**, 1569. (b) Wagner, R. W.; Lindsey, J. S. *J. Am. Chem. Soc.* **1994**, *116*, 9759. (c) Sedghi, G.; Sawada, K.; Esdaile, L. J.; Hoffmann, M.; Anderson, H. L.; Bethell, D.; Haiss, W.; Higgins, S. J.; Nichols, R. J. *J. Am. Chem. Soc.* **2008**, *130*, 8582. (d) Jurow, M.; Schuckman, A. E.; Batteas, J. D.; Drain, C. M. *Coord. Chem. Rev.* **2010**, *254*, 2297. e) Sedghi, G.; García-Suárez, V. M.; Esdaile, L. J.; Anderson, H. L.; Lambert, C. J.; Martín, S.; Bethell, D.; Higgins, S. J.; Elliott, M.; Bennett, N.; Macdonald, J. E.; Nichols, R. J. *Nature Nanotechnol.* **2011**, *6*, 517. (f) Sedghi, G.; Esdaile, L. J.; Anderson, H. L.; Martin, S.; Bethell, D.; Higgins, S. J.; Nichols, R. J. *Adv. Mater.* **2012**, *24*, 653. (g) Bruce, R. C.; Wang, R.; Rawson, J.; Therien, M. J.; You, W. *J. Am. Chem. Soc.* **2016**, *138*, 2078.

[34] (a) Kim, D.; Osuka, A. *J. Phys. Chem. A* **2003**, *107*, 8791. (b) Senge, M. O.; Fazekas, M.; Notaras, E. G. A.; Blau, W. J.; Zawadzka, M.; Locos, O. B.; Ni Mhuircheartaigh, E. M. *Adv. Mater.* **2007**, *19*, 2737. (c) Collins, H. A.; Khurana, M.; Moriyama, E. H.; Mariampillai, A.; Dahlstedt, E.; Balaz, M.; Kuimova, M. K.; Drobizhev, M.; Yang, V. X. D.; Phillips, D.; Rebane, A.; Wilson, B. C.; Anderson, H. L. *Nature Photonics* **2008**, *2*, 420. d) Aratani, N.; Kim, D.; Osuka, A. *Chem. Asian J.* **2009**, *4*, 1172. (e) Fisher, J. A. N.; Susumu, K.; Therien, M. J.; Yodh, A. G. *J. Chem. Phys.* **2009**, *130*, 134506. (f) Pawlicki, M.; M. Morisue, M.; Davis, N. K. S.; McLean, D. G.; Haley, J. E.; Beuerman, E.; Drobizhev, M.; Rebane, A.; Thompson, A. L.; Pascu, S. I.; Accorsi, G.; Armaroli, N.; Anderson, H. L. *Chem. Sci.* **2012**, *3*, 1541.

[35] (a) Zimmerman, J. D.; Diev, V. V.; Hanson, K.; Lunt, R. R.; Yu, E. K.; Thompson, M. E.; Forrest, S. R. *Adv. Mater.* **2010**, *22*, 2780. (b) Wu, H.-P.; Ou, Z.-W.; Pan, T.-Y.; Lan, C.-M.; Huang, W.-K.; Lee, H.-W.; Reddy, N. M.; Chen, C.-T.; Chao, W.-S.; Yeh, C.-Y.; et al., *Energy Environ. Sci.* **2012**, *5*, 9843. (c) Shiu, J.-W.; Chang, Y.-C.; Chan, C.-Y.; Wu, H.-P.; Hsu, H.-Y.; Wang, C.-L.; Lin, C.-Y.; Diau, E. W.-G. *J. Mater. Chem. A* **2015**, *3*, 1417. (d) Chiang, Y.-H.; Chou, H.-H.; Cheng, W.-T.; Li, Y.-R.; Yeh, C.-Y.; Chen, P. *ACS Energy Lett.* **2018**, *3*, 1620. (e) Lai, T.; Xiao, L.; Deng, K.; Liang, T.; Chen, X.; Peng, X.; Cao, Y. *ACS Appl. Mater. Interfaces* **2018**, *10*, 668.

[36] (a) Imahori, H. *J. Phys. Chem. B* **2004**, *108*, 6130. (b) Nakamura, Y.; Aratani, N.; Osuka, A. *Chem. Soc. Rev.* **2007**, *36*, 831.

Reference

[37] Susumu, K.; Shimizu, T.; Tanaka, K.; Segawa, H. *Tetrahedron Lett.* **1996**, *37*, 8399.

[38] Osuka, A.; Shimidzu, H. *Angew. Chem. Int. Ed Engl.* **1997**, *36*, 135.

[39] Jin, L.-M.; Chen, L.; Yin, J.-J.; Guo, C.-C.; Chen, Q.-Y. *European J. Org. Chem.* **2005**, *2005*, 3994.

[40] Arnold, D. P.; Johnson, A. W.; Mahendran,M. *J. Chem. Soc., Perkin Trans.*, **1978**, *35*, 366.

[41] (a) Arnold, D. P.; Nitschinsk, L. J. *Tetrahedron*, **1992**, *48*, 8781. (b) Arnold, D. P.; and Heath, G. A. *J. Am. Chem. Soc.*, **1993**, *115*, 12197. (c) Arnold, D. P.; James, D. A.; Kennard, C. H. L.; Smith, G. *J. Chem. Soc., Chem. Commun.*, **1994**, 2131. (d) Arnold, D. P.; Hartnell, R. D.; Heath, G. A.; Newby, L.; Webster, R. D. *Chem. Commun.*, **2002**, 754. (e) Arnold, D. P.; Heath, G. A.; James, D. A. *J. Porphyrins Phthalocyanines*, **1999**, *3*, 5.

[42] Taylor, P. N.; Huuskonen, J.; Aplin, R. T.; Anderson, H. L.; Rumbles, G.; Williams, E. *Chem. Commun.* **1998**, 909.

[43] Lin, V. S.; DiMagno, S. G.; Therien, M. J. *Science* **1994**, *264*, 1105.

[44] Screen, T. E. O.; Blake, I. M.; Rees, L. H.; Clegg, W.; Borwick, S. J.; Anderson, H. L. *J. Chem. Soc. Perkin 1* **2002**, 320.

[45] Esdaile, L. J.; Jensen, P.; McMurtrie, J. C.; Arnold, D. P. *Angew. Chem. Int. Ed Engl.* **2007**, *46*, 2090.

[46] Esdaile, L. J.; Senge, M. O.; Arnold, D. P. *Chem. Commun.* **2006**, 4192.

[47] Pereira, A. M. V. M.; Neves, M. G. P. M. S.; Cavaleiro, J. A. S.; Jeandon, C.; Gisselbrecht, J.-P.; Choua, S.; Ruppert, R. *Org. Lett.* **2011**, *13*, 4742.

[48] Ryan, A. A.; Plunkett, S.; Casey, A.; McCabe, T.; Senge, M. O. *Chem. Commun.* **2013**, *50*, 353.

[49] Kato, K.; Fujimoto, K.; Yorimitsu, H.; Osuka, A. *Chem. Eur. J.* **2015**, *21*, 13522.

[50] Arnold, D. P.; Nitschinsk, L. J. *Tetrahedron* **1992**, *48*, 8781.

[51] Song, J.; Jang, S. Y.; Yamaguchi, S.; Sankar, J.; Hiroto, S.; Aratani, N.; Shin, J.-Y.; Easwaramoorthi, S.; Kim, K. S.; Kim, D.; Shinokubo, H.; Osuka, A. *Angew. Chem.* **2008**, *120*, 6093.

[52] Maeda, C.; Shinokubo, H.; Osuka, A. *Org. Lett.* **2010**, *12*, 1820.

[53] Song, J.; Aratani, N.; Heo, J. H.; Kim, D.; Shinokubo, H.; Osuka, *J. Am. Chem. Soc.* **2010**, *132*, 11868.

[54] (a) Tsuda, A; Furuta, H.; Osuka, A. *Angew. Chem*. **2000**, *112*, 2649; *Angew. Chem. Int. Ed.* **2000**, *39*, 2549. (b) Tsuda, A.; Furuta, H.; Osuka, A. *J. Am. Chem. Soc.* **2001**, *123*,

10304. (c) Tsuda, A.; Osuka, A. *Science* **2001**, *293*,79. (d) Hiroto, S.; Osuka, A. *J. Org. Chem.* **2005**, *70*, 4054. (e) Ikeue,T.; Aratani, N.; Osuka, A.; *Isr. J. Chem.* **2005**, *45*, 293.

[55] (a) Crossley M. J.; King, L. G. *J. Chem. Soc., Chem. Commun.,* **1984**, *352*. 115. (b) Crossley M. J.; Burn, P. L. *J. Chem. Soc., Chem. Commun.*, **1987**, *39*. 116. (c) Crossley M. J.; Burn, P. L.; *J. Chem. Soc., Chem. Commun.*,**1991**, 1569.

[56] Ono, N.; Hironaga, H.; Ono, K.; Kaneko, T. Murashima, T.; Ueda, T.; Tsukamura, Ogawa, T. *J. Chem. Soc., Perkin Trans. 1*, **1996**, 417.

[57] Crossley, M. J.; Prashar, J. K. *Tetrahedron Lett.* **1997**, *38*, 6751.

[58] Mitsushige, Y.; Yamaguchi, S.; Lee, B. S.; Sung, Y. M.; Kuhri, S.; Schierl, C. A.; Guldi, D. M.; Kim, D.; Matsuo, Y. *J. Am. Chem. Soc.* **2012**, *134*, 16540.

[59] Yang, L.-L.; Hu, X.-L.; Tang, Z.-Q.; Li, X.-F. *Chem. Lett.* **2015**, *44*, 1515.

[60] Fujimoto, K.; Osuka, A. *Chem. Sci.* **2017**, *8*, 8231.

[61] Kurumisawa, Y.; Higashino, T.; Nimura, S.; Tsuji, Y.; Iiyama, H.; Imahori, H. *J. Am. Chem. Soc.*, **2019**, *141*, 9910.

[62] Alonso, C. M. A.; Neves, M. G. P. M. S.; Tomé, A. C.; Siva, A. M. S.; Cavaleiro, J. A. S. *Tetrahedron*, **2005**, *61*, 11866.

[63] (a) Lewtak, J. P.; Gryko, D. T. *Chem. Commun.* **2012**, *48*, 10069. (b) Lewtak, J. P.; Koszarna, B.; Charyton, M. K.; Gryko, D. *J. Porphyr. Phthalocyanines* **2020**, *24*, 448.

[64] Higashino, T.; Yamada, T.; Sakurai, T.; Seki, S.; Imahori, H. *Angew. Chem. Int. Ed.*, **2016**, *55*, 12311.

[65] Kato. K.; Kim, J. O.; Yorimitsu, H.; Kim, D.; Osuka, A. *Chem. Asian J.*, **2016**, *11*, 1738.

[66] (a) Anderson, H. L.; Martin, S. J.; Bradley, D. D. C. *Angew. Chem. Int. Ed. Engl.* **1994**, *33*, 655. (b) Lin, V. S.-Y.; Therien, M. J. *Chem. Eur. J.* **1995**, *1*, 645. (c) Taylor, P. N.; Anderson, H. L. *J. Am. Chem. Soc.* **1999**, *121*, 11538. (d) Sugiura, K.; Fujimoto, Y.; Sakata, Y. *Chem. Commun.* **2000**, *2*, 1105. (e) Yang, J.; Lee, J.-E.; Lee, C. Y.; Aratani, N.; Osuka, A.; Hupp, J. T.; Kim, D. *Chem. Eur. J.* **2011**, *17*, 9219. (f) O'Sullivan, M. C.; Sprafke, J. K.; Kondratuk, D. V.; Rinfray, C.; Claridge, T. D. W.; Saywell, A.; Blunt, M. O.; O'Shea, J. N.; Beton, P. H.; Malfois, M.; Anderson, H. L.; *Nature* **2011**, *469*, 72. (g) Tait, C. E.; Neuhaus, P.; Peeks, M. D.; Anderson, H. L.; Timmel, C. R. *J. Am. Chem. Soc.* **2015**, *137*, 8284. (h) Kamonsutthipaijit, N.; Anderson, H. L. *Chem. Sci.* **2017**, *8*, 2729.

[67] (a) Hisaki, I.; Hiroto, S.; Kim, K. S.; Noh, S. B.; Kim, D.; Shinokubo, H.; Osuka, A. *Angew. Chem. Int. Ed.* **2007**, *46*, 5125. (b) Tokuji, S.; Yorimitsu, H.; Osuka, A. *Angew.*

Chem. Int. Ed. **2012**, *51*, 12357. (c) Fukui, N.; Yorimitsu, H.; Osuka, A. *Angew. Chem. Int. Ed.* **2015**, *54*, 6311.

[68] (a) Sessler, J. L.; Johnson, M. R. *Angew. Chem. Int. Ed. Engl.* **1987**, *26*, 678. (b) Osuka, A.; Maruyama, K. *J. Am. Chem. Soc.* **1988**, *110*, 4454.

[69] (a) Fujisawa, K.; Satake, A.; Hirota, S.; Kobuke, Y. *Chem. Eur. J.* **2008**, *14*, 10735. (b) Song, J.; Jang, S. Y.; Yamaguchi, S.; Sankar, J.; Hiroto, S.; Aratani, N.; Shin, J.-Y.; Easwaramoorthi, S.; Kim, K. S.; Kim, D.; et al., *Angew. Chem. Int. Ed.* **2008**, *47*, 6004. (c) Regehly, M.; Wang, T.; Siggel, U.; Fuhrhop, J. H.; Röder, B. *J. Phys. Chem. B* **2009**, *113*, 2526.

[70] (a) Mathey, F. *Chem. Rev.* **1988**, *88*, 429. (b) Hissler, M.; Dyer, P. W.; Réau, R. *Coord. Chem. Rev.* **2003**, *244*, 1. (c) Crassous, J.; Réau, R. *Dalton Trans.* **2008**, 6865. (d) Matano, Y.; Imahori, H. *Org. Biomol. Chem.* **2009**, *7*, 1258. (e) Ren, Y.; Baumgartner, T. *Dalton Trans.* **2012**, *41*, 7792. (f) Duffy, M. P.; Delaunay, W.; Bouit, P.-A.; Hissler, M. *Chem. Soc. Rev.* **2016**, *45*, 5296.

[71] Examples of 2,5-diarylthiophenes: (a) Urselmann, D.; Antovic, D.; Müller, T. J. J. *Beilstein J. Org. Chem.* **2011**, *7*, 1499. Examples of 2,5-diarylphospholes: (b) Hay, C.; Hissler, M.; Fischmeister, C.; Rault-Berthelot, J.; Toupet, L.; Nyulászi, L.; Réau, R. *Chem. Eur. J.* **2001**, *7*, 4222. (c) Saito, A.; Miyajima, T.; Nakashima, M.; Fukushima, T.; Kaji, H.; Matano, Y.; Imahori, H. *Chem. Eur. J.* **2009**, *15*, 10000. (d) A. Arkhypchuk, I.; Orthaber, A.; Ott, S. *Eur. J. Inorg. Chem.* **2014**, *2014*, 1760.

[72] Saito, A.; Matano, Y.; Imahori, H. *Org. Lett.* **2010**, *12*, 2675.

[73] Gaussian 09, Revision E.01, Frisch, M. J.; Trucks, G. W.; Schlegel, H. B.; Scuseria, G. E.; Robb, M. A.; Cheeseman, J. R.; Scalmani, G.; Barone, V.; Mennucci, B.; Petersson, G. A.; Nakatsuji, H.; Caricato, M.; Li, X.; Hratchian, H. P.; Izmaylov, A. F.; Bloino, J.; Zheng, G.; Sonnenberg, J. L.; Hada, M.; Ehara, M.; Toyota, K.; Fukuda, R.; Hasegawa, J.; Ishida, M.; Nakajima, T.; Honda, Y.; Kitao, O.; Nakai, H.; Vreven, T.; Montgomery, J. A., Jr.; Peralta, J. E.; Ogliaro, F.; Bearpark, M.; Heyd, J. J.; Brothers, E.; Kudin, K. N.; Staroverov, V. N.; Keith, T.; Kobayashi, R.; Normand, J.; Raghavachari, K.; Rendell, A.; Burant, J. C.; Iyengar, S. S.; Tomasi, J.; Cossi, M.; Rega, N.; Millam, J. M.; Klene, M.; Knox, J. E.; Cross, J. B.; Bakken, V.; Adamo, C.; Jaramillo, J.; Gomperts, R.; Stratmann, R. E.; Yazyev, O.; Austin, A. J.; Cammi, R.; Pomelli, C.; Ochterski, J. W.; Martin, R. L.; Morokuma, K.; Zakrzewski, V. G.; Voth, G. A.; Salvador, P.; Dannenberg, J. J.; Dapprich, S.; Daniels, A. D.; Farkas, O.; Foresman, J.

B.; Ortiz, J. V.; Cioslowski, J.; Fox, D. J. *Gaussian 09*, revision D.01; Gaussian, Inc.; Wallingford, CT, **2013**.

[74] (a) Fox, S.; Boyle, R. W. *Tetrahedron* **2006**, *62*, 10039. b) Jiao, C.; Wu, J. *Synlett* **2012**, 171. (c) Mori, H.; Tanaka, T.; Osuka, A. *J. Mater. Chem. C* **2013**, 1, 2500. (d) Higashino, T.; Imahori, H. *Dalton Trans*. **2015**, *44*, 448.

[75] (a) Nakano, A.; Aratani, N.; Furuta, H.; Osuka, A. *Chem. Commun.* **2001**, 1920. (b) Sahoo, A. K.; Mori, S.; Shinokubo, H.; Osuka, A. *Angew. Chem. Int. Ed.* **2006**, *45*, 7972.; *Angew. Chem.* **2006**, *118*, 8140. (c) Fukui, N.; Yorimitsu, H.; Lim, J. M.; Kim, D.; Osuka, A. *Angew.Chem. Int. Ed.* **2014**, *53*, 4395.; *Angew. Chem.* **2014**, *126*, 4484. (d) Fukui, N.; Arai, S.; Shinokubo, H.; Yorimitsu, H.; Osuka, A. *Heterocycles,* **2015**, *90*, 252.

[76] (a) Fox, S.; Boyle, R. W. *Chem. Commun.* **2004**, 1322. (b) Shen, D.-M.; Liu, C. Chen, Q.-Y. *Chem. Commun*. **2005**, 4982. (c) Hayashi, S.; Matsubara, Y.; Eu, S.; Hayashi, H.; Umeyama, T.; Matano, Y.; Imahori, H. *Chem. Lett.* **2008**, *37*, 846. (d) Lash, T. D.; Smith, B. E.; Melquist, M. J.; Godfrey, B. A. *J. Org. Chem.* **2011**, *76*, 5335. (e) Ishizuka, T.; Saegusa, Y.; Shiota, Y.; Ohtake, K.; Yoshizawa, K.; Kojima, T. *Chem. Commun.* **2013**, *49*, 5939. (f) Ota, K.; Tanaka, T.; Osuka, A. *Org. Lett.* **2014**, *16*, 2974. (g) Fukui, N.; Lee, S.-K.; Kato, K.; Shimizu, D.; Tanaka, T.; Lee, S.; Yorimitsu, H.; Kim, D.; Osuka, A. *Chem. Sci.* **2016**, *7*, 4059.

[77] (a) Fagan, P. J.; Nugent, W. A.; *J. Am. Chem. Soc*. **1988**, *110*, 2310. (b) Fagan, P. J.; Nugent, W. A.; Calabrese, J. C. *J. Am. Chem. Soc*. **1994**, *116*, 1880. (c) Yan, X.; Xi, C. *Acc. Chem. Res*. **2015**, *48*, 935.

[78] (a) Sato, F.; Urabe, H.; Okamoto, S. *Chem. Rev.* **2000**, *100*, 2835. (b) Yamaguchi, S.; Jin, R.; Tamao, K.; Sato, F. *J. Org. Chem.* **1998**, *63*, 10060. (c) Matano, Y.; Miyajima, T.; Nakabuchi, T.; Matsutani, Y.; Imahori, H. *J. Org. Chem.* **2006**, *71*, 5792.

[79] (a) Shinokubo, H.; Osuka, A. *Chem. Commun.* **2009**, 1011. (b) M. O. Senge, *Chem. Commun.* **2011**, *47*, 1943. (c) Yorimitsu, H.; Osuka, A. *Asian J. Org. Chem.* **2013**, *2*, 356.

[80] Higashino, T.; Nishimura, I.; Imahori, H. *Chem. Lett.* **2019**, *48*, 257.

[81] (a) Baumgartner, T. *Acc. Chem. Res.* **2014**, *47*, 1613. (c) D. Joly, P.-A. Bouit, M. Hissler, *J. Mater. Chem. C* **2016**, *4*, 3686.

[82] (a) Fujimoto, K.; Yorimitsu, H.; Osuka, A. *Chem. Eur. J.* **2015**, *21*, 11311. (b) Kato, K.; Furukawa, K.; Osuka, A. *Angew. Chem. Int. Ed.* **2018**, *57*, 9491.

Reference

[83] (a) Fujimoto, K.; Kasuga, Y.; Fukui, N.; Osuka, A. *Chem. Eur. J.* **2017**, *23*, 6741. (b) Fukui, N.; Fujimoto, K.; Yorimitsu, H.; Osuka, A. *Dalton Trans.* **2017**, *46*, 13322.

[84] Matano, Y.; Matsumoto, K.; Terasaka, Y.; Hotta, H.; Araki, Y.; Ito, O.; Shiro, M.; Sasamori, T.; Tokitoh, N.; Imahori, H. *Chem. Eur. J.* **2007**, *13*, 891.

[85] (a) Song, H.; Cissell, J. A.; Vaid, T. P.; Holten, D. *J. Phys. Chem. B* **2007**, *111*, 2138. (b) Pawlicki, M.; Latos-Grażyński, L. *Chem. Asian J.* **2015**, *10*, 1438. (c) Sung, Y. M. ; Oh, J.; Cha, W.-Y.; Kim, W.; Lim, J. M. Yoon, M.-C.; Kim, D. *Chem. Rev.* **2017**, *117*, 2257.

[86] Matano, Y.; Saito, A.; Suzuki, Y.; Miyajima, T.; Akiyama, S.; Otsubo, S.; Nakamoto, E.; Aramaki, S.; Imahori, H. *Chem. Asian J.* **2012**, *7*, 2305.

[87] Seybold, P. G.; Gouterman, M. *J. Mol. Spectrosc.* **1969**, *31*, 1.

[88] (a) Tsuji, H.; Sato, K.; Sato, Y.; Nakamura, E. *J. Mater. Chem.* **2009**, *19*, 3364. (b) Tsuji, H.; Sato, K.; Sato, Y.; Nakamura, E. *Chem. Asian J.* **2010**, *5*, 1294. (c) Matano, Y.; Saito, A.; Fukushima, T.; Tokudome, Y.; Suzuki, F.; Sakamaki, D.; Kaji, H.; Ito, A.; Tanaka, K.; Imahori, H. *Angew. Chem. Int. Ed.* **2011**, *50*, 8016.

[89] (a) Schleyer, P. von R.; Maerker, C.; Dransfeld, A.; Jiao, H.; Hommes, N. J. R. van E. *J. Am. Chem. Soc.* **1996**, *118*, 6317. (b) Chen, Z.; Wannere, C. S.; Corminboeuf, C.; Puchta, R.; Schleyer, P. von R. *Chem. Rev.* **2005**, *105*, 3842.

[90] (a) Gust, D.; Moore, T. A.; Moore, A. L. *Acc. Chem. Res.* **2001**, *34*, 40. (b) Holten, D.; Bocian, D. F.; Lindsey, J. S. *Acc. Chem. Res.* **2002**, *35*, 57. (c) Imahori, H. *J. Phys. Chem. B* **2004**, *108*, 6130. (d) Ethirajan, M.; Chen, Y.; Joshi, P.; Pandey, R. K. *Chem. Soc. Rev.* **2011**, *40*, 340. (e) Ding, Y. ; Zhu, W.-H.; Xie, Y. *Chem. Rev.* **2017**, *117*, 2203. (f) Song, H.; Liu, Q.; Xie, Y. *Chem. Commun.* **2018**, *54*, 1811.

[91] (a) Carvalho, C. M. B.; Brocksom, T. J.; Thiago de Oliveira, K. *Chem. Soc. Rev.* **2013**, *42*, 3302. (b) Hayashi, H.; Touchy, A. S.; Kinjo, Y.; Toude, Y.; Kurotobi, K.; Umeyama, T.; Matano, Y.; Imahori, H. *ChemSusChem* **2013**, *6*, 508. (c) Chen, Q.; Brambilla, L.; Daukiya, L.; Mali, K. S.; De Feyter, S.; Tommasini, M.; Müllen, K.; Narita, A. *Angew. Chem. Int. Ed.* **2018**, *57*, 11233. (d) Wu, L.; Li, F.; Rao, Y.; Wen, B.; Xu, L.; Zhou, M.; Tanaka, T.; Osuka, A.; Song, J. *Angew. Chem. Int. Ed.* **2019**, *58*, 8124.

[92] Saegusa, Y.; Ishizuka, T.; Komamura, K.; Shimizu, S.; Kotani, H.; Kobayashi, N.; Kojima, T. *Phys. Chem. Chem. Phys.* **2015**, *17*, 15001.

[93] Higashino, T.; Nishimura, I.; Imahori, H. *Chem. Eur. J.* **2019**, *25*, 13816.

[94] Chen, X.; Jin, J.; Wang, Y.; Lu, P. *Chem. Eur. J.* **2011**, *17*, 9920.

[95] Shin, J.-Y.; Kim, K. S.; Yoon, M.-C.; Lim, J. M.; Yoon, Z. S.; Osuka, A.; Kim, D. *Chem. Soc. Rev.* **2010**, *39*, 2751.

[96] (a) Herges, R.; Geuenich, D. *J. Phys. Chem. A* **2001**, *105*, 3214. (b) Geuenich, D.; Hess, K.; Köhler, F.; Herges, R. *Chem. Rev.* **2005**, *105*, 3758.

[97] Grzybowski, M.; Skonieczny, K.; Butenschön H.; Gryko, D. T. *Angew. Chem. Int. Ed.*, **2013**, *52*, 9900.

[98] (a) Reimers, J. R.; Hush, N. S.; Crossley, M. J. *J. Porphyrins Phthalocyanines*, **2002**, *6*, 795; (b) Ito, S.; Hiroto, S.; Lee, S.; Son, M.; Hisaki, I.; Yoshida, T.; Kim, D.; Kobayashi, N. Shinokubo, H. *J. Am. Chem. Soc.*, **2015**, *137*, 142.

[99] (a) Wu, Y.-T.; Siegel, J. S. *Chem. Rev.*, **2006**, *106*, 4843. (b) Kawase, T.; Kurata, H. *Chem. Rev.*, **2006**, *106*, 5250. (c) Segawa, Y.; Yagi, A.; Matsui, K.; Itami, K. *Angew. Chem. Int. Ed.*, **2016**, *55*, 5136. (d) Rickhaus, M.; Mayor, M.; Juríček, M. *Chem. Soc. Rev.*, **2016**, *45*, 1542. (e) Pun, S. H.; Miao, Q. *Acc. Chem. Res.*, **2018**, *51*, 1630.

[100]   (a) Shen, Y.; Chen, C.-F. *Chem. Rev.*, **2012**, *112*, 1463. (b) Li, C.; Yang, Y.; Miao, Q. *Chem. Asian J.*, **2018,** *13*, 884. (c) Dhbaibi, K.; Favereau, L.; Crassous, J. *Chem. Rev.*, **2019**, *119*, 8846. (d) Kato, K.; Segawa, Y.; Itami, K. *Synlett*, **2019**, *30*, 370. (e) Mori, T. *Chem. Rev.*, **2021**, *121*, 2373.

[101]   (a) Kiel, G. R.; Patel, S. C.; Smith, P. W.; Levine, D. S.; Tilley, T. D. *J. Am. Chem. Soc.*, **2017**, *139*, 18456. (b) Evans, P. J.; Ouyang, J.; Favereau, L.; Crassous, J.; Fernández, I.; Perles, J.; Martín, N. *Angew. Chem. Int. Ed.*, **2018**, *57*, 6774. (c) Cruz, C. M.; Castro-Fernández, S.; Maçôas, E.; Cuerva, J. M.; Campaña, A. G. *Angew. Chem. Int. Ed.*, **2018**, *57*, 14782. (d) D. Reger, P. Haines, F. W. Heinemann, D. M. Guldi and N. Jux, *Angew. Chem. Int. Ed.*, **2018**, *57*, 5938. (e) Nakakuki, Y.; Hirose, T.; Sotome, H.; Miyasaka, H.; Matsuda, K. *J. Am. Chem. Soc.*, **2018**, *140*, 4317. (f) Schuster, N. J.; Hernández Sánchez, R.; Bukharina, D.; Kotov, N. A.; Berova, N.; Ng, F.; Steigerwald, M. L.; Nuckolls, C. *J. Am. Chem. Soc.*, **2018**, *140*, 6235. (g) Saal, F.; Zhang, F.; Holzapfel, M.; Stolte, M.; Michail, E.; Moos, M.; Schmiedel, A.; Krause, A.-M.; Lambert, C.; Würthner, F.; Ravat, P. *J. Am. Chem. Soc.*, **2020**, *142*, 21298.

[102]   (a) Zhong, H.; Wu, C.-H.; Li, C.-Z.; Carpenter, J.; Chueh, C.-C.; Chen, J.-Y.; Ade, H.; Jen, A. K.-Y. *Adv. Mater.,* **2016**, *28*, 951. (b) Laventurea, A.; Stanzelb, S.; Paynea, A.-J.; Lessardb, B. H.; Welcha, G. C. *Synth. Met.,* **2019**, *250*, 55.

[103]   Dore, A.; Fabbri, D.; Gladiali, S.; Valle, G. *Tetrahedron: Asymmetry*, **1995**, *6*, 779.

[104]   Maclean, A.; Foran, G.; Kennedy, B.; Turner, P.; Hambley, T. *Aust. J. Chem.,* **1996**, *49*, 1273.

Reference

[105]   PLATON, a multipurpose crystallographic tool, Utrecht Univesity, Utrecht (The Netherlands); Spek. A. L. *J. Appl. Crystallogr*., **2003**, *36*, 7.

[106]   Gasparro, F. P.; Kolodny, N. H. *J. Chem. Educ.,* **1977**, *54*, 258.

[107]   Goediche, C.; Stegemeyer, H. *Tetrahedron Lett*., **1970**, *12*, 937.

[108]   Higashino, T.; Nishimura, I.; Imahori, H. *Chem. Eur. J.*, **2020**, *26*, 12043.

List of Publications

The content of this thesis is composed of the following papers.

Chapter 1

"Synthesis of Phosphole-bridged Porphyrin Dimers"

Tomohiro Higashino, <u>Issei Nishimura</u>, Hiroshi Imahori, *Chemistry Letters*, **2019**, *48*, 257–259.

(Chapter 1 is the author's version of a submitted work that was subsequently accepted for publication in *Chemistry Letters*, copyright © Chemical Society of Japan after peer review. To access the final edited and published work, see the following website: http://www.journal.csj.jp/doi/10.1246/cl.180943)

Chapter 2

"Phosphole-fused Dehydropurpurins via Titanium-mediated [2+2+1] Cyclization Strategy"

Tomohiro Higashino, <u>Issei Nishimura</u>, Hiroshi Imahori, *Chemistry – A European Journal*, **2019**, *25*, 13816–13823.

(Chapter 2 is the author's version of a submitted work that was subsequently accepted for publication in *Chemistry – A European Journal*, copyright © John Wiley & Sons, Inc. after peer review. To access the final edited and published work, see the following website: https://onlinelibrary.wiley.com/doi/abs/10.1002/chem.201903269)

Chapter 3

"Unique Role of Heterole-fused Structures in Aromaticity and Physicochemical Properties of 7,8-Dehydropurpurins"

Tomohiro Higashino, <u>Issei Nishimura</u>, Hiroshi Imahori, *Chemistry – A European Journal*, **2020**, *26*, 12043–12049.

(Chapter 3 is the author's version of a submitted work that was subsequently accepted for publication in *Chemistry – A European Journal*, copyright © John Wiley & Sons, Inc. after peer review. To access the final edited and published work, see the following website: https://onlinelibrary.wiley.com/doi/10.1002/chem.202001361)

List of Publications

Chapter 4

"Synthesis of Thiophene-fused Porphyrin Dimers as Effective π-extended Helical Chromophores"

Issei Nishimura, Tomohiro Higashino, Hiroshi Imahori, *Chemical Communications*, **2021**, *57*, 9606–9609.

(Chapter 4 is the author's version of a submitted work that was subsequently accepted for publication in *Chemical Communications*, copyright © Royal Chemical Society after peer review. To access the final edited and published work, see the following website: https://pubs.rsc.org/en/content/articlelanding/2021/CC/D1CC04215G)

Other publications:

(1) "Exploration on the Combination of Push-Pull Porphyrin Dyes and Copper(I/II) Redox Shuttles toward High-performance Dye-sensitized Solar Cells"

Tomohiro Higashino, Iiyama, Hitomi, Issei Nishimura, Hiroshi Imahori, *Chemistry Letters*, **2020**, *49*, 936–939.

(2) "Effects of meso-diarylamino Group of Porphyrins on Optical and Electrochemical Properties"

Tomohiro Higashino, Yamato Fujimori, Issei Nishimura, Hiroshi Imahori, *Journal of Porphyrins and Phthalocyanines*, **2020**, *24*, 67–74.

Acknowledgement